

DI 212749

# *Hydrodynamics, Sediment Transport and Daily Morphological Development of a Bar-Beach System*



Rijkswaterstaat  
Rijksinstituut voor Kust en Zee/RIKZ  
Bibliotheek (Den Haag)

B-2311 712

Felix C.J. Wolf

## **Uitnodiging**

tot het bijwonen van  
de verdediging van mijn  
proefschrift

op maandag 11 oktober 1993  
om 14.30 uur precies

in het Academiegebouw  
van de Universiteit  
Utrecht, Domplein 29  
te Utrecht

Aansluitend op de  
promotie vindt in het  
Academiegebouw een  
receptie plaats

Wilfried ten Brinke  
Pal Maleterstraat 35  
3573 PE Utrecht  
Tel. 030 - 734866



# **Hydrodynamics, Sediment transport, and Daily Morphological Development of a Bar-Beach System**



Hydrodynamics, Sediment transport, and Daily Morphological Development  
of a Bar-Beach System

Hydrodynamica, sedimenttransport en dagelijkse morfologische ontwikkeling  
van een brandingsbank-strand systeem

(met een samenvatting in het Nederlands)

**Rijkswaterstaat**

Rijksinstituut voor Kust en Zee/RIKZ  
Bibliotheek (Den Haag)

B-2311 712

PROEFSCHRIFT

TER VERKRIJGING VAN DE GRAAD VAN DOCTOR AAN DE UNIVERSITEIT  
UTRECHT OP GEZAG VAN DE RECTOR MAGNIFICUS, PROF.DR. H.O. VOORMA  
INGEVOLGE HET BESLUIT VAN HET COLLEGE VAN DECANEN IN HET OPENBAAR  
TE VERDEDIGEN OP VRIJDAG 14 NOVEMBER 1997 DES MORGENS TE 10.30 UUR

DOOR

FELIX CAROLUS JOHANNES WOLF

GEBOREN OP 7 FEBRUARI 1962 TE ARNHEM

Promotores: Prof.dr. J.H.J. Terwindt  
Prof.dr.ir. L.C. van Rijn  
Vakgroep Fysische Geografie

Co-promotor: Dr. P. Hoekstra  
Vakgroep Fysische Geografie

Dit proefschrift werd mede mogelijk gemaakt door financiële steun van het Rijksinstituut voor Kust en Zee (RIKZ, projecten Kustgenese en Kust2000), het Instituut voor Marien en Atmosferisch Onderzoek Utrecht (IMAU) en door het Koninklijk Nederlands Aardrijkskundig Genootschap (KNAG).

## STELLINGEN

behorende bij het proefschrift getiteld:

Hydrodynamics, Sediment Transport  
and the Daily Morphological Development of a Bar-Beach System

door

Felix C.J. Wolf,

in het openbaar te verdedigen op 14 November 1997 te Utrecht

### I

Het effect van een storm op de meest landwaarts gelegen brandingsbank wordt behalve door de hydrodynamische eigenschappen van de storm sterk bepaald door de antecedente morfologie van het meest kustnabije deel van de brandingszone.

### II

Tijdens dissipatieve condities kunnen de golven in het binnenste deel van de brandingszone niet accuraat beschreven worden door de meest gangbare golftheorieën.

### III

Hoewel de hoogfrequente oscillaties de oscillerende waterbeweging en het aan de golven gerelateerde sediment transport domineren, kan de bijdrage van het laagfrequente deel niet verwaarloosd worden.

### IV

De ontwikkeling van de meest kustwaarts gelegen brandingsbank wordt niet altijd veroorzaakt door twee tegengestelde sediment transport vectoren maar kan eveneens het gevolg zijn van gradiënten in een landwaarts of een zeewaarts gericht sediment transport.

### V

Als het aankomt op de subtiële zelforganisatie van brandingsbanken, weten we alleen maar dat we ons bevinden in "the right ball park".

Stive, M.J.F., 1995. De Kust is vrij, Inaugurale reden, Faculteit der Civiele Techniek, Technische Universiteit Delft.

## VI

Geografisch onderzoek naar kustontwikkelingen is meer gebaat met onderzoek naar schaalproblematiek, dan met onderzoek dat poogt natuurlijke processen op een steeds gedetailleerdere fysische wijze te beschrijven.

Naar : Kwadijk , J.C.J., 1993. The impact of climate change on the discharge of the River Rhine, proefschrift Universiteit Utrecht, vakgroep Fysische Geografie.

## VII

In tegenstelling tot het achterland, is het aan de kust niet duidelijk welke bank men met *de* bank bedoelt.

## VIII

Modellen die gebruik maken van siliconen genereren meer turbulentie dan modellen die gebruik maken van silicaten.

## IX

Huisvrouwen zijn veelzijdig indien zij zowel email als Email gebruiken.

## X

Zowel de voor- als de tegenstanders van een nieuwe luchthaven in zee zullen waarschijnlijk het onderspit delven.

## XI

One does not discover new oceans without losing sight of the shore.

After: Andre Gide (French writer, 1869-1951)

“ And I tell you, if you have the desire for knowledge and the power to give it physical expression, go out and explore. If you are a brave man you will do nothing; if you are fearful you may do much, for none but cowards have need to prove their bravery. Some will tell you that you are mad, and nearly all will say, “What is the use?” For we are a nation of shopkeepers, and no shopkeeper will look at research which does not promise him a financial return within a year. And so you will sledge nearly alone, but those with whom you sledge will not be shopkeepers: that is worth a good deal. If you march your Winter Journeys you will have your reward, so long as all you want is a penguin’s egg. ”

Apsley Cherry Garrard - The Worst Journey in the World  
(First published by Penguin Books, 1922; reprinted by Picador, 1994)

For my parents:  
For offering me the opportunities  
to come this far





<b>CONTENTS</b>	
<b>FIGURES</b>	<b>14</b>
<b>PHOTOS</b>	<b>18</b>
<b>TABLES</b>	<b>19</b>
<b>APPENDICES</b>	<b>20</b>
<b>APPRECIATIONS AND ACKNOWLEDGEMENTS</b>	<b>21</b>
<b>1 INTRODUCTION</b>	<b>23</b>
1.1 Motives and scope of study	23
1.2 Outline of this thesis	26
<b>2. NEARSHORE BAR MORPHODYNAMICS - PREVIOUS RESEARCH AND DETAILED RESEARCH AIMS</b>	<b>27</b>
2.1 Introduction	27
2.2 Medium scale dynamics of nearshore bars	27
2.3 Mechanisms for the formation and development of nearshore bars	31
2.4 Hydrodynamic processes associated with the shoaling and breaking of high-frequency waves	37
2.5 Sediment transport processes associated with the formation and development of bars	40
2.6 Overview of hypothesis and research questions	43
<b>3 FIELD SITE AND DATA ACQUISITION</b>	<b>45</b>
3.1 Hydrodynamic setting	45
3.2 Morphological setting	47
3.3 Morphology of the field site	51
3.4 Measuring approach and observation periods	52
3.5 Hydrodynamic data acquisition	53
3.6 Sediment transport data acquisition	56
3.7 Morphologic data acquisition	61

4.	HYDRODYNAMICS OF BREAKING AND SHOALING WAVES	65
4.1	Introduction	65
4.2	Environmental conditions during measurements	65
4.3	Data validation and calibration	68
4.4	Analysis of wave hydrodynamics	69
4.4.1	Analysis and interpretation methods	69
4.4.2	Results and discussion	72
4.4.3	Conclusions	86
4.5	Analysis of the velocity field	86
4.5.1	Introduction	86
4.5.2	Analysis and interpretation methods	87
4.5.3	Results and discussion	90
4.5.4	Conclusions	113
4.6	Final discussion and conclusions	114
5.	INNER NEARSHORE SEDIMENT CONCENTRATIONS AND SEDIMENT FLUXES	117
5.1	Introduction	117
5.2	Data validation and calibration	118
5.3	Sediment concentrations	120
5.3.1	Analysis and interpretation methods	120
5.3.2	Results and discussion of instantaneous concentrations	122
5.3.3	Results and discussion of time-averaged concentrations	137
5.3.4	Conclusions	142
5.4	Instantaneous suspended sediment transport	143
5.4.1	Analysis and interpretation methods	143
5.4.2	Results and discussion	144
5.4.3	Conclusions	149
5.5	Depth integrated, time-averaged suspended sediment transport	149
5.5.1	Analysis and interpretation methods	149
5.5.2	Results and discussion	152
5.5.3	Conclusions	155
5.6	Bedload transport	156
5.6.1	Analysis and interpretation methods	156
5.6.2	Results and discussion	157
5.6.3	Conclusions	162
5.7	Total net sediment transport	
5.7.1	Ratio between suspended and bedload transport	162
5.7.2	Discussion	162
5.7.3	Conclusions	164
5.8	Sediment transport patterns in the inner nearshore zone	165
5.8.1	Introduction	165
5.8.2	Estimation of cross-shore sediment transport using relative wa height	166
5.8.3	Observations	168
5.8.4	Model computations	171
5.8.5	Conclusions	175
5.9	Final discussion and conclusions	175

6.	MORPHOLOGICAL DEVELOPMENTS AND MORPHODYNAMIC MODEL COMPUTATIONS	181
6.1	Introduction	181
6.2	Offshore wave conditions and initial cross-shore profiles	182
6.2.1	Single storm event (1991 data set)	182
6.2.2	Sequence of storms (1992 data set)	185
6.2.3	Initial profile characteristics 1991-1992	185
6.3	Cross-shore morphologic response of beach and shoreline	187
6.3.1	Response to a single storm (1991)	187
6.3.2	Response to a sequence of storms (1992)	189
6.4	Cross-shore morphologic response of the inner nearshore bar	193
6.4.1	Response to a single storm (1991)	193
6.4.2	Response to a sequence of storms (1992)	196
6.5	Cross-shore morphologic response of the outer nearshore bar	202
6.5.1	Response to a single storm (1991)	202
6.5.2	Response to a sequence of storms (1992)	203
6.6	Longshore variability of beach and outer nearshore response	204
6.7	Conclusions morphological behaviour nearshore zone	208
6.8	Morphodynamic computations in the nearshore zone	209
6.8.1	Introduction and methods	209
6.8.2	Model input	210
6.8.3	Hydrodynamic calculations	212
6.8.4	Morphodynamic calculations	217
6.9	Conclusions morphodynamic computations	228
6.10	Final discussion and conclusions	229
7.	SYNTHESIS	235
7.1	Introduction	235
7.2	Main results	235
7.3	Small and medium scale morphodynamic processes involved in the inner nearshore bar development	237
7.4	Development of the inner nearshore bar on a medium to large time scale	239
7.5	Final remarks and recommendations	241
	A SUMMARY	243
	SAMENVATTING	245
	REFERENCES	249
	APPENDICES	261
	CURRICULUM VITAE	267

## FIGURES

- 1.1 Morphodynamic system
- 2.1 Profiles showing the response of an inner bar during a storm and during the following recovery period
- 2.2 Bar formation and modification by plunging and spilling breakers
- 2.3 Bar formation as explained by the convergence of sediment.
- 2.4 Velocity vectors beneath a standing wave
- 3.1 Geographical location of field site
- 3.2 Offshore wave height distribution for three wave-period intervals (YM6 buoy, 1979-1991)
- 3.3 Average directional spreading of offshore wave field (YM6 buoy, 1979-1991)
- 3.4 Mean monthly offshore wave height (YM6 buoy, 1979-1991)
- 3.5 Nearshore morphology near Egmond aan Zee in 1967 and 1973
- 3.6 Cross-shore profile at Egmond aan Zee and morphological terminology
- 3.7a Field area showing data acquisition platforms and measuring transections
- 3.7b Cross-shore profile showing the location of measurements poles
- 3.8 Arrangement of the intake nozzles of the pump sampler and the OBSs on the BERT
- 3.9 Beach profiles surveyed
- 3.10 Field lay-out of Sub-Aquatic Profiler (SAP)
- 4.1 Offshore significant wave height during BERT measurements (October-November 1992)
- 4.2 Hydrodynamic zonation in the inner nearshore
- 4.3 Nearshore profile and beach profile with the range of cross-shore positions of the BERT
- 4.4 Relation between wave steepness, water depth and hydrodynamic conditions
- 4.5 Relation between relative wave height, water depth and hydrodynamic conditions
- 4.6 Relation between duration asymmetry and amplitude asymmetry
- 4.7 Example of wave profile shape
- 4.8 Application domain of various wave theories and position of measurements
- 4.9 Shape of wave profile, measured and theoretical
- 4.10 Wave frequency spectra of surface wave recordings
- 4.11 Relation between local wave height and low-frequency to high-frequency ratio of the surface wave height
- 4.12 Relation between offshore wave height and low-frequency wave height
- 4.13 Relation between onshore and offshore, significant, orbital peak velocities at 0.1 m above the bed
- 4.14 Relation between relative wave height and onshore, significant, peak velocities at 0.1 m above the bed
- 4.15 Relation between mean velocities at 0.1 m above the bed and breaker type for the different hydrodynamic zones
- 4.16 Relation between measured undertow and predicted undertow according to Svendsen (1984), Stive and Wind (1986) and Van Rijn (1990)
- 4.17 Relation between amplitude asymmetry of the velocity at 0.1 m above the bed and breaker type
- 4.18 Relation between duration asymmetry of the velocity at 0.1 m above the bed and breaker type
- 4.19 Relation between relative wave height and amplitude asymmetry of the velocity at 0.1 m above the bed
- 4.20 Relation between percentage of breaking waves and amplitude asymmetry of the velocity at 0.1 m above the bed



- 4.21 Relation between percentage of breaking waves and duration asymmetry of the velocity at 0.1 m above the bed
- 4.22 Examples of frequency spectra of near bed velocities
- 4.23 Relation between relative wave height and significant, low-frequency, orbital peak velocity at 0.1 m above the bed
- 4.24 Relation between duration asymmetry of the waves and duration asymmetry of the velocity at 0.1 m above the bed
- 4.25 Examples of orbital velocity profile of the velocity at 0.1 m above the bed
- 4.26 Wave profile and orbital velocity profile of near-bed velocity
- 4.27 Shape of orbital velocity profile, measured and theoretical
- 4.28 Relation between measured and theoretical significant, onshore, orbital peak velocity at 0.1 m above the bed
- 4.29 Relation between the ratio measured to theoretical, significant, onshore peak velocity at 0.1 m above the bed and the relative wave height
- 4.30 Relation between measured and theoretical, significant, offshore, orbital peak velocity at 0.1 m above the bed
- 4.31 Relation between measured and theoretical amplitude asymmetry of the velocity at 0.1 m above the bed
- 4.32 Relation between mean, cross-shore velocity at 0.1 m and at 0.3 m above the bed
  
- 5.1 Calibration tank for the optical backscatter sensors
- 5.2 Time series of velocity and concentration at the lowest OBS level (0.07 m above the bed) in various hydrodynamic zones
- 5.3 Time series of velocity and concentration at the lowest OBS level (0.07 m above the bed) in (non-) breaking zone
- 5.4 Velocity spectra and concentration spectra of lowest OBS (0.07 m above the bed)
- 5.5 Cross-spectra and squared coherence of lowest OBS (0.07 m above the bed)
- 5.6 Time-series of velocity and concentration of EMF and OBS at 0.07, 0.12, 0.17 and 0.26 m above the bed of series 2310-5 (breaking conditions)
- 5.7 Correlation between suspended sediment concentration at 0.07 and 0.12 m and between suspended sediment concentration at 0.07 and 0.26 m
- 5.8 Concentration and cross-spectra at upper OBS level (0.26 m above the bed) and lowest OBS (0.07 m above the bed)
- 5.9 Examples of sediment concentration profiles, measured and theoretical
- 5.10 Influence of current- and wave-related bed roughness on computed suspended-sediment profiles
- 5.11 Effect on using different factors for estimating the  $D_{50}$  of the suspended sediment from the  $D_{50}$  of the bed sediment
- 5.12 Mean grain size ( $D_{50}$ ) of the bedload sediment and of the suspended sediment as a function of the elevation above the bed
- 5.13 Explication of advective sediment transport
- 5.14 Relation between relative wave height and concentration at 0.06 m and at 0.6 m above the bed
- 5.15 Relation between net, mean, and oscillating suspended sediment fluxes in the cross-shore direction at 0.17 m above the bed and the relative wave height
- 5.16 Relation between low-frequency and high-frequency oscillating suspended sediment fluxes in the cross-shore direction at 0.17 m above the bed and the relative wave height
- 5.17 Vertical distribution of cross-shore suspended sediment transport modes
- 5.18 Vertical distribution of longshore suspended sediment transport modes
- 5.19 Example of computed concentration profiles, velocity profiles and the resulting suspended sediment transport profiles
- 5.20 Relation between relative wave height and depth-integrated, suspended-sediment transport in the cross-shore direction



- 5.21 Relation between depth-averaged cross-shore mean current at 0.1 m above the bed and depth-integrated, suspended-sediment transport in the cross-shore direction
- 5.22 Relation between measured and computed depth-integrated, suspended-sediment transport in the cross-shore direction
- 5.23 Relation between cross-shore and longshore depth-integrated, time-averaged, suspended-sediment transport
- 5.24 Relation between relative wave height and net, cross-shore, bedload transport
- 5.25 Relation between significant, onshore, orbital peak velocity and onshore bedload transport
- 5.26 Relation between mean cross-shore velocity at 0.1 m and offshore bedload transport
- 5.27 Relation between mean cross-shore velocity at 0.1 m and net bedload transport in the cross-shore direction
- 5.28 Relation between the ratio onshore, significant, orbital peak velocity to mean velocity, and net bedload transport in the cross-shore direction
- 5.29 Relation between measured and computed (TRANSPOR model) bedload transport
- 5.30 Relation between measured bedload and suspended sediment transport and diameter of the sediment ( $D_{50}$ )
- 5.31 Relation between the relative wave height and total, cross-shore, sediment transport
- 5.32 Relation between the measured and computed (TRANSPOR model) total, cross-shore, sediment transport
- 5.33 Relation between relative wave height and mean suspended sediment transport, oscillating suspended sediment transport, bedload transport and fitted curves
- 5.34 Relation between suspended sediment transport and relative wave height for different sediment transport modes
- 5.35 Sediment transport direction in the inner nearshore during 1991 storm
- 5.36 Measured nearshore profiles and calculated hydrodynamics and sediment transport on 3 October 1992
- 5.37 Measured nearshore profiles and calculated hydrodynamics and sediment transport on 9 October 1992
- 5.38 Sediment transport and sediment transport gradients at the inner nearshore bar during four different offshore wave height ranges
- 5.39 Spatial distribution of suspended sediment transport modes around a breakpoint
- 5.40 Spatial distribution around a breakpoint of the total sediment transport
  
- 6.1 Definition sketch of morphometric bar properties
- 6.2 Offshore hydrodynamics and morphologic surveys in 1991
- 6.3 Offshore hydrodynamics and morphologic surveys in 1992
- 6.4 Nearshore profile at the start of the field measurements in 1991 and 1992
- 6.5 Beach profile response of profile 39.500 in 1991
- 6.6 Position shoreline in 1991 (profile 39.500)
- 6.7 Location of the shoreline at 39.500 profile in 1992
- 6.8 Beach profile response at profile 39.500 in 1992
- 6.9 Relation between location of the crest and of the trough of the inter-tidal bar (1992 data)
- 6.10 Morphologic response of the inner nearshore zone (SAP profile) in 1991
- 6.11 Relation between location and the elevation of the crest of the inner nearshore bar in 1991
- 6.12 Morphologic response of the inner nearshore zone (SAP profile) in 1992
- 6.13 The elevation and location of the crest of the inner nearshore bar at SAP profile as a function of time (1992 data)
- 6.14 Relation between location and the elevation of the crest of the inner nearshore bar in 1992
- 6.15 Relation between the location and the landward slope of the inner nearshore bar in 1992

- 6.16 Outer nearshore zone development in 1991 (profile 39.500)
- 6.17 Outer nearshore zone development in 1992 (profile 39.500)
- 6.18 Variation in response of the shoreline along the field site in 1992
- 6.19 Total beach volume and volumetric changes between 1 October and 9 November 1992 in 9 profiles along the field site
- 6.20 Response of the outer nearshore bar along the field site in 1992
- 6.21 Cross-shore profile and computed (UNIBEST-TC model) and measured wave height in the nearshore zone on 16 October 1991
- 6.22 Cross-shore profile and computed (UNIBEST-TC model) and measured wave height in the nearshore zone on 3 November 1991
- 6.23 Influence of varying breaker coefficient on predicted wave height at pole 2 at inner nearshore bar (data of 16 October 1991)
- 6.24 computed (UNIBEST-TC model) and measured mean cross-shore velocity at frame on outer nearshore bar and at pole 2 at inner nearshore bar (data of 16 October 1991)
- 6.25 Computed (UNIBEST-TC model) and measured profile development 3 - 7 October 1992
- 6.26 Computed (UNIBEST-TC model) and measured profile development 9 - 13 October 1992
- 6.27 Computed (UNIBEST-TC model) and measured profile development 15 - 26 October 1992
- 6.28 Computed (UNIBEST-TC model) profiles at the end of run 1 (7 Oct.), at the end of run 2 (13 Oct.) and at the end of run 3 (26 Oct.)
- 6.29 Measured and computed (UNIBEST-TC model) profiles of first (3 - 7 October 1992) and second run (9 - 13 October 1992); computed profiles computed with breaking wave delay
- 6.30 Relation between location of the shoreline and location of the crest of the inner nearshore bar in 1992
- 6.31 The location of the trough of the inner nearshore bar at SAP profile as function of time in 1992
- 6.32 Position of the crest of the inner nearshore bar and suggested dynamic equilibrium
- 7.1 Sediment transport vectors and the resulting morphologic development of the shoreline and inner nearshore bar during non-storm and storm-periods in the autumn and winter

## PHOTOS

- 3.1 Beach-based Electronic Registration Tower (BERT)
- 3.2 Bedload sampler as used in the field
- 3.3 Sub-Aquatic Profiler (SAP) positioned in front of Tractor with winch.

## TABLES

- 2.1 Bar migration characteristics during various field experiments at Duck
  
- 3.1 Grain size distribution of beach and surf zone
- 3.2 Locations of hydrodynamic data sampling
- 3.3 Sampling characteristics of hydrodynamic data acquisition
- 3.4 Sampling characteristics of sediment transport data acquisition
  
- 4.1 Daily averaged D50 values bottom samples near the BERT
- 4.2 Calibration coefficients EMF (BERT)
- 4.3 Hydrodynamic conditions from inner nearshore measurements
- 4.4 Wave asymmetry
- 4.5 Wave height and -period in different frequency domains
- 4.6 Mean velocities, significant orbital peak velocities and velocity asymmetries at 0.1 m above the bed
- 4.7 Cross-shore peak velocities (high-frequency/low-frequency) at 0.1 m above the bed
- 4.8 Mean velocities, significant peak velocities and velocity asymmetries at 0.1, 0.3 and 0.7 m above the bed in cross-shore direction
  
- 5.1 Hydrodynamic conditions and time-averaged concentrations
- 5.2 Hydrodynamic conditions and suspended transport modes at 0.17 m above the bed
- 5.3 Hydrodynamic conditions, time-averaged suspended transport and bedload transport
  
- 6.1 Offshore wave characteristics in 1991
- 6.2 Storm characteristics in 1992
- 6.3 Morphologic characteristics nearshore bars in 1991 and 1992
- 6.4 Descriptive statistics of the inner nearshore bar 1991
- 6.5 Descriptive statistics of the inner nearshore bar 1992

## APPENDICES

- A. Short description of UNIBEST-TC model
- B. Model parameters UNIBEST-TC model



## APPRECIATIONS AND ACKNOWLEDGEMENTS

Whilst walking on a Dutch beach in the spring of 1985 we suddenly found ourselves in front of what I now would call a 'drain-rip'. Sand grains were moved down the beach by flowing water. Someone asked me, believing that a future hydrographer should know the answer, *why* does a storm move sand to the sea? I did not know. Shortly before writing this part of my thesis I remembered this event and realised that this question and other questions about the dynamics of nature have provided me with the necessary inspiration to carry out this study. I believe it is essential that people around you are asking such questions because they force you to discuss these matters and keep the inspiration alive. So, let me begin by thanking those people without whom this thesis would not have been possible.

I would like to thank my 'promoters': prof. dr. Joost Terwindt and prof. dr. ir. Leo van Rijn. Joost for giving me the freedom to follow my own, winding path and Leo for all discussions about the hydrodynamics, the sediment-transport and the morphology. Moreover, I would like to thank Leo for frankly sharing his views about planning a Ph.D. study (*'dat lukt je nooit'*). I also like to show my sincere appreciation to my 'co-promotor' dr. Piet Hoekstra who scrutinised and structured this thesis in the very detail and made sure that I had the best working conditions possible.

Several departments and people from *Rijkswaterstaat* offered their help and skills to make every field campaign a success. Thanks are due to the National Institute for Coastal and Marine Management (RIKZ) for providing the financial means to carry out this study. Drs. Pieter van Vessem and dr. Jan Mulder of the RIKZ are thanked for handling many logistic matters. The North-Holland Directorate of *Rijkswaterstaat* assisted during all field experiments. I highly appreciate their help and technical knowledge. Ing. Jan Visser, ing. Jeroen van der Kuijp, Paul Dekker, Peter van den Boogaard, Lück Overmars, André Jansen, Chris Roosendaal, trainees and the crews of the research vessels are thanked for doing numerous jobs for me under often unfavourable weather conditions. I would also like to thank the Geosurvey department of *Rijkswaterstaat*, section marine and terrestrial surveys, in Delft and Nieuwegein for providing and operating several total stations. I owe a very special thanks to Tjip Vonk. He made, together with his wife Nel, every field campaign a valuable and enjoyable experience. Besides, he introduced me to Mart Gul and his beach crew who also offered irreplaceable technical assistance.

The laboratory of physical geography of the Utrecht University, section electronics, is thanked for designing, building, installing and servicing the electronics for the Sub-Aquatic Profiler (SAP) and the Beach based Electronic Registration Tower (BERT). Theo Tiemissen, Bas van Dam, Marcel van Maarsenveen, Jaap van Barneveld and others are thanked for sharing their technical knowledge and for their fine craftsmanship. I highly appreciate that they always showed their interest about the measurements, even during their own vacations and during stormy Sundays. 'Pak' Theo Tiemissen is also thanked for taking care of many logistic and financial matters.

A number of former undergraduate students offered me more than just 'a helping hand' during the field experiments. In 1991, Klaas Houwman, Jaap Goudriaan, Arjan van der Weck, Janneke van Oort assisted during the day while Tjeerd Nijeholt was busy during day and night. Yolanda Onneweer, Fred Tank, Willem van der Lee,



Gert de Vaan and Lucas Meursing are thanked for their help during the 1992 field experiments.

The analysis of all field data was a job that would still be foregoing without the help of Willem van der Lee and Ruud Klein. They did a large number, often unpleasant, computer jobs for me. Killian Hekhuis did a lot of computer programming in the early stage of the research.

I am most grateful to my (former) colleagues at the department of Physical Geography of the Utrecht University who contributed much to this thesis and created the enjoyable atmosphere at the department. Very special thanks to my trailblazer dr. A. Kroon. Aart, thanks for your humour (*das ist das Man trotzdem Alles lacht*). Also thanks to my former roommate Ad Stolk who showed an everlasting interest in every aspect of my research. I had many fruitful but loud discussions with my part-time roommate Kathelijne Wijnberg (sorry neighbours!). I sincerely like to thank her for the very pleasing and optimal sharing of the room and especially of the 'Mac'. Klaas Houwman and Gerben Ruessink generously provided me with loads of computer programs and knowledge about 'their' Terschelling measurements. Eric-Jan Houwing en Claus Kruyt learned me practical jokes and the right fieldwork attitude. Jan van de Meene and Claire Jeuken proved that you do not have to walk the polonaise to have a great wedding-party. The muddy boys Willem van der Lee, Wilfried ten Brinke and Bart Kornman are thanked for the entertaining stories about the operational aspects of their cohesive sediment studies. Pieter Augustinus helped me with financial and logistic matters. Alfred Coerts is thanked for the rapid clearing of my desk when I came in and for tapping beer at 5:30 am at my M.Sc. party. All other (former) colleagues, especially those of the coastal section and the 'gruppo fluvial', are thanked for continuously showing me that physical geography is more than several random walking sand grains near Egmond. And not in the last place, I like to thank Celia Roovers for her eternal smile and for correcting series of signs of which I thought that it represented something logically.

My friends encouraged me, made me laugh, invited me for great meals and, above all, did me realise that one should never write a thesis without beer and sports. I sincerely like to thank them and hope that our friendship will continue in the future. I especially would like to thank: Willem-'racket van de maand'-Pieter with whom I played many squash games; Iris for her love, her friendship and for giving me so much 'joie de vivre' (*tof !*); José who gave me moral support and talked with me about the facts of life; Jeroen and Ilja who invited me for many dinners and parties which always passed in a homely atmosphere; Bart, Karel and Yde who are friends for life; Celia, Aart and Rogier who improved my *parallel-swung* ('*aah, 's goud*'); Jan, Wilfried and Aart for the Sunday-evening discussions, mainly about the looks of waitresses; and Jacqueline for asking me to join her on a holiday at the time when I needed it most.

Dit proefschrift zou er nooit zijn gekomen zonder mijn Vader en Moeder, mijn broers Otto en Marco en bijna zwager Willem, mijn (schoon)zussen Regina, Petra, Cecile en Angela en mijn nichtjes Mayke, Lisanne en Veerle. Hun interesse, hun ondersteuning en het plezier dat zij mij gedurende de afgelopen jaren gaven waren onmisbaar. Bedankt!

Felix Wolf  
Utrecht, September 1997

## 1. INTRODUCTION

### 1.1 Motives and scope of study

To prevent the Netherlands from flooding, the Dutch have always found solutions for problems caused by the sea. The earliest man-made changes along the coast of the Netherlands were the construction of groins, jetties and seawalls. Groins were designed to trap sediment moving alongshore. Jetties were built to constrain the flow of water at inlets. However, these construction works also affect wave refraction, wave breaking and surf zone circulation. In addition, they can interrupt bar-beach systems (Short, 1992). Finally, seawalls often induce slow and accelerated erosion and a resulting reduction of beach width.

It is because of these undesired effects and the increasing significance of the coastal areas for ecology, economy, culture and recreation, that the scale and types of shore protection have changed in recent decades. Instead of large, 'hard' coastal protection works, current engineering solutions to combat coastal erosion are custom made and 'soft'. Nowadays, sand nourishment is, in the Netherlands, a common measure to combat coastal erosion. The result is a temporarily widened (upper) beach with a shape and sediment composition often out of equilibrium with the natural processes.

In spite of all the measures taken, parts of the Dutch coast are still subject to erosion. Thus coastal protection works will still be needed in the future. Despite the shift towards more 'natural' ('soft') protection works, their effect on coastal behaviour, i.e. the morphologic development of the shoreface, surf zone, beach and dunes, is still hard to assess. It is especially difficult to predict the coastal developments along time scales of years and decades, and to improve coastal management i.e. to reduce the negative effects of protection works, because not enough is understood about the physical processes involved in coastal development. Even the development of cross-shore profiles along time scales of days are hardly understood. To this end a multi-disciplinary research programme was initiated in 1985. This programme, entitled 'Coastal Genesis', and the follow-up research programme ('Coast 2000') should extend the knowledge of physical processes, increase the capabilities of process-orientated models and by doing so predict future coastal developments to make efficient management of the coastal zone possible. The study described in this thesis is part of both research programmes.

The physical processes in the coastal system may be broadly subdivided into two types, hydrodynamic and morphodynamic. The differences between hydrodynamic and morphodynamic processes lie in the direction of the process. Hydrodynamic processes involve the effect of an external force on water motion. These processes are related to fluid mechanics (e.g. wave propagation). Morphodynamic processes are the mutual, and often non-linear, interactions between hydrodynamic forces and morphology, and involve the motion of sediment. In a morphodynamic system like the coast, hydrodynamics induce a sediment transport and a net sediment transport is reflected in a change of the morphology. This changed morphology influences and interacts again with the hydrodynamics. The result will be another net sediment transport and a further adaptation of the morphology to the changed conditions (Fig. 1.1). It is these morphodynamic processes which are responsible for the coastal development. Knowledge of how present morphodynamic processes operate, and



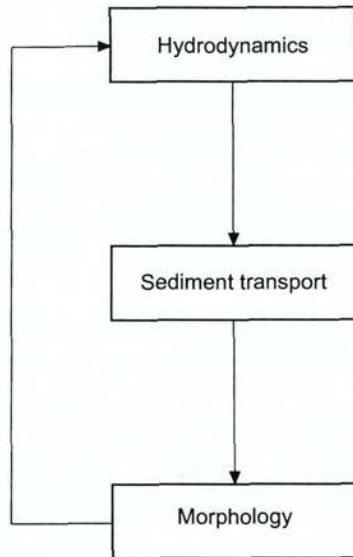


Figure 1.1 Morphodynamic system

how their present rates vary in time and space, is, therefore, essential to improve the understanding of coastal development.

Morphodynamic processes in the coastal zone vary both cross-shore and alongshore, i.e. are three-dimensional. Longshore variations occur when, e.g., the coast is interrupted by groins, or when the nearshore morphology shows alongshore variations. As will be shown in Chapter 3 (field site), there are no man-made structures near the field site and large morphological gradients are only noticeable over larger (more than 1 kilometre) distances. Thus, it is assumed that the cross-shore processes govern the morphodynamics of the beach and nearshore zone (cf. Short, 1979; Greenwood, 1987; Kraus and Horikawa, 1990). Three-dimensional monitoring of morphodynamic processes requires a large number of (specific) instruments, equipment, personnel and involves high costs. Financial and logistic support were, however, limited. So, also from a practical point of view, a three-dimensional monitoring of the morphodynamic processes was not possible. The emphasis in this study is on *cross-shore* morphodynamic processes and field measurements, therefore, were executed along cross-shore profiles.

Nearshore breaker bars are prominent features in coastal profiles along the Dutch coast and in coastal environments elsewhere. These bars are often not static features, but migrate and are reformed under the influence of the varying tidal- and wave conditions, i.e. they may receive, store and feed large quantities of sediment from and to adjacent areas (e.g. Allen and Psuty, 1985; Wijnberg, 1995). Nearshore bars also filter or reflect the incoming waves and thereby influence the development of the zone landward from the bar, e.g. a beach may be sheltered from the fully impact

of storm waves (e.g. Takeda and Sunamura, 1992). Finally, bars also determine the cross-shore distribution of the longshore current. Hence, nearshore bars may in three ways be significant for development of an entire coastal profile. A better understanding of nearshore breaker bar developments may, therefore, result in a improved understanding of the behaviour of cross-shore profiles and of three-dimensional developments.

Kroon (1994) studied the morphodynamic behaviour of a swash bar and two nearshore breaker bars at Egmond aan Zee. The results of his study revealed the morphodynamics of the beach on time-scales from days to weeks and the development of the cross-shore profile from years to decades. Due to a lack of suitable equipment, the morphodynamics of the surf zone on time scales from days to weeks were not thoroughly investigated. Especially unclear was the behaviour of the inner nearshore bar and the processes leading to this behaviour. The aim of this study which is a continuation of Kroon's study is, therefore, to examine the inner nearshore bar developments at Egmond aan Zee.

Studies aiming at a better understanding of nearshore morphodynamics, must, inevitably, limit their objectives to a certain spatial and temporal scale. One is forced to choose a scale of investigation, because an independent causal variable at a certain level may appear as a dependent effect on another level of study (de Boer, 1992). Moreover, individual processes may take a different course within particular time intervals (Renwick, 1992; Larson and Kraus, 1995). For instance, hydraulic movements react almost instantaneously to changes in the morphology, whereas morphological changes in response to variations in the water movement occur more slowly. In this thesis, the morphodynamic analysis is performed on two scales, the medium and the small scale. Here, small scale refers to processes acting on a range from centimetres to metres and from seconds to hours. Medium scale processes are operating over a range from metres to a kilometre and over days to weeks. Finally, processes acting over months and over kilometres are, classified as acting on a large-scale. The medium scale represents geomorphological processes such as the development and transformation of bars over tens of metres and over weeks to months, the small scale represents fluid processes and sediment transport in response to fluctuations in energy level over centimetres and from seconds to minutes. Hence, the focus of this thesis is not on the statistical observational approaches, e.g. to reveal the position of inner bars in a 'beach state' model (cf. Wright and Short, 1984; Lippmann and Holman, 1990), but instead a more deterministic approach is adopted by understanding the inner nearshore bar as a sediment response to particular aspects of the small-scale water motions.

Laboratory and field experiments have emphasised the complexities of the processes influencing the formation and development of nearshore bars and suggest that no single mechanism can explain the range of morphological and sediment transport patterns observed. It is increasingly evident that the importance of any mechanism varies temporally (e.g. between storm and non-storm conditions), spatially (e.g. alongshore and cross-shore) and with the geographical location. The latter determines e.g. the sediment size, the nearshore slope and the offshore wave climate. From all possible mechanisms explaining inner nearshore bar behaviour, this study focuses on processes related to the shoaling and breaking of wind-waves. These processes are believed to be the main agent steering the behaviour of nearshore bars. Hence, the more specific aim of this study is to examine to what extent inner nearshore bar



development relates to the hydrodynamics and sediment transports associated with the shoaling and breaking of wind-waves. A detailed elaboration of the research aims is given in the next chapter.

## **1.2 Outline of this thesis**

The outline of this thesis is as follows:

Chapter 2 reviews previous research regarding the formation and development of breaker bars and the nearshore hydrodynamics and sediment transport involved. The chapter defines the research topics addressed by this study

Chapter 3 starts with a description of the temporal and spatial characteristics of the field site. The temporal aspect involves a description of the morphological developments over recent decades; the spatial element involves a description of the Holland coast. Field data is essential for studying inner nearshore bar behaviour and many instruments are needed to measure the hydrodynamics, the sediment transport and the morphological development. The measuring approach, the instruments and the instrumental arrangement that were used to collect the field data are also presented in Chapter 3.

Chapter 4 is a study of the hydrodynamics of wind waves, the aim of which is to determine the relevant processes involved in the shoaling and breaking of these waves. The velocity field induced by these waves is also studied.

Chapter 5 is an analysis of the nearshore sediment transport, the aim of which is to determine the modes, magnitude and direction of the nearshore sediment transport and to relate these to the observed hydrodynamics. Chapter 5 also studies the sediment transport patterns acting on a medium scale that may have caused the observed morphological developments

Chapter 6 first reveals the morphological behaviour of the nearshore bars under changing hydrodynamic conditions. Thereafter, it is studied whether the observed hydrodynamics, sediment transport and morphological developments can be simulated using a physical-mathematical model.

Chapter 7 is a synthesis of this study.

## 2. NEARSHORE BAR MORPHODYNAMICS - PREVIOUS RESEARCH AND DETAILED RESEARCH AIMS

### 2.1 Introduction

To position this study within morphodynamic research, a literature review is first presented. Previous studies that analysed the morphodynamics of coastal breaker bars have led to four important groups of theories regarding nearshore breaker bar formation and behaviour. All theories will be discussed, together with their advantages and objections. Next, a review of the most important hydrodynamic phenomena in the surf zone is given. Third, the sediment transport in the surf zone is explained. As this study is a continuation of Kroon's study (1994), frequent reference will be made to his work to explain the starting points of this present study.

### 2.2 Medium-scale dynamics of nearshore bars

A nearshore breaker bar can be described as a submerged or emerged accumulation of sand, or other unconsolidated material, more or less parallel to the coast and built in shallow water by waves and currents. Bars may occur singly or as a series of such features. The Egmond aan Zee field site incorporates two nearshore bars: an inner nearshore bar and an outer nearshore bar. As several researchers (e.g. Goldsmith et al., 1982; Short and Aagaard, 1993; Kroon, 1994) clearly showed, inner and outer nearshore bars have different length scales and inner nearshore bars seem to be more mobile than outer ones (Kroon, 1994; Ruessink and Kroon, 1994); outer nearshore bars tend to migrate only during periods of severe storms (Birkemeier, 1984; Aagaard, 1990; Kroon, 1994). The variation in the response of nearshore bars is likely the result of a cross-shore variation in the relative wave height ( $H_b/h$ ). As a result, the inner nearshore bar is more frequently located in the breaker zone and the changes take place on a smaller time scale than the outer bar. Thus, outer and inner nearshore bars show different behaviour and are studied separately in the remainder of this section.

The most comprehensive data set regarding nearshore bar development on medium scales has been collected at the Coastal Engineering Research Center's Field Research Facility at Duck, North Carolina, USA. The results for different experiments are summarised in Table 2.1. Mason et al. (1984) and Sallenger et al. (1985) studied the behaviour of a cross-shore profile during two succeeding storms at the Duck field site. The maximum significant wave heights and maximum spectral peak ( $T_p$ ) wave periods during these storms were 2 and 4 m and 15 and 12 s, respectively. Before the first storm, nearshore morphology was characterised by a well-developed berm and a relatively small nearshore bar (Fig. 2.1). The bar height was about 0.3 m and the bar was positioned only 13 m offshore. The first storm eroded the berm and moved the bar 57 m offshore while migration rates of  $2.2 \text{ m hr}^{-1}$  ( $\sim 53 \text{ m day}^{-1}$ ) were measured. After the peak of the first storm, the bar became crescentic while the bar also moved along the shore. This resulted in large alongshore differences in migration direction. For instance, the bar showed an apparent landward migration of 36 m at the main survey line while 69 m northward of this line the bar migrated 18 m offshore. These developments occurred very rapidly (onshore migration rates of  $0.5 - 1.2 \text{ m hr}^{-1}$   $\sim 12 - 29 \text{ m day}^{-1}$ ) even though wave energy was decreasing. An outer bar emerged at a



distance of 350 m during the first storm. During the second storm, the outer bar became better developed and migrated offshore.

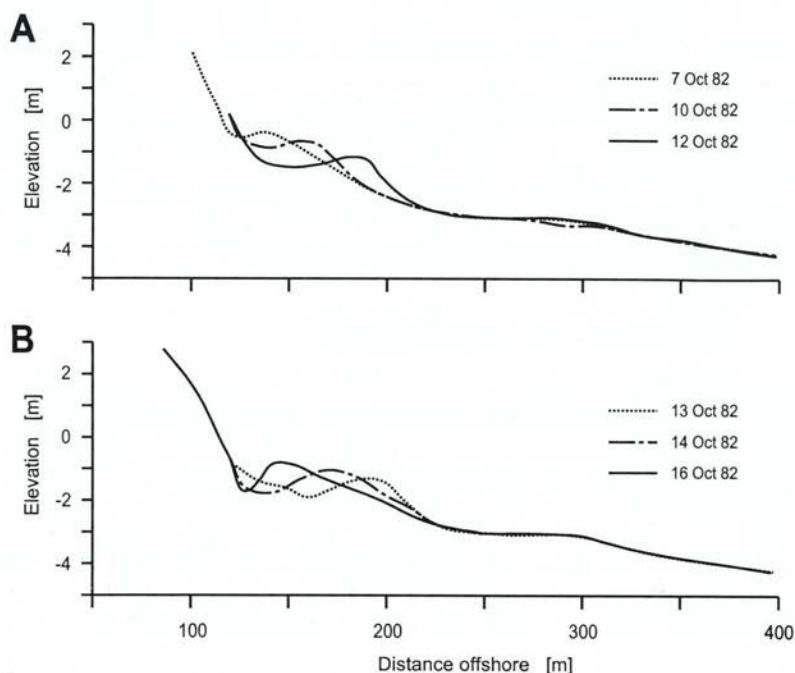


Figure 2.1 Profiles showing the response of an inner bar during (A) a storm and (B) during the following recovery period. Distance seaward is relative to a baseline approximately 110 m landward of MSL (after Sallenger et al., 1985).

Table 2.1 Bar migration characteristics during various field experiments at Duck

Reference	Year	Storm Characteristi c	Height bar [m]	Depth above bar crest [m]	Onshore migr. speed [m day <sup>-1</sup> ]	Offshore migr. speed [m day <sup>-1</sup> ]
Mason et al. (Duck82)	1984	$H_{\text{peak}} = 2.2 \text{ m}$ $T_{\text{peak}} = 17 \text{ s}$	0.3 1.1	0 1.8	12 - 29	17 - 53
Birkemeier	1984	$H_{\text{peak}} = 3.5 \text{ m}$	1	2.0		>30
Howd and Birke- meier (Duck85)	1987	$H_{\text{peak}} = 2 \text{ m}$	0.7	1.0		50 (max.)
Larson and Kraus	1992a, 1992b		0.9 0.4	1.6 3.8	1.5 0.6	2.9 1.1

The dynamics of an inner and outer bar during storms and quiet weather periods over a 3.5 year period at the Duck field site was reported by Birkemeier (1984). Minor storms resulted in an offshore movement of the inner bar (height of 0.3 - 2 m, depth of 0.6 to 1.5 m) while during larger storms both the inner and outer (height of 0.3 - 1.2 m, depth of 3-4 m) nearshore bar moved offshore. The storm induced changes occurred rapidly, over periods of one to five days. Onshore bar movement which occurred during periods of low waves was affected by the post-storm wave conditions and the post-storm configuration of the profile. During storms offshore migration rates were measured as high as  $30 \text{ m day}^{-1}$  for the inner bar while during calm conditions the onshore migration rates were as low as  $0.5 \text{ m day}^{-1}$  for the outer bar.

Howd and Birkemeier (1987) studied the storm-induced morphological changes during the Duck85 experiment (see also Mason et al., 1987). This experiment largely confirmed the earlier findings at the Duck field site. It became clear that the initial response of the nearshore is the formation of a linear sand bar which migrates offshore to a distance of 60-80 m. This offshore migration was rapid during the Duck85 experiment, with the bar crest moving seaward at rates up to  $2.1 \text{ m hr}^{-1}$  ( $\sim 50 \text{ m day}^{-1}$ ). Surveys done the day after the peak in incident wave energy show the bar becoming crescentic.

Larson and Kraus (1992a, 1992b) analysed surveys (1981-1989, with bi-weekly intervals) from the Duck field site. The average migration speed for the outer bar was about one-third of that of the inner bar but this was due to the effect that the inner nearshore bar is more frequently subject to wave breaking than the outer nearshore bar. These speeds were determined assuming that the movement is constant between two surveys. However, because bar movement in general is rapid (e.g. Sallenger et al., 1985) and often is associated with storms, this method underestimates migration speeds. Thus the calculated speed of the bars during onshore movement is a better estimation than that of the offshore movement of the bars. Regression relationships were derived for some combinations of (inner and outer) bar and deep water wave properties but the coefficients and regression analyses were mostly of qualitative nature. These low regression coefficients are due to the large average spacing in time between two surveys (10 days) and due to the variation of the wave height within this period. In addition, the migration of longshore bars is not only a function of the wave characteristics but also of other factors such as the water level variations, the location and shape of the bars and the duration of a given set of conditions.

Lippmann and Holman (1990) and Lippmann et al. (1993) studied the behaviour of the nearshore zone at Duck on a daily basis and for a number of years using the video method of Lippmann and Holman (1989). They found that linear bars occur under the highest wave conditions but are unstable (mean residence time  $\sim 2$  days) while shore-attached rhythmic bars are most stable (mean residence time  $\sim 11$  days) and generally form 5-6 days following peak wave events. Changes in incident wave height preceded cross-shore bar migration by less than 1 day. Offshore bar movement was found to be more determined by the incident wave height than by the preceding morphology but for onshore migration bars the preceding morphology is more important. The influence of extreme events ( $H_{s, \text{ offshore}} > 3 \text{ m}$  for more than 6 h) depended heavily on the presence of an outer nearshore bar and usually resulted in both immediate alterations to the cross-shore profile and subsequent monthly



averaged bar migration. Without the presence of an outer bar, the inner nearshore bar migrated further seaward, than when a well-defined outer bar existed.

Research at field sites in Canada (e.g. Greenwood and Davidson-Arnott, 1975; 1979; Greenwood and Osborne, 1991), in Australia (e.g. Wright and Short, 1984), in Denmark (e.g. Aagaard, 1991), in Ireland (e.g. Carter and Kitcher, 1979) and in the Netherlands (e.g. Kroon, 1994; Ruessink and Kroon, 1994) largely confirm the above observations regarding nearshore bar behaviour although the time spacing between two succeeding surveys during these experiments was often larger than at Duck. Orme (1985) presented onshore migration rates of longshore bars observed at the coast of Japan ( $2 - 5 \text{ m day}^{-1}$ ), Quebec ( $0.8 - 10 \text{ m day}^{-1}$ ), Oregon ( $1 - 5 \text{ m day}^{-1}$ ) and California ( $9 - 30 \text{ m day}^{-1}$ ) of which the latter rates were comparable with the rates observed at Duck. The lower rates are, apart from different environmental conditions (e.g. size of the bar), also due to large intervals between two succeeding surveys. In this interval, bars may be arrested for longer times (e.g. Aagaard, 1988) despite the occurrence of storms (Davidson-Arnott, 1981, 1989). Carter and Kitcher (1979) studied the influence of the tide on bar formation and migration and found that during lower waves and an increasing tidal range, bars moved quickly onshore. Others (e.g. Dhyr-Nielsen and Sørensen, 1970; Sunamura and Takeda, 1993) stated that a large tidal range hinders the formation of bars because the break point is rapidly changing with the tidal cycle. Takeda and Sunamura (1992) studied the relation between the position of nearshore bars and the amount of beach erosion. They found that the beach is not likely to be eroded by storm waves when an inner bar is present in the nearshore zone and/or an outer bar is closer to the shoreline. During storm-wave attack the eroded beach sediment is transported and contributes to the bar development. Hence, the location of a nearshore bar relative to the beach may determine its own development. The influence of the nature of the offshore wave field on the existence and development of bars was mentioned by Guillén and Palanques (1993). Sea-dominated coasts (e.g. the Dutch coast) have often a higher number of bars than swell-dominated coasts (e.g. the Australian coast). Moreover, the influence of the preceding morphology on the development of bars is lower at sea-dominated coasts than at swell-dominated coasts (Guillén and Palanques, 1993). Other factors affecting nearshore bar development are grain size (e.g. Short, 1986) and nearshore slope (e.g. Hayes, 1972).

In summary, nearshore bars have a certain number of universal characteristics but their appearance and behaviour varies depending on the environmental setting. Outer bars are often linear while inner bars are more rhythmic. Bars may be very dynamic, migrating seawards during storms and landwards during low wave conditions but bars may also be arrested in place. Whether a bar moves or not, the direction of the bar movement and the rate of migration may depend on the nature of the offshore wave conditions (e.g. wave height, duration), on the distance of the bar from the shore, on the size of the bar, on the sediment size, on the nearshore gradient and on the tidal range. Antecedent wave conditions, which are incorporated in the preceding profile may also play an important role in the nearshore bar development. All these variable bar characteristics and developments have lead to several hypotheses for nearshore bar formation and development. These theories are discussed in the next section.

Nearshore breaker bars are difficult to examine in the field, especially under storm conditions. Initially, therefore, the theories explaining nearshore bar behaviour have been largely based on either laboratory tests (e.g. Rector, 1954; Sunamura and Horikawa, 1974) or mathematical models (e.g. Bowen and Inman, 1971; Lau and Travis, 1973). In the last decade, however, due to new and improved techniques, field studies have become increasingly important in the verification and establishment of theories regarding bar morphodynamics.

The following groups of theories have emerged during the recent decades:

- the 'breakpoint hypothesis' which relates bar behaviour to processes associated with the transformation of high-frequency ( $T < 20$  s) wind-waves in the surf zone (e.g. wave asymmetry, wave breaking, undertow) (e.g. Miller, 1976; Dally, 1987);
- theories that relate bar behaviour to the presence of low-frequency ( $T > 20$  s) or infragravity waves. This group can be divided into two mechanisms:
  - infragravity waves with a cross-shore standing pattern. This pattern causes gradients in the cross-shore drift and oscillatory currents by which sediment may converge at fixed locations on the bed (e.g. Holman and Bowen, 1982; Bowen and Huntley, 1984)
  - infragravity waves that are forced by radiation stress variations due to grouped high-frequency waves which have a pattern of alternating low and high waves. The stirring of the sediment is caused by high-frequency waves while infragravity waves govern the transport which may result in the formation of a bar (e.g. O'Hare and Huntley, 1994)
- The overtake of harmonic waves (e.g. Boczar-Karakiewicz and Davidson-Arnott, 1987; Boczar-Karakiewicz et al., 1995) which leads to a regular pattern of an alternatively increasing and decreasing wave heights.

Once bars begin to form, the possibility arises of a resonant interaction between the bed and the wave field (O'Hare and Davies, 1993). It is, therefore, not always clear to what extent these theories, often originally intended to explain the *formation* of bars, also explain the further *development* (e.g. migration) of bars. This study does not address this question because, at the field site, bars are present throughout the year. Hence, it is assumed that all theories may also be used to explain the further development of bars.

The breakpoint theory relies on the (sudden) changes in processes occurring when waves break. Characteristics of the breaking wave itself or breaking induced currents are used to explain the formation and movement of bars. In a laboratory, Miller (1976) found that the vortex of plunging breakers excavates a trough and forms a bar just at the seaward side of the breakpoint (Fig. 2.2a). Miller (1976) observed that spilling breakers erased the bar. The offshore movement of bars was explained by the shifting of the breakpoint of plunging breakers. The breaker-induced return flow of plunging breakers, causing an offshore-directed sediment transport, is not present, or may be weak when the breakers are of the spilling type. Therefore, a spilling breaker causes a landward migrating bar because the vortex of spilling breakers is limited to the upper part of the water column (Fig. 2.2b). King and Williams (1949) observed the morphologic response of steep waves in a wave tank. They found that sand on the



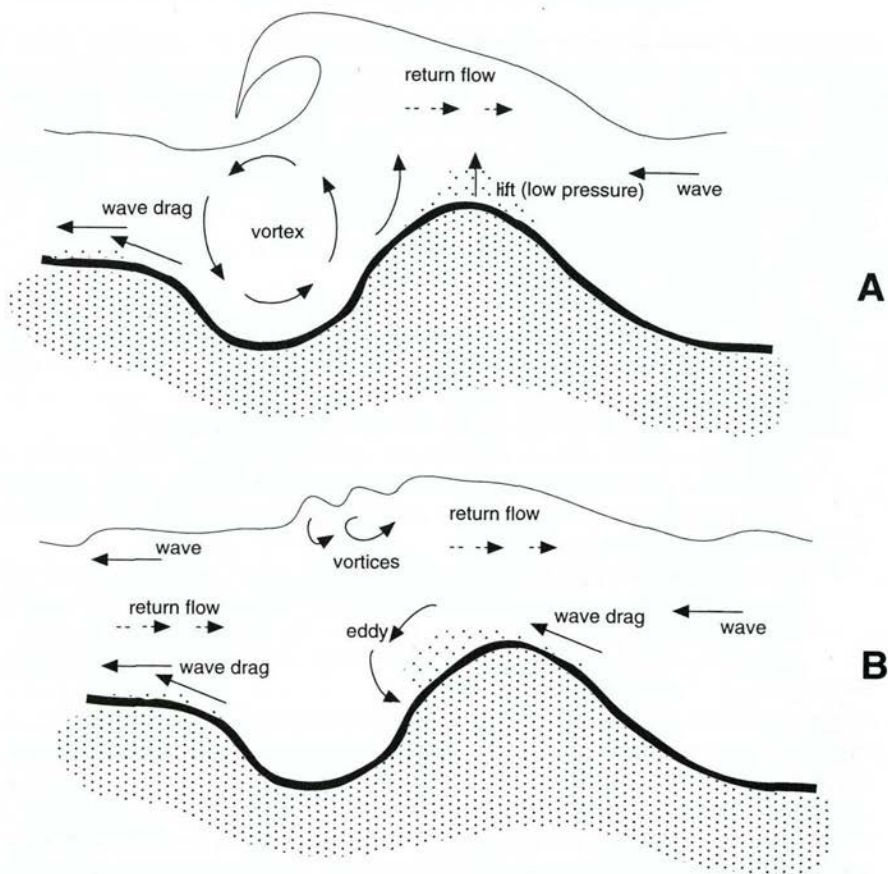


Figure 2.2 Bar formation and modification by plunging (A) and spilling (B) breakers (after Greenwood and Davidson-Arnott, 1979).

seaward side of the breakpoint moved in the onshore direction, while at the landward side sand moved offshore. In this way, a bar was formed near the breakpoint. Similar theories have been proposed in which the position of the bar is confined to the breakpoint (e.g. Dhyr-Nielsen and Sørensen, 1970; Greenwood and Davidson-Arnott, 1979; Dally and Dean, 1984; Dally, 1987). The speed at which the bar was formed was found to increase with increasing breaker vortices (Miller, 1976; Sunamura and Maruyama, 1987). Multiple bars were formed by the breaking and successive reforming of waves (Fig. 2.3). It was also found that sediment on the seaward side may have been transported landward due to drift velocities which were the result of increasing wave asymmetry towards the breakpoint. Seaward transport is driven by a net offshore flow, the undertow, which may be caused by the non-uniform distribution of momentum over depth, the so-called Stokes drift, the mass transport in breaking waves and a possible wind set-up. Greenwood and Davidson-Arnott (1979) suggested that rip-currents may also generate an offshore sediment transport towards the breakpoint.

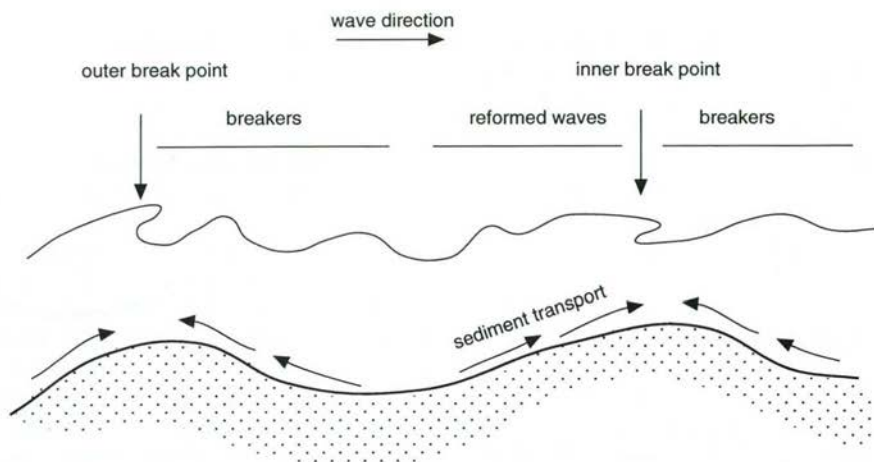


Figure 2.3 Bar formation as explained by the convergence of sediment. More bars are formed when the waves break, reform and break again (after Dyrh-Nielsen and Sorensen, 1970).

Despite the simplicity and attractiveness of this theory, some doubt about its validation has been expressed. For instance, field studies have shown that the bar crest location is not always related to the breakpoint (e.g. Mason et al., 1984; Sallenger et al., 1985; Seymour and Aubrey, 1987). In many cases, multiple bars are observed in fully-saturated surf zones (i.e. where waves break over a wide region) in which there are no easily identifiable fixed breakpoints (e.g. Sallenger and Howd, 1989). In such cases, it is difficult to see how the breakpoint hypothesis can be valid. Greenwood and Davidson-Arnott (1979) found, in a field study, that the breakpoint of the waves was, in most cases, located at the seaward side of the bars and not on the crests. A similar result was found by Sunamura and Maruyama (1987) using monochromatic waves in a large wave tank, and by Sanchez-Arcilla et al. (1994) executing a study in a large wave tank with random waves. Although the breakpoint hypothesis requires plunging breakers (Miller, 1976), Orme (1985) notes that these may also destroy a bar. Others (e.g. Dally, 1987; Greenwood and Davidson-Arnott, 1979 and Sunamura, 1985) claim that spilling breakers may also form bars. The offshore movement of the bar during storms was explained by spilling breakers that start to break further offshore, but still at the seaward side of the bar, thus resulting in a larger head loss and, in turn, in larger (breaker induced) offshore currents. The onshore movement was explained in a similar way (Greenwood and Davidson-Arnott, 1979). Sunamura and Takeda (1984), reasoned that a bar migrates in the onshore direction when waves are breaking on the seaward slope of the bar. After breaking, the waves reform into bores which advance over the bar and move material towards the landward side of the bar. These bores may originate from plunging or spilling breakers (Battjes, 1988). Another factor influencing the formation and movement of bars is the tide. Dyrh-Nielsen and Sørensen (1970) argue that, on a tidal coast, the breakpoint will move continuously. Hence, there will be no formation of a distinct bar. A small tidal



range as a condition for bar formation was also proposed by Davidson-Arnott (1975) and Greenwood and Davidson-Arnott (1975).

Theories relating bar morphology to standing infragravity waves emerged after the recognition that the cross-shore length scales of standing infragravity waves and bar scales are of the same order of magnitude (e.g. Short, 1975; Bowen, 1980). Standing infragravity waves are formed when progressive infragravity waves, also called 'surf beat' (Munk, 1949), are reflected from the shoreline thereby interfering with incoming waves, to form standing waves. The mean cross-shore drift velocities associated with standing infragravity waves cause a sediment-transport pattern that results in the accumulation of sediment under either a node or antinode of a standing wave (Carter et al., 1972; Lau and Travis, 1973; Bowen, 1980; O'Hare and Davies, 1993) (Fig. 2.4). The dominant transport mode, suspended load or bedload, determines whether the bar will form under either antinodes (suspended load dominant) or at a node (bedload dominant; Short, 1975). Bar formation is also thought to be the result of edge waves which are long waves trapped to the shore by refraction. Longshore variability and rhythmicity, in particular, can be explained by standing edge waves (Holman and Sallenger, 1993). Aagaard (1990) and Bauer and Greenwood (1990) carried out field measurements that largely supported the idea that infragravity waves play an important role in nearshore morphology.

Studies suggesting that the scales of (standing) infragravity waves are in line with the spacing of nearshore bars (e.g. Dally 1987; O'Hare and Davies, 1993) have raised a number of objections. First, the scales of standing waves were calculated using theoretical models that assume that the waves reflect against a vertical wall and that the profile is a planar beach. Both assumptions are highly unrealistic. The second criticism is that the models require certain, often unmeasured but *a priori* adapted inputs (e.g. long wave climate). A similar criticism applies to the period of the standing long waves and the dominant transport mode, i.e. bedload or suspended transport. To verify the theory, the dominant transport mode should be determined along the entire profile. In addition, the theory itself requires only one transport mode to be dominant over the entire profile, which does not necessarily have to be the case. Finally, Davidson-Arnott (1988) observed that gentle slopes often have more bars; this seems to be in contrast to the infragravity theory because gentle slopes have lower reflection coefficients. Field studies (e.g. Allen and Psuty 1987; Davidson-Arnott and McDonald, 1989; Sallenger and Holman, 1987; Noble and Lees, 1990; Ruessink et al., in prep) and laboratory studies (e.g. Dally, 1987; Dean et al., 1992) found no clear relation between standing infragravity waves and bar morphology. Most field studies only measured significant infragravity energy during storm conditions. However, the spectra during these events were often broad banded and showed no distinct peaks (Huntley et al., 1981; Oltman-Shay and Guza, 1987). Because only a small number of bars are commonly present, the theory requires sharp peaks in the wave spectra. In addition, during periods of low waves, when there is hardly any infragravity energy, bars often move onshore. Hence, this theory can not explain onshore bar movement.

The second mechanism associated with the presence of low-frequency (infragravity) waves is the bar formation due to the high-frequency wave/low-frequency wave coupling. Offshore waves approaching the shore have often a grouped structure which results in a pattern of alternating high and low waves. These high-frequency wave variations result in variations of the radiation stress (Longuet-Higgins and Steward, 1962, 1964) which, in turn, forces a low-frequency wave ('bound long

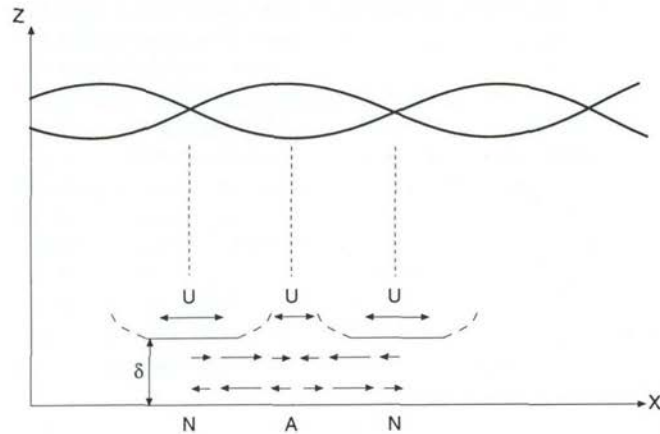


Figure 2.4 Velocity vectors beneath a standing wave. The X-axis is the cross-shore axis and the Z-axis is the vertical axis;  $\delta$  is the thickness of the bottom boundary layer;  $N$  signifies a node and  $A$  is an antinode (after Carter et al., 1973).

wave'). Before entering the surf zone, this long wave is coupled to the wave group variations and has the form of an elevation of the still water level beneath lower waves and a depression of the still water level beneath higher waves. As the wave propagates into the surf zone, the bound long wave lags behind the wave groups and when the short waves break, the bound long wave is released as a free wave. If the high-frequency waves can mobilise sediment from the bed, then there is the possibility that sediment transport may occur. The direction of the sediment transport is determined by the correlation between the bottom velocity due to the high-frequency waves (which mobilises sediment) and the velocity due to the low-frequency (bound) waves (which transports sediment). In case of a region with a fixed correlation between the envelope of the high-frequency waves and the low-frequency waves, a net sediment transport will occur in that region. If several of these regions are present in the surf zone, then there will be a convergence or divergence of sediment that may lead to the formation of a bar.

There is limited evidence that such regions do exist in real surf zones (e.g. Jaffe et al., 1984; Beach and Sternberg, 1991). In addition, the high-frequency wave/low-frequency wave mechanism does neither include the contribution from mean currents nor the contribution of the asymmetry of the high-frequency waves to the sediment transport. The wave coupling mechanism is, in many respects, similar to the standing infragravity wave mechanism. It is, therefore, subject to the same criticisms. The need for a narrow-banded infragravity wave spectrum to produce stable regions of sediment convergence and divergence is in particular unrealistic. Field experiments have, however, made clear that a coupling between high-frequency waves and low-frequency waves is feasible (e.g. Guza et al., 1985; Foote et al., 1992) and may influence bar development. Yet, the exact sediment transport mechanisms and spatial variability of these mechanisms are to be revealed.

The basis for the explanation of the formation of nearshore bars by the wave overtake mechanism (e.g. Boczar-Karakiewicz et al., 1995) is the alternating reinforcement and



cancellation of two harmonic waves. These waves are related to an, a priori, defined regular wave train, having a known constant amplitude and a single frequency equal to the peak wave frequency of the storm-generated wave spectrum. The amplitude of these waves varies along the cross-shore profile while their phase-difference remains constant. Since the amplitudes of these two waves are different, they will interfere, alternatively reinforcing and cancelling at positions which, for a uniform water depth, are periodically spaced along the direction of the wave propagation. This leads to spatial gradients in the sediment fluxes and zones will develop where sediment converges and zones where sediment diverges, i.e. bar formation.

The main disadvantage of this mechanism is that it becomes invalid at the inner nearshore zone (Boczar-Karakiewicz et al., 1995). Therefore, It can not explain the formation of e.g. inner nearshore bars. In addition, the interference between two wave harmonics is damped in a naturally occurring spectrum of wind-generated waves (e.g. Doering and Bowen, 1995).

In conclusion, there is still no consensus about the processes that influence bar development and migration. This is because most theories are hard to verify in the field, especially as detailed morphological and hydrodynamic measurements are frequently lacking. While it is possible, and very probable, that different mechanisms may be important, the formation of bars is most easily linked with the breaking of wind-waves because many breaking related processes can be visually verified. The break point hypothesis is the most intuitive and attractive mechanism explaining bar development and because of costs and operational constraints, this study focuses on the processes related to the transformation of wind-waves. As a matter of fact, a dense array of instruments is needed to verify the other theories.

The previous section has shown that the response of (inner) bars to storm and non-storms is difficult to predict because it is determined by a large number of factors. The most prominent changes in bars are determined by:

- variations in the offshore wave conditions, i.e. the alternation of storm and non-storm periods which also govern the shoaling and breaking of high-frequency wind-waves in the surf zone;
- the position of the bar in the cross-shore profile as an outer nearshore bar behaves differently than an inner nearshore bar.

Previous studies regarding nearshore bar behaviour (except the Duck measurements) often monitored nearshore bar behaviour over a short time-span (<10 days) and with rather large intervals (several days) between two succeeding surveys. The Duck-measurements have made clear that nearshore bar development can be fast (order 1 day) and an intensive monitoring is thus necessary.

Therefore, assuming that the shoaling and breaking of high-frequency wind-waves is the main mechanism steering inner nearshore bar development, it is necessary:

- to study how the inner nearshore bar responds to daily changes in the shoaling and breaking of high-frequency waves over the bar, i.e. to non-storm and storm periods;
- to study how the response of the inner nearshore bar to non-storm and storm conditions depends on the antecedent cross-shore profile configuration.

It is generally acknowledged that in the surf zone hydrodynamic processes induce sediment transport processes and the integration of sediment transport processes leads to morphological development. To study whether inner nearshore bar developments are related to the break point hypothesis, it is also necessary to analyse the hydrodynamic and sediment transport processes induced by shoaling and breaking high-frequency waves. Basic characteristics of these phenomena are described in the following sections.

## **2.4 Hydrodynamic processes associated with the shoaling and breaking of high-frequency waves**

In this section the propagation and transformation of high-frequency waves are considered. These waves play an important role in the nearshore zone because they generate many (secondary) water motions that drive currents, sediment transports and morphologic changes. When waves enter the surf zone they become non-linear and may break. Hence, the regular offshore waves are transformed in many other wave motions (e.g. turbulence, low-frequency waves). The transformation-processes are, however, poorly understood.

In shallow water where the waves are close to breaking they become very non-linear, typically characterised by a gradual peaking of the wave crest, a flattening of the trough and a relative steepening of the face. This development of a surface wave is also evident in the wave-induced velocity field and the variation of the near-bed orbital motion will deviate significantly from the sinusoidal prediction of the linear wave theory. Although also other effects, e.g. streaming (e.g. Fredsøe and Deigaard, 1992), may cause a landward directed net current near the bed, it is believed that velocity asymmetry is the main cause for onshore sediment transport. Investigations of wave shape and the internal velocity field in the surf zone have been carried out in numerous laboratory studies and in a few field studies. Miller and Zeigler (1965, In: Yu et al., 1993) found that the internal velocity structure of waves is strongly related to the wave shape, i.e. the wave asymmetry. Kroon (1994) performed measurements in the inner nearshore zone at Egmond and found velocity-asymmetry values ranging from 0.52 ( $U_{on} \approx 1.2 U_{off}$ ) to 0.64 ( $U_{on} \approx 1.8 U_{off}$ ). He also found that the degree of asymmetry increased with the relative wave height which means that the asymmetry increases towards the breaking region.

As waves propagate into shallower water, the process of shoaling leads to increasing wave heights. Eventually, the waves will begin to break because their steepness, i.e. the forward wave orbital velocity, becomes too large. Breaking will, theoretically, occur when the breaker height-to-water depth ratio is about 0.78 (Galvin, 1972). Field measurements have shown, however, that a more appropriate breaker ratio is in the range of 0.4-0.6 (Huntley and Bowen, 1975; Sallenger and Holman, 1985). Non-breaking (Stokes drift) and breaking (surface roller) waves generate an onshore directed flow at the surface which is compensated by a mean offshore flow, the undertow. This mean flow, which is concentrated in the lower part of the water column, is obviously an important control on the rate and direction of the net sediment transport.

After a wave has broken, the wave is transformed into a bore or into swash. The relative wave height ( $H_b/h$ ) generally decreases from a value of about 0.8 at the point of wave breaking to about 0.5 in the inner nearshore zone (Fredsøe and Deigaard,



1992). Kroon (1994), however, found that under swash conditions the relative wave height may be as high as 1.1. In the swash zone, low-frequency motions are significant and become dominant for gentle slopes (e.g. Hamm et al., 1993).

The above résumé makes clear that the net onshore-offshore sediment transport appears to be controlled by the differences between the onshore transport due to the asymmetry of the waves and the offshore transport in the undertow. Under low waves, the undertow is weak and the asymmetry in the cross-shore velocity, with higher onshore than offshore velocities, leads to a net onshore sediment transport. During storms, both the undertow and the velocity asymmetries increase (e.g. Davidson-Arnott and McDonald, 1989; Greenwood and Osborne, 1990; Masselink and Black, 1995) but the undertow commonly dominates the near-bed velocity field. Moreover, the findings of Hazen et al. (1990) showed that the undertow may continue to increase even though the wave conditions are locally saturated at the point of measurement. If the undertow dominates the near bed velocity field it will cause a net offshore sediment transport. Therefore, the undertow was thought to be a major control on the beach erosion and the subsequent deposition of this sediment on nearshore bars (e.g. Dally and Dean, 1984; Roelvink and Stive, 1989).

Field experiments with random waves and non-barred profiles indicate that the undertow is zero at the seaward side of the surf zone and increases gently to a maximum around the mid-surf zone position and sharply decreases in the direction of the shore (e.g. Masselink and Black, 1995). In contrast to a non-barred profile, where variations in the high-frequency wind wave oscillatory currents and mean currents are strongly depth-dependent, the nearshore velocity field across barred coasts is constrained by its position with respect to bars. Greenwood and Osborne (1990) found that during a storm event ( $H_{s, \max} = 1.5$  m), the undertow in a barred nearshore was neither temporally nor spatially consistent. Before the peak of the storm, higher mean cross-shore and offshore directed velocities ( $0.20 \text{ m s}^{-1}$ ) were found at the seaward side of a nearshore bar (located 30 m offshore) than at the landward side ( $0.16 \text{ m s}^{-1}$ ). After the peak of the storm, the mean cross-shore velocity, still offshore directed, increased towards the shore. The wave-induced oscillatory current and the velocity asymmetry always decreased in the onshore direction. Similar findings were reported by Allen et al. (1991). In addition, they found that the undertow had its maximum at the bar crest (70 m offshore) and that the spatial variability of the undertow was larger than the temporal variation.

An alternative nearshore circulation system was presented by Shepard and Inman (1950). Their horizontal circulation cell hypothesis consists of weak onshore mass transport in the breaker zone, longshore feeder currents and narrow, strong, and offshore-directed rip currents (i.e. a three-dimensional situation). However, in storms, the two-dimensional vertical circulation (undertow) is observed to be the dominating pattern (e.g. Short, 1978; Wright et al., 1982; Greenwood and Osborne, 1990).

The rapid transformation of waves in the surfzone has been very difficult to describe, especially for plunging breakers, and practically no theories are available that can be used as a basis for a hydrodynamic description or for sediment transport calculations. Theories, originally developed for use in particular conditions, are often extended to a wider range of conditions to cover the entire surf zone. Then, many wave theories are available to determine the onshore- and offshore orbital peak-velocity and the velocity asymmetry near the bed. Analytical theories have been developed for deep (Stokes theories) and shallow water (Cnoidal theories) while also numerical methods based on



Fourier approximation methods (e.g. Covocoidal theories) have been derived. Roelvink (1987) measured peak onshore and offshore velocities during a large-scale flume experiment. The onshore orbital, peak velocities were reasonably well described by the linear wave theory, the Rienecker-Fenton Fourier approximation theory and the Covocoidal theory, even at high relative wave heights ( $H_s/h = 0.6$ ). The offshore orbital, peak velocities under the wave trough were overpredicted by the linear wave theory (about 20%) and underpredicted by the Rienecker-Fenton and Covocoidal theories, even for non-breaking waves ( $H_s/h = 0.3$ ). Kroon (1994) found in field studies that the onshore orbital, peak velocities can be reasonably well described by the linear wave theory. The offshore orbital peak velocity could also be described by the linear wave theory when a correction factor was used. Kroon (1994) also compared measured velocity asymmetries with those computed by some wave theories. He concluded that only the Covocoidal theory reasonably predicted the measured velocity asymmetries although a small systematic overestimation was present.

In summary, the wave transformation processes are still at an early stage of understanding. Besides, large spatial and temporal gradients of the different water motions exist in the surf zone. More research on different geographical locations is necessary to verify the previous research and establish some consistency in the relative importance of the different water motions in the surf zone. The bar development shows different behaviour during periods of breaking waves (storms) than during non-breaking waves (quiet weather). Hence, hydrodynamic analysis should identify the different processes involved with either non-breaking or breaking waves.

The previous review largely dealt with high-frequency wind waves. Researchers (e.g. Wright et al., 1991; Osborne and Greenwood, 1992; Russell, 1993) have, however, made clear that sediment transport is also coupled with low-frequency wave motions. Besides, low-frequency waves may even become dominant close to the shore (Huntley, 1976; Holman, 1981).

In conclusion, to study to what extent nearshore bar developments are related to the hydrodynamics associated with the shoaling and breaking of high-frequency wind-waves it is necessary :

- to determine the relative contribution of high-frequency versus low-frequency oscillations under different hydrodynamic conditions
- to measure and describe the transformation of wind-waves in the nearshore zone by considering the wave shape and wave dimensions as a function of the position in the surf zone, i.e. in non-breaking waves, breaking waves and swash. In this framework:
  - to verify the application of present wave theories for non-breaking and, especially, breaking conditions
- to analyse and describe in detail the velocity field around the breakpoint including the absolute and relative importance of wave asymmetry versus undertow

## 2.5 Sediment transport processes associated with the formation and development of bars

Research on sediment transport has led to a better understanding of some basic processes. However, there is insufficient expertise at present to describe and predict directions and rates of sediment transport in the surf zone. In addition, the significance of sediment transport mechanisms involved in the formation and development of nearshore bar systems has not yet been fully explored. This is reflected in the poor prediction capabilities of the existing sediment transport- and coastal-profile models (Brøker-Hedegaard et al., 1992; Sherman and Bauer, 1993). To improve these models, many questions regarding the physical processes behind the transport of sediment will first have to be answered.

The total sediment transport may be divided into bedload and suspended load transport but in the field, it is very difficult to distinguish clearly between the two modes of transport. The suspended sediment transport is often extrapolated to the bed and because sediment concentration increases rapidly in the near bed region, this leads to suspended sediment transports that are largely determined by the extrapolation method. Here, bedload transport is defined as all sediment transported by rolling, sliding and saltation (Van Rijn, 1993). The remainder of the sediment transport is regarded as suspended transport.

The suspended sediment transport can be estimated using the time-averaged vertical profile of the concentration and velocity of the sediment. Alternatively, this flux can also be computed by combining the instantaneous vertical profiles of concentration and velocity. Regardless of the method used for calculating suspended sediment transport, knowledge of the concentration in the vertical is important. Earlier investigations revealed that the suspended sediment concentrations decrease rapidly with increasing elevation above the bed. The main (medium scale) factors influencing the concentration profile in the surf zone are:

- Cross-shore position: the highest concentrations are found near the breakpoint and near the swash in the inner surf zone.
- Position relative to breakpoint: maximum concentrations occur on the shoreward side of the breakpoint.
- Breaker type: plunging breakers induce a higher sediment concentration than spilling ones.

For the inner nearshore zone, Kroon (1994) found that higher concentrations are also associated with steeper vertical concentration profiles. His measurements revealed that the suspended sediment concentration near the bed (0.1 m) was about  $0.01 \text{ kg m}^{-3}$  in non-breaking waves,  $1\text{-}5 \text{ kg m}^{-3}$  in breaking waves and  $5\text{-}15 \text{ kg m}^{-3}$  under swash conditions.

The above factors lead to an irregular spatial distribution of the suspended sediment concentration across the surf zone which creates a potential for gradients in net sediment transport. These gradients may lead to net morphological changes e.g. the erosion of the beach or the creation of a bar. As indicated by the above list, high-frequency wind waves are undoubtedly the primary cause of sediment suspension. However, individual waves within a wave group induce more suspension than an individual wave that is uncorrelated with a wave group (Hanes and Huntley, 1986). Beach and Sternberg (1988) found, after performing measurements in the inner surf



zone of an oceanic beach, that the mean concentration associated with infragravity waves was 3 to 5 times higher than that associated with incident wave frequencies. Also, the development and decay of concentration in the vertical were strongly related to infragravity waves. Thus, sediment re-suspension is also correlated with longer time scales than those of incident waves, i.e. those of wave groups.

Owing to the invention and development of acoustical and optical devices, the knowledge about the vertical, temporal and spatial distribution of suspended matter has improved considerably. Recent research indicates that suspended sediment transport should not be estimated using the cross-product of the time-averaged velocity and time-averaged concentration because there is a time-lag between the maximum concentration and the maximum external force (Hanes, 1988; Beach et al., 1992; Osborne et al., 1990; Greenwood and Osborne, 1991). These time-lags depend on the height above the bed, the presence of small-scale bedforms (ripples) and the frequency of the forcing velocity (Beach and Sternberg, 1991). It is possible that the depth-integrated mean current flows in the opposite direction to the depth integrated sediment transport (e.g. Huntley and Hanes, 1987). Therefore, to analyse the various components of the suspended sediment transport, the net sediment transport is usually decomposed into steady and fluctuating components:

$$\langle u \cdot c \rangle = \langle u \rangle \cdot \langle c \rangle + \langle \tilde{u} \cdot \tilde{c} \rangle \quad (2.1)$$

where  $u$  and  $c$  are velocity and concentration respectively; the brackets represent a time average; and the tilde indicates the fluctuating (wave) component.

Hence, the direction of suspended sediment transport is determined by the different frequencies, mean, incident and infragravity, of the near-bed velocity field and the concentration. The direction of the mean flux is determined by the direction of the mean velocity and the direction of the instantaneous components is determined by the phase between the forcing of the fluid and the response of the sediment. In general, onshore transports are generated by incident wave frequencies (wave asymmetry effect); offshore transport by lower frequency motions (bound long waves, see section 2.3) and mean currents (undertow effect) (Hanes and Huntley, 1986; Doering and Bowen, 1989; Osborne et al., 1990; Kroon, 1994; Hoekstra et al., 1996).

The relative contributions of the mean and oscillating part of the transport may vary in the vertical. Huntley and Hanes (1987) found that the oscillating term was dominant near the bed while the time-averaged term dominated the upper part of the water column. The different frequencies contributing to the sediment flux vary, not only with height, but also with location in the surf zone (Osborne and Greenwood, 1992). This complicates the suspended sediment transport even further.

There is little understanding of bedload processes in the nearshore zone, and the existing knowledge is based on bedload transport in unidirectional flows (Sherman and Bauer, 1993). It is often difficult to distinguish and define a boundary between bedload and suspended load. Different criteria are used making it difficult, therefore, to evaluate the (relative) amounts of bedload and suspended load estimated in the different studies. Bowen (1980) proposed that the percentage of the bedload versus the suspended load rates should be determined by using the ratio of the orbital velocity and the sediment-fall velocity. However, both orbital velocity and sediment fall velocity vary considerably over the surf zone (Wolf, 1992, 1993; Kroon, 1994; Guillén

and Hoekstra, 1996). This implies that the relative contributions of the bedload and suspended load also vary considerably in the surf zone of Egmond. The relative contributions and directions of bedload and suspended load (Bailard and Inman, 1981; Hanes, 1988; Sternberg et al., 1989) are still under discussion. Komar (1978), who regarded all load under 0.1 m from the bottom as bedload, suggested that bedload accounts for 80% of the sediment transport in the surf zone. Beach and Sternberg (1992) found that 30% of the suspended sediment was carried within 0.035 m of the bed. Apart from the relative contributions, the directions of the bedload and suspended sediment transport may also differ (e.g. Ribberink and Al-Salem, 1992).

The medium-term change in the nearshore (bar) morphology is primarily associated with cross-shore sediment transport produced by wave action. However, only few field experiments with simultaneous sediment transport- and morphologic measurements have been executed. Jaffe et al. (1984) described the role of suspended sediment transport during the Duck82 field experiments. They observed that the onshore migration of a nearshore bar (located 75 m offshore) during a storm ( $H_{s, \max} = 1.6$  m) was associated with the gradients in the cross-shore suspended sediment transport. The time-averaged suspended sediment flux over the bar was onshore directed and had its maximum value at the landward slope of the bar. At the landward side of the trough of the bar, the time-averaged suspended sediment flux was offshore directed. These fluxes occurred even though the mean cross-shore current over the bar was offshore directed.

Osborne and Greenwood (1992) observed the local time-varying suspended sediment flux in a barred profile during a single storm ( $H_{s, \max} = 0.9$  m) and found that the onshore-offshore sediment transport was predominantly two-dimensional over a bar (located 90 m offshore). The relative influence of the high-frequency, low-frequency, and mean transport components varied spatially and temporally in association with the incident wave energy. The sediment transport across the barred nearshore was constrained by position with respect to the bars. On the lakeward side of the bar, wind wave oscillating velocities generated large rates of onshore transport near the bed while low-frequency oscillations produced an offshore transport often equal in magnitude to that induced by wind waves. On the bar crest, net sediment transport was close to zero, owing to a balance between the offshore mean transport and the onshore oscillatory transport. Landward of the bar crest and in the trough, sediment transport by wind waves decreased because of dissipation of energy during wave breaking. In contrast, the contribution to suspended sediment transport by low-frequency waves increased relatively and this transport was onshore directed. This transport approximated the offshore sediment transport induced by the mean currents.

Aagaard and Greenwood (1994) measured the sediment transport and morphologic development nearby a bar (175 m offshore) during a storm ( $H_{s, \max} = 1.2$  m). The time-averaged suspended sediment flux was offshore directed at the landward side of the bar while decreasing in the direction of the bar. At the seaward side of the bar, the time-averaged suspended sediment flux was onshore directed while the onshore fluxes decreased in the offshore direction. The total (i.e. averaged over the storm) relative magnitudes of mean and oscillatory suspended transports were almost equal over the entire surf zone. In contrast to the high-frequency and mean suspended fluxes, the low-frequency fluxes were not consistent in direction during the storm and over the surf zone. Low-frequency fluxes were quantitatively more important during



the waning of the storm and high-frequency fluxes during the early stages of the storm. Correlation of morphological changes with measured rates and directions of suspended sediment transports were partly successful.

Thornton et al. (1996) performed field measurement at Duck (DELILAH experiment) and studied mechanisms for bar generation with the Bowen (1980)-Bailard (1981) sediment transport model. The model identified that the generation of the bar (200 m offshore) was the result of onshore sediment transport from outside the surf zone by high-frequency velocity asymmetry converging with sediment from within the surf zone, where it is primarily suspended by strong longshore currents and short waves and transported offshore by undertow. The importance of the mean longshore current was contrary to the conventional assumption that the short waves cause the primary stress to mobilise and suspend the sediments. Inside the surf zone, the mean, high-frequency and low-frequency velocity components varied both spatially and temporally and were all of the same order.

In summary, the net cross-shore suspended sediment transport in the nearshore zone is a combination of:

- mean offshore sediment transport associated with the undertow;
- onshore or offshore sediment transport due to low-frequency oscillation in the cross-shore current velocity;
- onshore sediment transport due to high-frequency wave velocity asymmetry.

The contribution of the different components to the net sediment transport varies largely, both temporally and spatially, over nearshore bars. Clearly, to gain an understanding of sediment transport processes responsible for the development of the inner bar it is necessary:

- to study the relative contribution of the high-frequency oscillating, suspended sediment transport, the low-frequency oscillating, suspended sediment transport, the mean suspended sediment transport and bedload transport to the total sediment transport in the nearshore under different wave conditions;
- to study and describe the order of magnitude, direction and the dominant transport mechanism of the net sediment transport around a breakpoint, i.e. under different wave conditions;
- to study how the cross-shore distribution of the net sediment transport may lead to convergence and divergence of sediment fluxes around the inner nearshore bar.

## 2.6 Overview of hypothesis and research questions

In summary, the above literature review has reviewed the morphologic, hydrodynamic and sediment transport processes related to the development of an inner nearshore bar. It is not clear, however, to what extent the development of this bar may be attributed to processes related to the shoaling and breaking of wind-waves. The next hypothesis is, therefore, examined in this thesis:



- *inner nearshore bar development is determined by the hydrodynamics and sediment transports induced by shoaling and breaking of high-frequency wind-waves*

Based on the foregoing, the following research questions are defined:

- regarding the morphologic development:
  - how does the inner nearshore bar respond to daily changes in the shoaling and breaking of high-frequency waves over the bar, i.e. to non-storm and storm periods?
  - how does the response of the inner nearshore bar to non-storm and storm periods depend on the antecedent cross-shore profile configuration?
- regarding the hydrodynamic processes:
  - what is the relative contribution of high-frequency versus low-frequency oscillations under different morphological and hydrodynamic conditions?
  - how do the wave shape and wave dimensions vary as a function of the position in the surf zone, i.e. in non-breaking waves, breaking waves and swash?
  - which wave theory can describe the observed wave transformations?
  - how does the velocity field, especially the absolute and relative importance of wave asymmetry versus undertow, vary under waves around a breakpoint?
- regarding the sediment transport processes:
  - what is the relative contribution of the high-frequency oscillating, suspended sediment transport, the low-frequency oscillating, suspended sediment transport, the mean suspended sediment transport and bedload transport to the total sediment transport in the nearshore?
  - how does the relative contribution of these sediment transport mechanisms vary around a breakpoint, i.e. under different wave conditions?
  - what is the order of magnitude and direction of the net sediment transport around a breakpoint, i.e. under different wave conditions?
  - what is the degree of convergence or divergence of the sediment transport near the inner nearshore bar?

The following chapters (4-6) focus on these questions, while chapter 7 gives a synthesis.

### 3 FIELD SITE AND DATA ACQUISITION

#### 3.1 Hydrodynamic setting

The field site is a coastal area of about 1 kilometre alongshore and extends about 1 kilometre offshore. It is situated near the village of Egmond aan Zee. The central Dutch coastline is sandy, 124 km in length and the Egmond field site is part of the central stretch (Fig. 3.1). Both waves and tides affect the morphological behaviour of this mixed energy coast, and the nearer the waves are to the coast the more important they are (Dillingh and Stolk, 1989). Longshore differences in the offshore wave climate are small due to the short length and relative uniform orientation of the central Dutch coast. Larger differences in the hydrodynamics are experienced in the cross shore direction because of the slope of the cross-shore profile and the presence of bars.

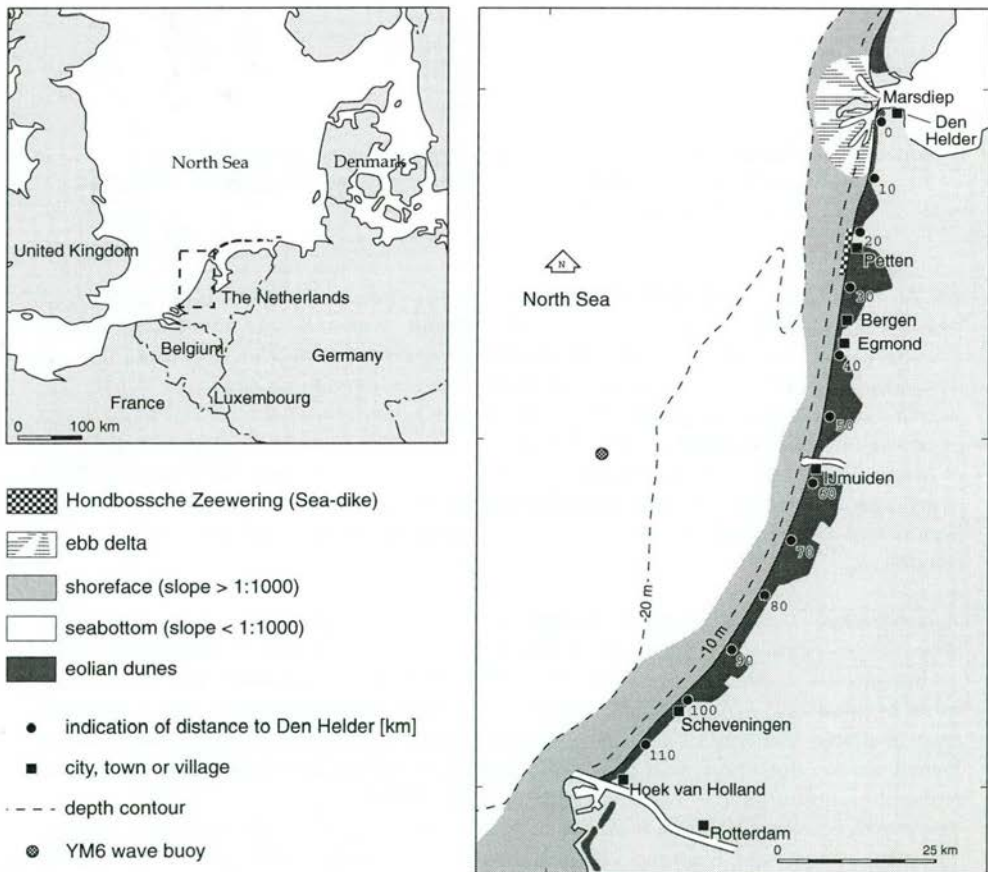


Figure 3.1 Geographical location of field site

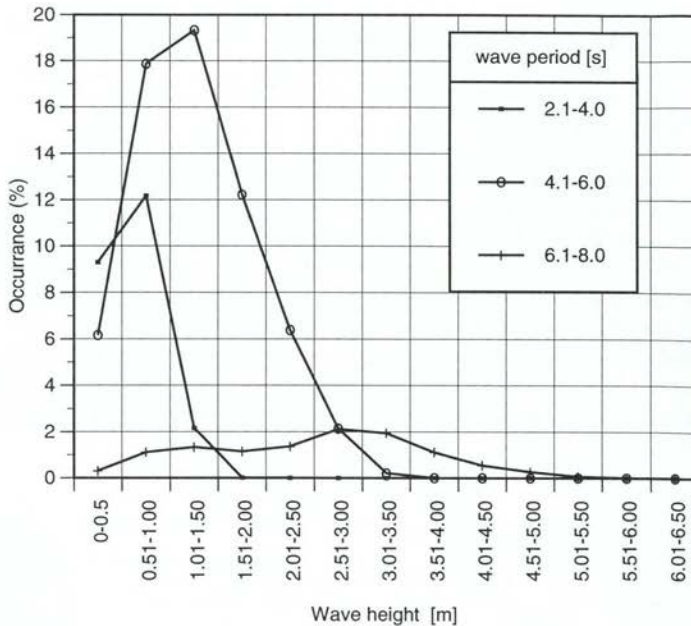


Figure 3.2 Offshore wave height distribution for three wave-period intervals using recordings from YM6 buoy averaged over all directions and over 1979-1991. Data from Roskam (1992).

As the field site is located on the semi-enclosed, shallow (< 200 meter) North Sea basin, the wind-fetch is restricted. Moreover, ocean swell can only approach the field site from the northern part of the North Sea. The wave climate, therefore, is dominated by wind waves related to low pressure areas moving from west (the Atlantic) to east (the European continent). Figure 3.2 illustrates the wave height-wave period relation as recorded by the YM6 wave buoy. This buoy is located at a distance of about 35 km offshore of IJmuiden where the water has a depth of 22 m (Fig. 3.1). The figure shows that the wave height mostly varies between 0 and 4 m and the wave period between 2 and 8 seconds. Higher waves are associated with longer wave periods.

The direction in which the waves spread is illustrated in Figure 3.3. Since the fetch is longer in the north-west, the larger waves approach the coast from this direction. Most of the waves approach the coast from the north-west and from the south-west quadrant and as the intensity of the fronts of the low-pressure areas is less in summer than in winter, the wave height also shows a seasonal fluctuation (Fig. 3.4) with the lowest waves occurring during April-August ( $H_s \sim 1.0$  m) and highest in the period November-January ( $H_s \sim 1.9$  m) (Augustein et al., 1990).

The mean tidal range varies from 1.4 m at Den Helder to 1.7 m at Hoek van Holland. The tidal range near Egmond varies between 1.2 m (neap tide) and 2.1 m (spring tide). At Egmond, the flood tide has a duration of four hours and the ebb tide, eight hours. The horizontal tide runs ahead of the vertical tide by about 45 minutes.

The semi-diurnal tide induces asymmetrical surface currents which may reach values of  $0.6\text{--}1.0\text{ ms}^{-1}$ , (Wiersma and van Alphen, 1988).



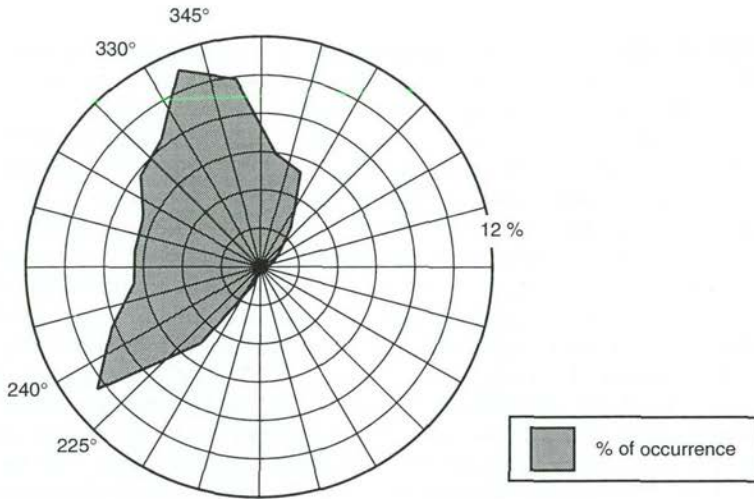


Figure 3.3 Average directional spreading of offshore wave field at YM6 buoy using recordings from 1979-1991. Data from Roskam (1992).

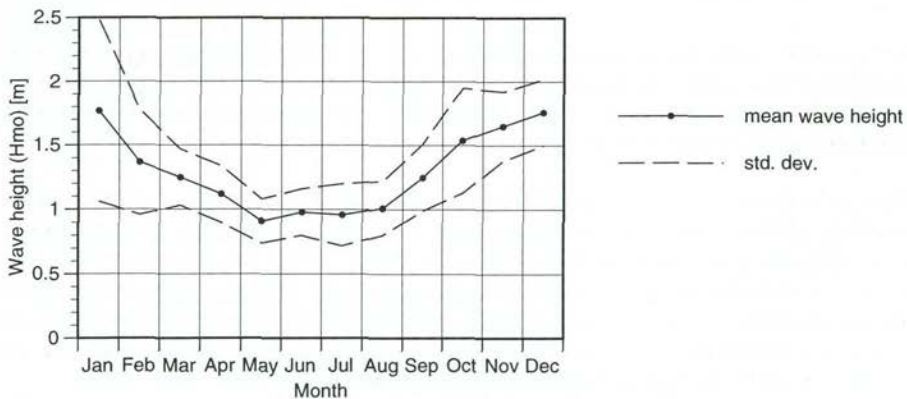


Figure 3.4 Mean monthly offshore wave height at YM6 buoy for the years 1979-1991, and standard deviation based on the years 1979-1988. Data from Roskam (1992).

### 3.2 Morphological setting

The geomorphological evolution of the Dutch coast started about 6000 years ago. At that time, the sea level rose and the former 'dry' North Sea became flooded again. In contrast to the Wadden area in the North and the Delta area in the South, the central stretch of the Dutch coast developed into what is now a 'closed', 'straight' coast with no tidal inlets or estuaries. This central stretch of this coastline is now considered.



The slope of the coastal zone, including the shoreface and surf zone, varies along the central stretch of the Dutch coast (Fig. 3.1). The steepest slopes are found near Egmond (1:150) and the mildest slopes (1:500) at both ends, at Den Helder and Hoek van Holland (Stolk, 1989). The width of this zone, which extends to approximately the 20 m depth contour, varies from 10 km in the North and the South to 2.5 km between Egmond and IJmuiden. Between one and four nearshore breaker bars are to be found in the surf zone, their number decreasing with the slope of the coastal zone. These bars are always present, but they show an annual net movement in an offshore direction as part of a migration cycle, in which a new bar emerges at the shoreline, moves offshore, and finally disappears near the seaward edge of the surf zone (Wijnberg, 1995). The speed of migration is in the order of tens of metres per year (de Vroeg, 1987; Wijnberg and Terwindt, 1995; Wijnberg, 1995). During a migration cycle a new bar emerges at the waterline so there are bars in different phases of the migration cycle present at the same time. The configuration of bars on two dates (1967 and 1973) is illustrated in Figure 3.5. It is clear from this figure that the bar configuration shows considerable changes over time. The outer bar may be crescentic (Fig. 3.5a) or straight (Fig. 3.5b); the inner nearshore bar may be attached to the shore. However, the location of the shore attachment areas also varies in time. A thorough analysis of these bathymetric data reveals that the phase of the migration cycle varies alongshore (Wijnberg and Wolf, 1994; Wijnberg, 1995).

The average subaerial beach width is about 100 m. Beaches are wider (>100 m) in areas with a prograding coastline and smaller (<100 m) in areas with a retreating coastline. The beach width may be strongly affected by the vicinity of coastal structures. For instance, in front of the Hondsbossche Zeewering there is no beach, while near the southern harbour mole of IJmuiden the beach width is more than 500 metres. Beach slopes vary from about 1:30 to 1:80. Most of the beaches along this central stretch of the Dutch coast show ridge-runnel systems during low wave periods, but these systems are eroded during storms (Stolk, 1989). Short (1991) concluded, using aerial photographs of the period 1976-1985, that the modal beach state was of the ridge-runnel/low tide terrace type.

There is no distinct longshore or cross-shore trend in the distribution of sediment size along the central stretch of the Dutch coast. The median grain size ( $D_{50}$ ) of beach sand along the coast varies between 150 and 300  $\mu\text{m}$  (van Bemmelen, 1988). The sediment size in the cross-shore direction may vary over more than 300  $\mu\text{m}$  and often over shorter distances than that alongshore. Coarser sediment, in the ranges 250-500  $\mu\text{m}$  and sometimes 500-2000  $\mu\text{m}$ , is found in the North. South of Bergen aan Zee, all sediment is within the 125-500  $\mu\text{m}$  range (Dillingh and Stolk, 1989; Stolk, 1989). The median grain size ( $D_{50}$ ) of the beach at the field site varies between 200 and 350  $\mu\text{m}$ . The subtidal sands are clearly finer than the inter tidal sands. That sediment size becomes finer offshore is illustrated in Table 3.1.

From past sampling it is known that in the 4 km south of the field area, sediment size has changed over the years. The beach sands became somewhat coarser: from 300  $\mu\text{m}$  in 1967 to 360  $\mu\text{m}$  in 1982. However, from within the field site to 8 km north of it, no such changes were noticed (van Bemmelen, 1988).

There is very little mud in the sediment at the field site, 0.5 % (beach), but this increases offshore to 1.4 % (1000 m offshore). It is therefore unlikely that mud has any influence on the cohesion of the sand and therefore on the sediment-transport processes (cf. Van den Velden, 1993) at the field site.

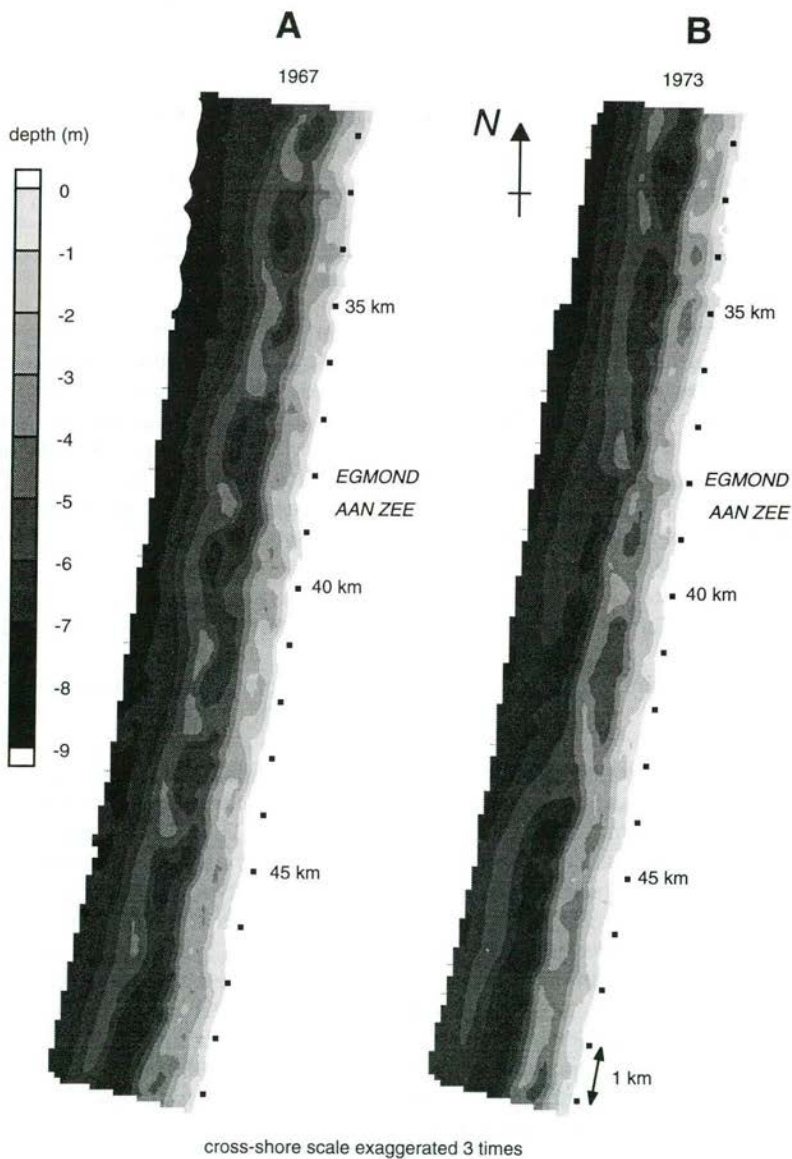


Figure 3.5 Nearshore morphology near Egmond aan Zee  
(A) in 1967  
(B) in 1973.



The beach slope varies around 1:30 with a distance between the low- and high tide mark of about 50 m. The width of the beach is about 80 m, the upper part of which is only flooded during periods of severe storms ( $H_{s, offshore} > 3$  m). During these storms, part of the foot of the dunes may be eroded by wave action. Two morphological features may be present on the lower part of the beach - a ridge-runnel (RR) or low-tide terrace (LTT) system - and occasionally during a year, a double ridge-runnel system. For a RR system to be transformed into a LTT system, a storm is needed (Short, 1991; van den Berg, 1977) while after a storm the LTT system converts back into a RR system again. The ridge of the RR system is a swash bar of about 0.2 to 1.4 m above the associated runnel formed mainly by swash and backwash processes. During periods of low and moderate wave conditions, the ridge-runnel system moves towards the dunes. The swash bar increase in height during this movement, and the runnel becomes shallower (van den Berg, 1977; Kroon, 1994). As the tidal range increases, i.e. from neap to spring tide, so does the speed of the onshore migrating swash bar. The ridge of the RR systems may be traversed, in a cross-shore direction, by small rips or 'drain-rips' (Short, 1991) which function, especially during low tide conditions, as drains for the runnel.

The morphometric characteristics of the inner nearshore bar vary because of processes acting on a small (daily) temporal scale and on a large (yearly) scale. On the latter time scale, the net offshore movement of this bar is about 20 m per year<sup>-1</sup>. During the offshore migration through the surf zone, the bar changes in form from asymmetric to symmetric (Houwing, 1991; Wolf, 1991). During the field experiments, the distance from the water line to the crest of the inner nearshore bar was about 200 m, with water depths above the crest varying from 1 to 2.5 m. The inner nearshore bar was oriented SSE-NNW at an angle of about 8 degrees with the coast. Using Wright and Short's (1984) model, the inner bar can be primarily classified as 'rhythmic bar and beach' (RBB) or 'longshore bar and through' (LBT). The RBB state is associated with periods of lower waves and that of the LBT with periods of higher waves (Short, 1991; Kroon, 1994). The rhythmic wave length of this bar varies between 200 and 700 metres.

The variability in morphology of the outer bar is less compared to that of the inner bar. The outer bar shows a stepwise, rather than gradual, mean annual net offshore migration of about 10-20 m, with the largest net migration seemingly occurring during the winter storms (Houwing, 1991). The crest of the outer bar was located at a distance of 550 m from the water line at a mean water depth of about 3.5 - 4 m during the field experiments. The outer bar is linear and shows no signs of rhythmicity within the spatial scale of the field site. However, on larger spatial scales the bar may be rhythmic (Fig. 3.5). The outer bar has an oblique orientation with respect to the coastline, also caused by its imbedding in a larger alongshore outer bar system.

### 3.4 Measuring approach and observation periods

The length of the observation period should be in accordance with the time and spatial scale of the system being studied. The observation period though is also constrained by the techniques available and the research time. The time scale of interest is here determined by the response of the morphology to changing hydrodynamic conditions. From existing literature and previous research on the Dutch



coast, it is clear that the surf zone system at Egmond has different time scales (e.g. Birkemeier, 1985, Kroon, 1994), varying from seconds (for the sediment transport processes) to years (for the morphological changes of the outer bar). As the inner nearshore bar is one of the main research subjects, it was clear that the length of the observation period is largely dictated by the specific time scales of the inner nearshore bar. These time scales are about one or two days for stormy periods (e.g. Sallenger, 1985), but more in the order of weeks for quiet weather periods (e.g. Orme 1985). To monitor the impact of multiple storms on the nearshore morphology, therefore, the observation period should be at least several weeks, preferably including November, when there is the greatest likelihood of storms (Stolk, 1991). In practice, though, the maximum length of the observation period was determined by the logistic (e.g. the availability of boats and personnel) and costs constraints.

The above considerations led to the implementation of two intensive field surveys in 1991 and 1992. Both field periods lasted from approximately 1 October to 10 November. The field lay-out of the instruments was largely the same during both observation periods.

Old and new techniques were used at the Egmond field site, based on previous fieldwork in the Netherlands (e.g. Kroon and van Rijn, 1990; Kroon, 1990,1991) and on field studies in the USA (e.g. the Duck experiments; e.g. Mason et al., 1984; Howd and Birkemeier, 1987). The instruments and their application are described in the following paragraphs.

### 3.5 Hydrodynamic data acquisition

Surf zone hydrodynamics vary considerably both in time and space because of changes in the hydrodynamic conditions offshore and the nearshore morphology. The objective of the hydrodynamic measurements was to give an accurate picture of the variation of waves, water levels and currents through the surf zone, relative to offshore hydrodynamic conditions. To this end, hydrodynamic data were gathered at different points along one cross-shore line, using different instruments which, in the surf zone, were attached to poles and a frame.

Table 3.2 Locations of hydrodynamic data sampling (distances and depths are approximated)

Location	Distance to waterline[m]	Water depth [m]	Instrument carrier	Attached instruments
Waterline	0	0	pole	CW, PG
Inner bar	230	1.5	pole	CW, PG, EMF
Outer bar	500	3.0	frame	S4-sensor
outer bar	550	3.5	pole	CW, PG, EMF
offshore	1900	15	buoy	-

CW = capacitance wire

PG = pressure gauge

EMF = electromagnetic flow meter

A field station was built near the dunes to accommodate the computers and the energy supply needed to collect and store the data. In the surf zone, three poles were jettied into the sand serving as a platform for instruments. The ca. 0.70 m diameter

poles were placed near the waterline ('pole 1'), near the inner bar ('pole 2') and near the outer bar ('pole 3'). The main reasons for these locations were that bars were the main subject of study and large gradients in hydrodynamic processes were expected over the two nearshore bars. Finally, a frame was positioned on top of the outer nearshore bar and a Wavec buoy was positioned offshore. The field layout is depicted in Figure 3.7 and summarised in Table 3.2. The instruments and data acquisition are described below.

To measure the offshore wave conditions a WAVEC wave-directional buoy (Datawell) was used to follow the moving water surface and measure its own vertical acceleration, pitch and roll angles and the magnetic field components. The elevation of the water surface and directional information are derived from these measurements. In the surf zone, the wave and water level fluctuations at the poles were measured with two devices: a pressure gauge (PG) and a capacitance wire (CW). The capacitance wire (CW) is highly reliable but may suffer mechanical damage due to floating debris or wave impact. To avoid long periods without recordings, a PG was installed to operate as a back-up sensor. The CW, manufactured by Endress and Hauser, is basically a capacitor. Consisting of two electrodes placed vertically in the water, one of which is a steel cable. The other electrode is the U-frame which holds the steel cable. The CW uses the differences in capacity between water and air as a measure for the water level. The length of the CW is not fixed but may be varied and adjusted to the expected wave and water level fluctuations. The length of the CW at pole 1 was 4 m; that at pole 2 and pole 3, 6 m. The accuracy of the instrument is about 1% of its length. The PG (Keller) had a measuring range of either 0-1000 or 0-2000 mbar with an accuracy better than 0.5%. The instantaneous currents at the poles were measured by electromagnetic flow metres (EMF; Delft Hydraulics). The EMF generates an electromagnetic field around a sphere, which when water flows around it, generates an electric current proportional to the speed of the water flow. The EMF measures the water flow along two perpendicular, horizontal axes oriented in a longshore and cross-shore direction, located several decimetres from the bed. The accuracy of the flow meters is  $0.01 \text{ m s}^{-1}$  (manufacturer's specification). The frame on the outer nearshore bar was equipped with a S4 sensor (Inter Oceans) which is a sphere with a diameter of ca. 0.4 m capable of measuring longshore- and cross-shore currents and pressure.

The calibrations of the CW and PG were performed before and after each field campaign. The CW was calibrated by slowly lowering and raising the water level and simultaneously measuring the output voltage of the CW and the height of the water column, the latter measured with a measuring tape. The voltage was linearly related to the height of the water column by regression analysis. The PG was calibrated using a 'dead-weight tester'. The EMFs were calibrated before and after the field campaigns at Delft Hydraulics, by towing the EMFs at different constant speeds through a tank. The calibration was performed in the range  $0\text{-}2.5 \text{ m s}^{-1}$  and both axes were calibrated independently. The calibration curves are linear and have high ( $R^2 \sim 0.99$ ) correlation coefficients. For the S4-sensor, the manufacturer's calibration coefficients were used.

Hydrodynamic data may be recorded in two ways: by storing the data near the instruments or by transmitting them via cables to the shore. The first method, has however, a number of disadvantages. For instance, it is not possible to monitor the

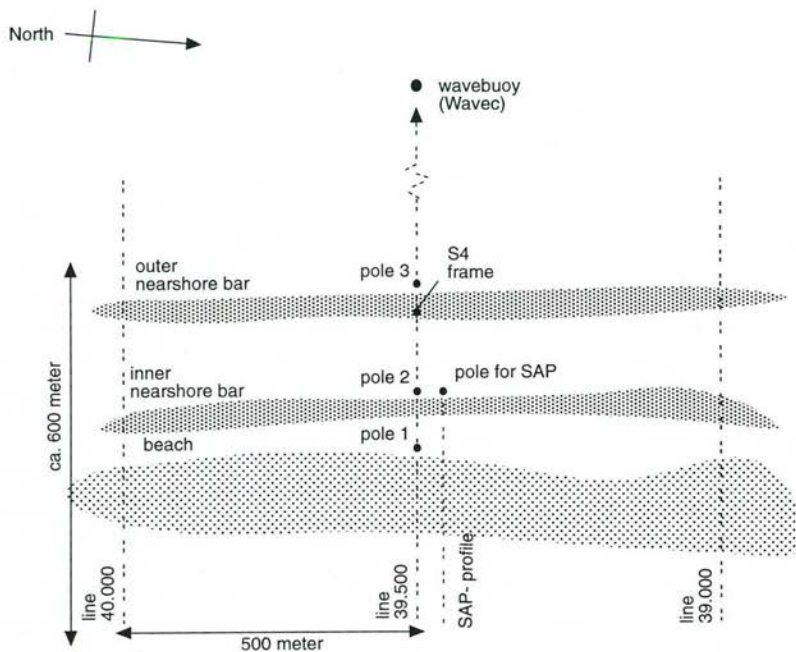


Figure 3.7a Field area showing data acquisition platforms and measuring transections.

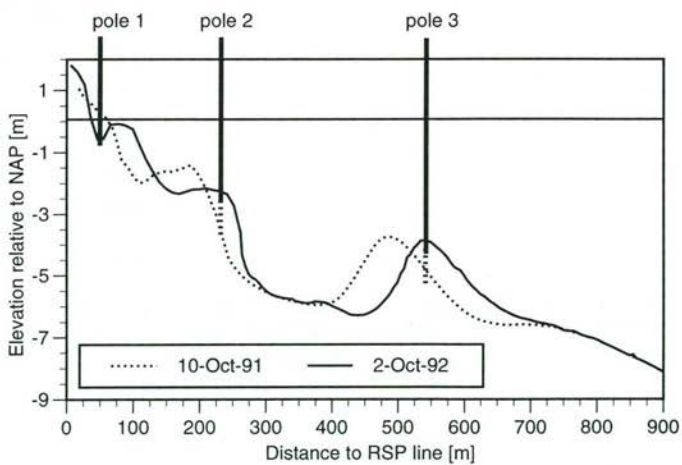


Figure 3.7b Cross-shore profile showing the location of measurements poles.



instruments while they are recording and failure cannot be detected until the instrument is lifted from its position. Moreover, when using high sampling rates, the electric power supply is often incapable of handling storage in an extensive series of multiple instruments over a long period of time. Using cables for data transmission, however, also has a number of disadvantages. First, the installation of the instruments involves higher costs and more manpower. Second, it is often not possible to move the instruments. Hence, once established, the field layout cannot be adapted for use under different conditions or for different purposes. The above considerations, together with the basic demand for reliable monitoring, even during stormy weather, lead to the conclusion that a fixed configuration with cables would be the best option for poles close to the shore. Further offshore, the costs of cables would be too high. It was decided to use radio telemetry to collect data from the outer nearshore (pole 3), thereby avoiding the disadvantages of storing the data near to the instruments. The Wavec data was transmitted to a receiver-coupled computer in Egmond aan Zee, which gathered, tested, processed and stored the incoming data. Some parameters and variables were displayed on-line, on a monitor, enabling direct verification. Data from the S4 sensor, however, were stored locally, near the recording instruments. The data sets from the other instruments were collected and stored in the field station on the beach. Data acquisition of the instruments on the two inner poles was handled by computers in the field station. The logging of the data from pole 3 (outer nearshore bar), was handled by a data logger located in a watertight container on the pole. The data from pole 3 was temporarily stored on the pole and thereafter transmitted at hourly intervals to the field station. This data was also stored on removable hard discs. The data of all poles were synchronised using the central computer in the field station. The sampling characteristics of all instruments are given in Table 3.3.

Table 3.3 Sampling characteristics of hydrodynamic data acquisition

Location	Platform	Data transmission	Instrument	Burst duration [min]	Burst interval [min]	Sampling rate [Hz]
Waterline	pole 1	cable	cw	60	60 <sup>1)</sup>	8 <sup>2)</sup> , 4 <sup>3)</sup>
Waterline	pole 1	cable	pg	60	60 <sup>1)</sup>	8 <sup>2)</sup> , 4 <sup>3)</sup>
Inner bar	pole 2	cable	cw	60	60 <sup>1)</sup>	8 <sup>2)</sup> , 4 <sup>3)</sup>
Inner bar	pole 2	cable	pg	60	60 <sup>1)</sup>	8 <sup>2)</sup> , 4 <sup>3)</sup>
Inner bar	pole 2	cable	emf	60	60 <sup>1)</sup>	8 <sup>2)</sup> , 4 <sup>3)</sup>
Outer-bar	frame	local storage	s4-sensor	40	180	2
Outer bar	pole 3	telemetry	cw	40	60	4
Outer bar	pole 3	telemetry	pg	40	60	4
Outer bar	pole 3	telemetry	emf	40	60	4
Offshore	wavec	telemetry	-	20	30	1.28

1) i.e. continuous sampling

CW = capacitance wire

2) 1991 field campaign

PG = pressure gauge

3) 1992 field campaign

EMF = electromagnetic flow meter

### 3.6 Sediment transport data acquisition

The aim of the sediment-transport measurements was to obtain a detailed data set of the hydrodynamics and the resulting sediment dynamics. It was decided, therefore, to concentrate the sediment-transport measurements at one location. The location

chosen was the beach face because there, it is possible to measure nearly all the variables that are important for sediment transport, such as, for example, the height of the instruments above the bed. Often these variables can not, or only with low spatial or temporal resolution, be measured in deeper water. A (scaffold) platform was built to house the instruments, and the power and logging devices. This was the so-called Beach based Electronic Registration Tower (BERT).

The BERT is a movable platform 2.5 m in length, 2.5 m in width and 2.5 m in height. The working platform is located about 2 m above the local bottom (Photo 3.1) and the instruments are attached to vertically adjustable poles situated at the sea facing front of the BERT. The instruments attached at the front end are: one capacitance wire (CW), three electromagnetic current metres (EMF), four optical backscatter sensors (OBS), ten intake nozzles connected with suspended sediment pumps and a bedload sampler (BS). Before starting a series of measurements, the BERT was located near the waterline during low tide. As the BERT was movable, the location could be carefully chosen with respect to morphological and Hydrodynamic characteristics of the inter-tidal beach (e.g. rip currents) which could influence the measurements. The wheels were then removed and the BERT was positioned on four runners (metal plates). Measuring sessions were performed during the rising and successive falling of the tide, each session lasting about 1 hour. After the falling water level had reached a position in which one or more of the instruments were above water level, the BERT was pulled onto the beach using a winch.

The CW and the EMF were of the same type as those used on the poles. The CW, 2 m in length, was placed on the BERT to record the local free water surface elevations. The three EMFs, measuring longshore and cross-shore velocities, were located at approximately 0.1, 0.3 and 0.7 m above the local bed. The desired height was achieved by lowering and lifting the pole to which the EMFs were attached. This adjustment was repeated at the beginning of each session, minimising the influence of possible erosion or accretion on the relative elevation of the EMFs. The calibration of the CW and the three EMFs was carried out in the same way as the CW and EMFs on the poles. The four OBSs (D&A instruments) measuring the instantaneous suspended sediment concentration, were located at heights of 1.5, 6.5, 11.5 and 21.5 cm above the lowest intake nozzle, transmitting infra-red signals and measuring the radiation scattered by the suspended matter. The amount of radiation is a measure for the amount of suspended matter. The sensors were located near the intake nozzles of the pump sampling system (Fig. 3.8) and attached to the same vertical adjustable pole. This pole was also used for re-establishing the desired height of the nozzles and OBSs at the beginning of each session. The OBSs were calibrated in a specially designed calibration tank at Utrecht University (see van de Meene, 1994).

The pump sampling system, driven by eight pumps on the platform, was used to determine the time-averaged suspended sediment concentration. These pumps were connected to eight intake nozzles in a vertical array (Fig. 3.8). The time-averaged suspended sediment concentrations were determined by pumping the water (with sediment) into buckets also positioned on the platform. When the 10-litre buckets were full, the pumps were stopped, the exact volume of water was determined and then poured off. The sediment was collected in calibration tubes where its dry mass could be determined. Thereafter, the suspended sediment samples were preserved and used for determining the fall velocity and other sediment characteristics.





Photo 3.1 Beach-based Electronic Registration Tower (BERT).



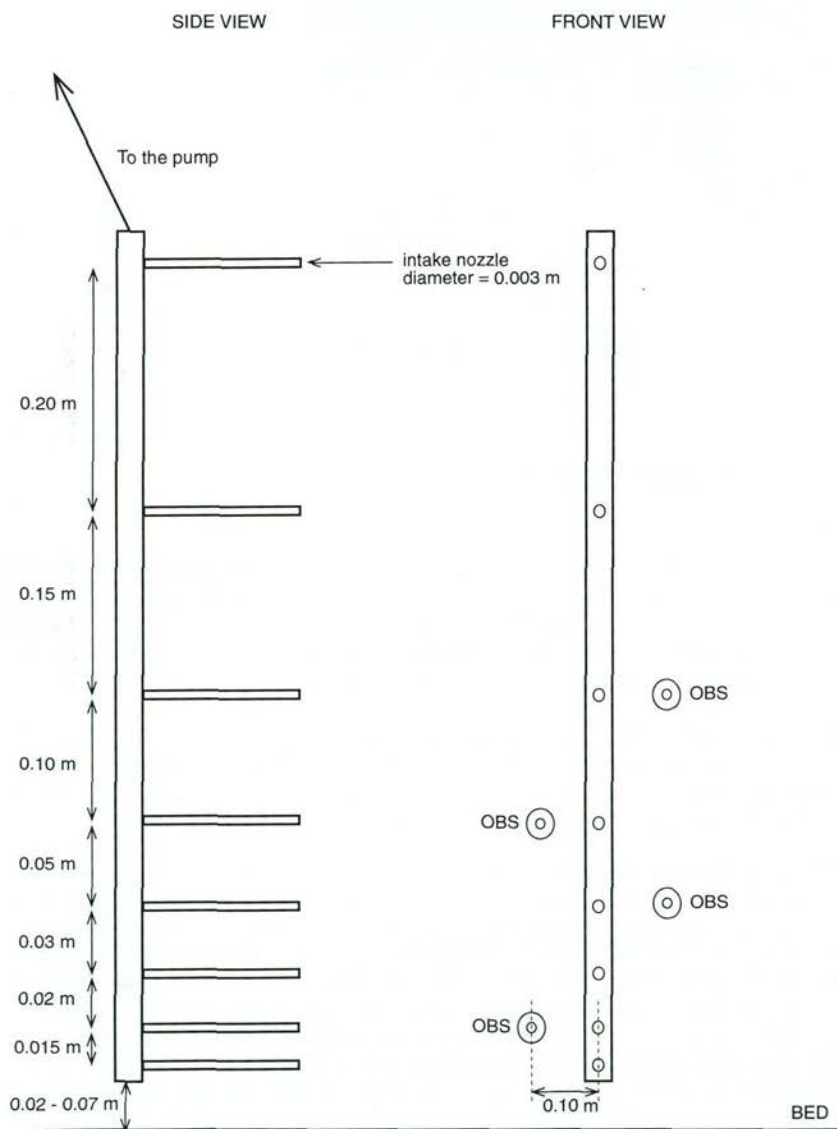


Figure 3.8 Arrangement of the intake nozzles of the pump sampler and the OBSs on the BERT.



Photo 3.2 Bedload sampler as used in the field.

The time-averaged bedload transport rate was determined using a bedload sampler consisting of an aluminium intake opening (0.093 m width and 0.044 m height) connected to a nylon bag with a mesh size of 150  $\mu\text{m}$  (Photo 3.2). The sampler was connected to a steel bar used to position it on the bottom. The steel bar could be mounted into two holding sockets while measurements were being taken.

The power supply, data acquisition and data storage facilities were located on the BERT. Data sampling and storage of the electronic instruments were operated by a datalogger with a memory module (Campbell, CR10). Power to operate the instruments and logger (12V/24V) was supplied by four accumulators.

At the beginning of each session, the CW, EMFs, OBSs and pump sampler were started synchronously. The sampling of the electronic instruments lasted 40 minutes and about 20 minutes was needed with the pump sampler to fill the buckets. During the operational time of electronic instruments and the pump sampler, a number of the bedload transport measurements were executed. Bottom samples were also taken and the breaker type determined. After the electronic instruments had finished recording, the amount of erosion or accretion near the EMF and OBS was determined using a vertical movable rod. Thereafter, the instruments were raised and visually inspected before being lowered again to start the next session. Each session lasted about an hour while the total number of sessions was commonly 4-6. After a number of sessions, the BERT was pulled out of the water, the memory modules were removed from the platform and the data was transferred to a computer. All sampling characteristics are summarised in Table 3.4.

Table 3.4 Sampling characteristics of sediment transport data acquisition

Instrument	Burst duration[min]	# of bursts in one session	Sampling frequency[hz]
CW	40	1	4
EMF	40	1	4
OBS	40	1	4
Pump	~20	1	continuous
Bedload	~3	~6	continuous

CW = capacitance wire

EMF = electromagnetic flow meter

OBS = optical backscatter sensor

### 3.7 Morphological data acquisition

The objective of the morphological data acquisition particularly for the beach and the inner nearshore bar, was to reveal the nature of the morphological changes. In addition, the reaction and response times of the beach and inner nearshore bar had to be determined. Because of variations in the reaction and response times, the intensity and the equipment used for morphological monitoring, varied cross-shore. The frequency of the morphological surveys was further determined by wave and weather conditions. Monitoring nearshore morphology during storms, for example, is extremely difficult and thus is only possible using techniques that can withstand storm conditions but nevertheless give reliable results. Finally, the increase in depth, in a cross-shore, and offshore direction, requires different techniques leading to different approaches for surveying the beach, the inner nearshore and the outer nearshore.

Beach profiles extending from the dune foot to the low-water line and regularly spaced over the one-km longshore section (Figure 3.9) were surveyed at frequent intervals during the field campaigns. The profiles were levelled using a Zeiss Elta 20 total station, a Polartrack total station, Depth-Of-Activity-Rods (DOAR) and (occasionally) an optical levelling instrument.

The Zeiss Elta 20 surveying instrument was used together with a triple prism unit on a stake, and is capable of measuring and recording single points. All angles and distances are internally stored and later transferred to a PC for calculating X, Y and Z values of the measured points. The Polartrack total station operates like the Elta 20 except that it is self-tracking and is directly linked to a PC. This means that the hand-held prism is constantly followed by the Polartrack and a continuous profile is obtained which is stored on-line, on disk. DOAR were used to survey the beach along several cross-shore lines because they make it possible to monitor the beach in detail and with high accuracy, high temporal resolution and little man effort. DOAR (see Greenwood and Hale, 1980) are rods with a length of 1 m and a diameter of 0.005 m. placed vertically in the bed with the assumption that this vertical position will remain constant. The elevation of the beach is measured from the top of the rod. Hence, the distance between the top of the rod and the bed, measured during successive days, gives a time-course of the local elevation changes. If, during one or more days, the bed elevation at the DOAR is measured with a levelling instrument, relative to a certain elevation date (i.e. NAP), the absolute elevation changes can be determined. The net elevation changes along a complete cross-shore profile may be determined by placing a number of DOAR in a cross-shore array. By using a washer, DOAR are



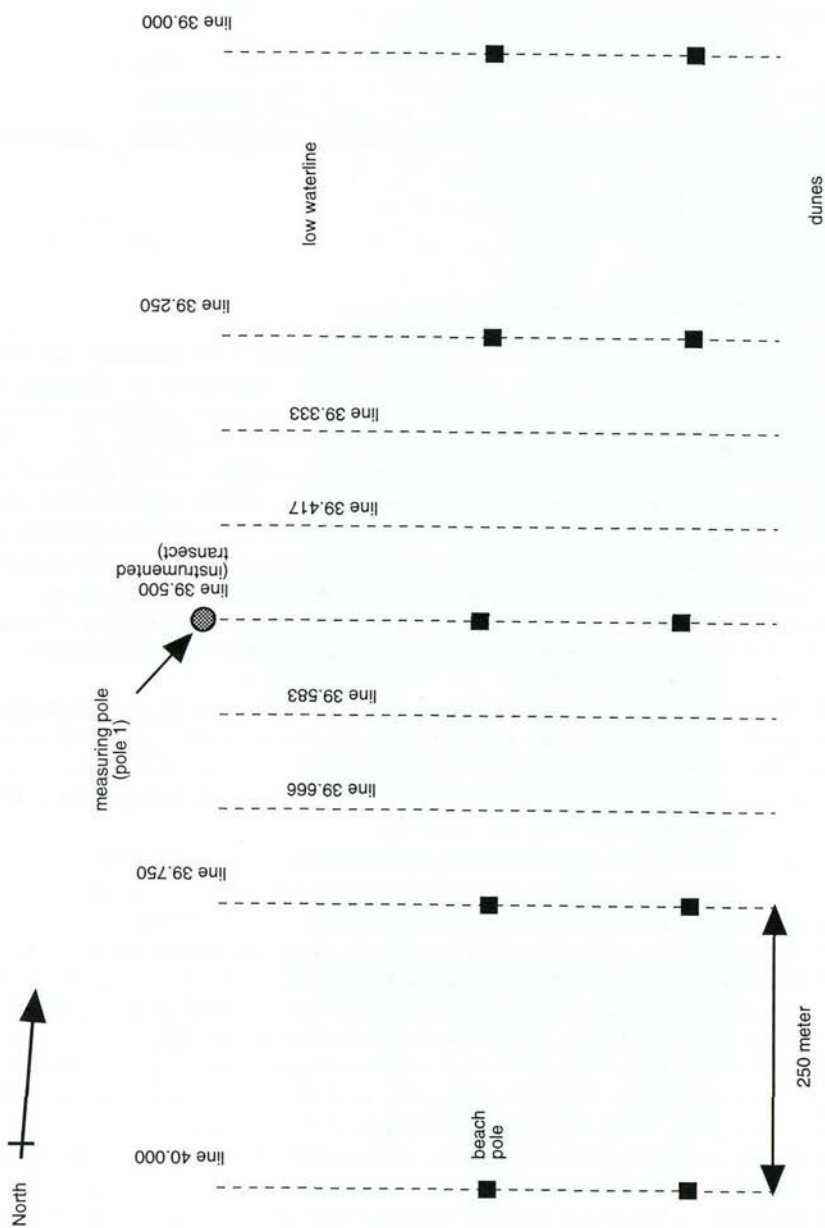


Figure 3.9 Beach profiles surveyed.

also capable of determining the gross elevation changes, but these are outside the scope of this study.

The vertical accuracy of the total stations is about 0.01 m in elevation and 0.1 m in position. The DOAR measurements have a vertical accuracy of 0.005 m and a position accuracy of 0.05 m. The optical levelling instrument has an accuracy of about 0.005 m in elevation and 0.025 m in position.

The inner nearshore measurements should reveal the morphological behaviour of the inner bar. As 'normal' geodetic survey procedures cannot be applied during storms, a sea-sledge was designed to monitor the inner bar. One cross-shore profile was surveyed with this sledge, the so-called Sub-Aquatic Profiler (SAP). The cross-shore profile was located 50 metres north of beach line 39500 (see Fig. 3.7), incorporating the lower beach and part of the inner nearshore bar. The SAP is a 3 x 2.5 x 1.2 meter sledge with a 7 metre long mast (Photo 3.3) weighting about 220 kg, the mobility of which is ensured by four wheels. Although the term 'sledge' is used, the use of wheels, instead of runners, minimises bed disturbance and -friction. One watertight PVC cylinder, containing two inclinometers and a compass, is placed on the SAP and a second watertight cylinder with a logger and batteries is attached crosswise. The position of the SAP is obtained by pointing an electronic survey instrument at a reflector at the top of the mast. This position is then adjusted for the longitudinal and transverse tilt of the SAP with the inclinometer values. The logging of the inclinometer values is controlled by a measuring wheel under the SAP. The SAP is pulled back and forth through the surf zone by a capstan (attached to a tractor) and a cable in a closed loop between the capstan and two pulleys, one of which is attached to a beach pole and the other to a pole in the surf zone (Figure 3.10).

During the field measurements in 1991 and 1992, the position of the SAP was obtained by using three electronic surveying instruments: a Zeiss Elta 20, a Polartrack and a Geodimeter 140T. The first two instruments are described above. The Geodimeter 140T is comparable with the Polartrack in operation and accuracy. Extensive trials with the SAP during April 1991 revealed that the horizontal accuracy is in the order of dm's and the vertical accuracy 0.05-0.1 cm, depending on the hydrodynamic conditions (Wolf, 1991).

The outer nearshore zone was surveyed by vessels equipped with echosounders. This inferred, however, that the outer nearshore could only be surveyed during quiet weather conditions.

The hydrographic survey consisted of cross-shore survey lines between beach poles 39.000 and 40.000. The spacing of the survey lines was 100 m between 39.250-39.750 and 250 metres between 39.000 - 39.250 and 39.750-40.000. The seaward limit of the survey lines was -15m NAP. This rather deep limit was chosen because the surveys were also used for other means. The landward limit was the inner bar (~ 1.5 m depth). The vertical accuracy of the sounding profiles is about 0.2 m and the position accuracy about 7.5 m.

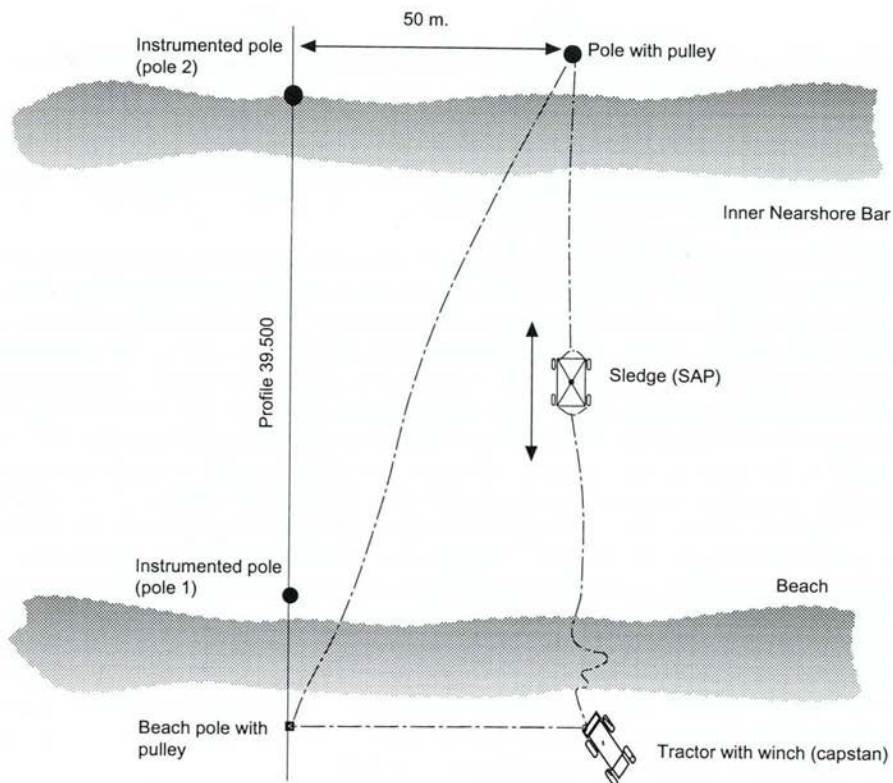


Figure 3.10 Field lay-out of Sub-Aquatic Profiler (SAP)



Photo 3.3. Sub-Aquatic Profiler (SAP) positioned in front of Tractor with winch.



## 4. HYDRODYNAMICS OF BREAKING AND SHOALING WAVES

### 4.1 Introduction

The central aim of this thesis is to understand the relation between inner nearshore bar developments and the hydrodynamics and sediment transports associated with the shoaling and breaking of high-frequency waves. This chapter concerns the hydrodynamics and the following research questions will be addressed (see chapter 2):

- what is the relative contribution of high-frequency versus low-frequency oscillations under different hydrodynamic conditions?
- how do the wave dimensions and wave shape vary as a function of the position in the surf zone, i.e. in non-breaking waves, breaking waves and swash?
- which wave theory can describe the observed wave transformations?
- how does the velocity field, especially the absolute and relative importance of wave asymmetry versus undertow, vary under waves around a breakpoint?

This chapter has the following outline. First, methods used to analyse the hydrodynamics of surface waves are discussed, followed by results. Second, hydrodynamics of the velocity field under shoaling and breaking waves are analysed. Finally, the results of these analyses are synthesised and the research questions are addressed.

The sediment transport measurements were not performed at the inner nearshore bar nor were they continuously carried out. To make the results of the sediment transport analysis applicable to the inner nearshore bar development, the results of the hydrodynamic analysis are related to the relative wave height ( $H_s/h$ ). This parameter appears to be useful in describing hydrodynamic and sediment transport phenomena in the inner nearshore zone (Kroon, 1994).

### 4.2 Environmental conditions during measurements

The data were obtained using the Beach based Electronic Registration Tower, the BERT (see Section 3.6) and measurements were taken from 23 October to 10 November 1992 (Section 4.3). It was rather rough weather during this period as can be seen from the offshore wave heights, varying between 0.5 and 2.5 m (Fig. 4.1). Note that as the Wavec buoy malfunctioned during the November measurements, the offshore wave height for November was estimated using a linear regression line between the pole 3 measurements and the WAVEC measurements in October. Apart from two series with non-breaking waves, the waves broke on the inner nearshore bar, or on the outer nearshore bar, or both, before reaching the BERT. Hence, the waves present near the BERT were mostly reformed waves. The measurements on the BERT registered non-breaking waves, breaking waves and swash. In fact, during nearly all measurements, breaking waves were present near the BERT. The position of the break point, however, shifted from the seaward side of the BERT (swash), to near the BERT (breaking waves) and finally to the landward side of the BERT (non-breaking waves). The shifting of the breaker line was induced by the vertical tide (Fig. 4.2).

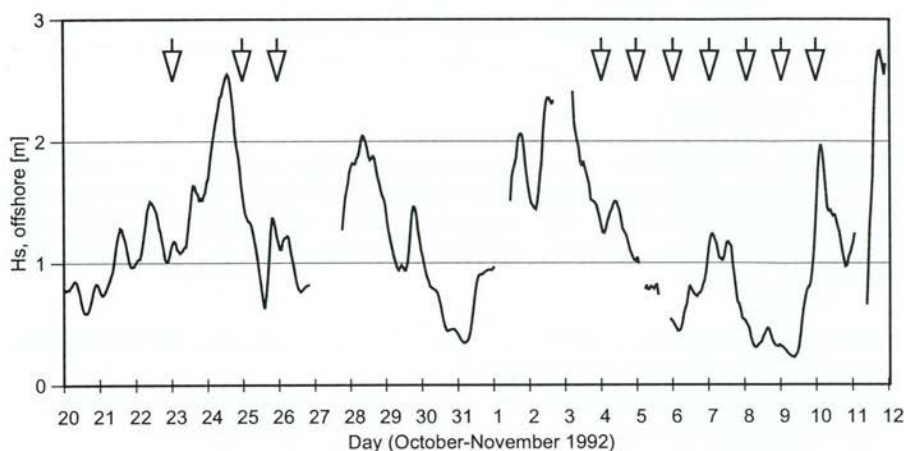


Figure 4.1 Offshore significant wave height ( $H_{s, \text{offshore}}$ ) in October-November 1992. Arrow indicates day on which measurements with the BERT were taken.

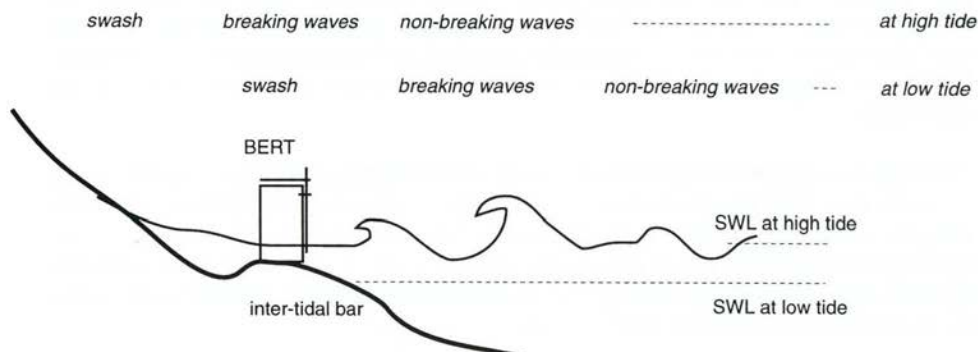


Figure 4.2 Hydrodynamic zonation in the inner nearshore and the lateral shift of the zones due to the tide.

All measurements were taken on top or at the seaward side of an inter-tidal bar, located near the low tide mark (Fig. 4.3). The profiles reveal that the shape and the volume of the inter-tidal bar near the BERT varied during the investigation period, one reason being that the BERT was positioned at different sites along the coastline while the characteristics of the bar also change along the coast. A second important reason is the changing hydrodynamic conditions during succeeding days of the measuring period and the resulting morphological changes, not only in the inter-tidal bar but also for the seaward boundary, i.e. the location and shape of the inner nearshore bar (Chapter 6). The elevation of the base of the BERT was around 0 m NAP and this varied less than 0.4 m. NAP is the Dutch Ordnance Level, which is about equal to mean sea level (MSL).

No signs of small bedforms (e.g. ripples) were found near the BERT either before or after a series of measurements and no bedform monitoring was performed during the measurements. The observed orbital velocities were  $0.6 - 1.3 \text{ ms}^{-1}$ ; the sediment

diameter ( $D_{50}$ ) was circa 350-400  $\mu\text{m}$ . These values and the bedform classification of Allen (1982, in Van Rijn, 1993) indicate that, for most of the time, a flat bed must have been present.

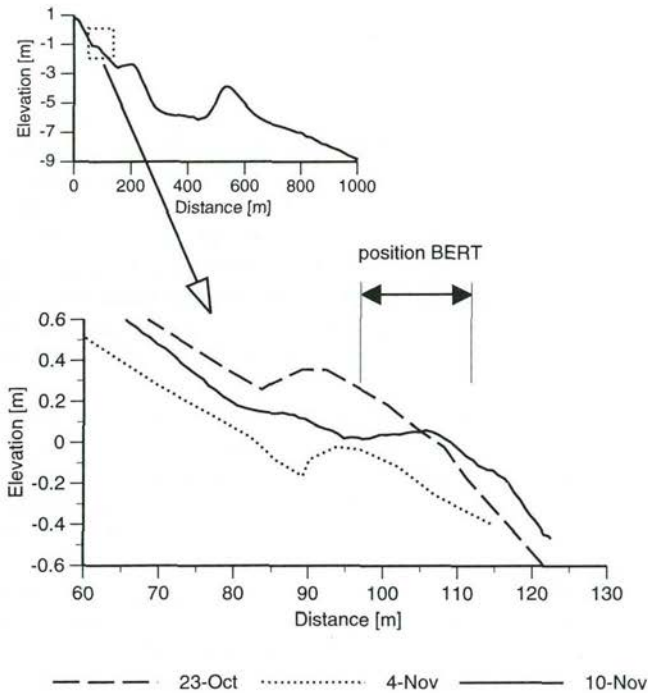


Figure 4.3 Nearshore profile and beach profile (1992) with the range of cross-shore positions of the BERT.

Table 4.1 Daily averaged  $D_{50}$  values from bottom samples near the BERT

Date	Median grain size, $D_{50}$ ( $\mu\text{m}$ )
23-Oct-1992	406
25-Oct-1992	355
26-Oct-1992	366
04-Nov-1992	349
05-Nov-1992	418
06-Nov-1992	423
07-Nov-1992	370
08-Nov-1992	348
09-Nov-1992	347
10-Nov-1992	400



Sediment samples of the bed were taken during all measurements. The  $D_{50}$  values were determined in a settling tube. At least three samples, each taken during different measurement sessions, were used to calculate the daily averaged values. The grain size shows large variation, although all samples were collected on the seaward side of the inter-tidal bar (Table 4.1).

#### 4.3 Data validation and calibration

Fifty six measurement sessions were carried out over a period of 14 days. Before using the recorded time-series of the electronic instruments, i.e. the capacitance wire (CW), electromagnetic flow meters (EMF) and optical backscatter sensors (OBS), recorded in each session, the instruments were first inspected to see if they had recorded relevant data. If two of these instruments were found not to be working correctly then the results of the entire session were excluded from further analysis. The remaining 47 sessions were analysed by examining the time-series for overflow values and spikes. An overflow value is a value beyond the measuring range. A spike is defined as a value that differs from the previous value in such a way that the gradient  $\Delta V/\Delta t$  is larger than 4. The value  $\Delta V$  is the difference in value and the  $\Delta t$  is the sample period.

The CW series did not show any overflow values or spikes. Therefore none of the recorded CW series was excluded from further analysis. The EMF series, however, showed variations in overflow values of between 0 and 10 per cent and in the number of spikes of between 0 and 600. One of the main causes for the presence of overflow values is that the sensor is temporarily above water level. Thus the highest percentage of overflow values were recorded at the highest EMF. The highest percentage of spikes was also found at the highest EMF because these may also be caused by the entrainment of air bubbles in the water due to breaking waves. The entire session was rejected if more than two of the time series taken during a session had more overflow values or spikes of more than 1 per cent. Another 9 series of measurements were rejected from further analysis, bringing the total number of validated sessions to 38. The overflow values and spikes in the time series of the remaining 38 sessions were replaced by the mean of the previous and next value. If there were two or three overflow values in a row, these were replaced by the mean of the values on both sides of the range of overflow values.

The CW was calibrated before the field campaigns. The hardware and software were adjusted in such a way that the offset was zero and the gain equal to unity. The EMF was calibrated both before and after the field campaign. The EMF calibration curves were forced through zero so that only their (linear) slope are of importance. The averaged value of both calibrations is used in the analysis of the EMF data. The EMF calibration coefficients are summarised in Table 4.2

Table 4.2 Calibration coefficients EMF (BERT) before and after field campaign, and used in data analysis

	calibration coefficients (m/s/V)					
	before		after		used	
sensor	x-axis	y-axis	x-axis	y-axis	x-axis	y-axis
EMF <sub>10</sub>	0.9685	0.9658	0.9829	0.9783	0.9757	0.9721
EMF <sub>30</sub>	0.9483	0.9535	0.9571	0.9637	0.9527	0.9586
EMF <sub>70</sub>	0.9750	0.9537	0.9650	0.9531	0.9700	0.9534

Subscript of EMF denotes height (in cm) above the bed.

## 4.4 Analysis of wave hydrodynamics

### 4.4.1 Analysis and interpretation methods

#### *general hydrodynamic conditions*

The general hydrodynamic conditions are characterised by determining the following variables and parameters

- significant wave height ( $H_s$ )
- significant wave period ( $T_s$ )
- mean water depth ( $h$ )
- relative wave height ( $H_s/h$ )
- significant wave steepness ( $H_s/L_s$ )
- breaker type
- percentage of breaking waves

These variables have been chosen because they are thought to be important for the direction and magnitude of the sediment transport. The first five parameters were computed using a 40 minute time series while the final two parameters were determined over 5 minutes (300 s).

#### *wave asymmetry*

Waves approaching the coast are subject to a shoaling process which causes the waves to deform. The wave shape changes from a symmetrical form into a wave with a relatively short, high crest and a shallow, wide trough. This asymmetrical wave shape induces asymmetry in the near-bed velocities. When averaged over a wave cycle, the asymmetry of the velocities leads to a net sediment transport because of the non-linear velocity-transport relationship (e.g. Shi and Larsen, 1984; Doering, 1988).

In fact, asymmetry may result from a difference in either the duration or the magnitude of onshore movement versus the offshore movement or by a combination of both. Consequently, both the asymmetry in amplitude and in duration have to be evaluated. The asymmetry in amplitude is defined as :

$$A_{a,\eta} = \frac{\eta_{crest}}{\eta_{crest} + \eta_{trough}} \quad (4.1)$$

$\eta_{crest}$  = elevation of the wave crest relative to Still Water Level (SWL) [m]

$\eta_{trough}$  = elevation of the wave trough to SWL [m]

$A_{a,\eta}$  = amplitude asymmetry of the surface-waves [-]

The asymmetry in duration is defined as:

$$A_{d,\eta} = \frac{T_{crest}}{T_{crest} + T_{trough}} \quad (4.2)$$



- $A_{a,\eta}$  = duration asymmetry of the surface-waves [-]  
 $T_{crest}$  = time interval between a zero up crossing and the next zero down crossing [s]  
 $T_{trough}$  = time interval between a zero down crossing and the next zero up crossing [s]

The asymmetries are 'significant' because they are calculated using the highest one-third of the waves in each time series. To detect individual waves, the time series have to be demeaned by applying one or other of the two following methods. In the first method, the entire time series is used to calculate a second-order polynomial by using a least squares solution. However, in the nearshore zone, waves with an amplitude asymmetry occur rather frequently. In asymmetric waves, though, the amplitude of the crest is higher than that of the trough. Hence, the polynomial used to remove the trend will be dominantly affected by the wave crest instead of the crest and trough having equal influence. To use this a priori knowledge of asymmetric waves, a second method to calculate the polynomial was applied which divides the time series into twenty subseries and then calculates their mean values in order to determine a second-order polynomial. In either method, once the time series have been de-meaned, a zero down crossing method is used to detect individual waves.

A further point of consideration is how to calculate the amplitude and duration asymmetry. The series-averaged asymmetry can be determined by calculating the asymmetry for each individual wave and thereafter averaging the individual asymmetries. A second method is to average the crest height (crest duration) and trough heights (trough duration) over all waves and then to calculate the amplitude asymmetry.

The above mentioned calculation methods were applied to all measured time series but only small differences ( $<0.01$ ) were found using any combination of demeaning and asymmetry calculation and the linear regression coefficients between all methods were high ( $r^2 \sim 0.95$ ). It was decided to calculate the asymmetries using the first-mentioned de-meaning procedure and the time-averaged values of the trough and crest.

#### *shape of the surface-waves*

Wave shape may be described using various wave theories but first an average wave shape is calculated to test the applicability of these theories for breaking and shoaling waves. By calculating an average wave shape, it is also possible to examine to what extent wave asymmetry reflects the wave shape. The average shape is determined using Houwman and Hoekstra's (1994) approach, as follows:

1. Apply high pass ( $T < 20$  s) filtering of the original time series to make an individual wave detection possible.
2. Select the highest one-third section of all recorded waves.
3. Calculate a spline function, i.e. a piecewise polynomial which passes exactly through all points, for each individual wave selected. Normalise this spline function by using the positive maximum elevation and calculate for every one-hundredth part of each wave.
4. Calculate the mean value and standard deviation of each of the 100<sup>th</sup> parts.
5. Normalise the mean wave shape again because individual differences cause the crests of all waves not to coincide exactly.



#### *wave spectra*

Spectra of the surface-wave elevations reveal the distribution of wave energy over the different frequencies. Through spectra the potential and relative contribution of infragravity and incident wave energy to sediment transport can be examined. Moreover, energy peaks can be isolated and their importance recognised for revealing the processes responsible for sediment transport.

Spectra were calculated using a discrete Fourier transform method. A cosine taper was used in the time domain and a Hanning filter in the frequency domain. The series were divided into 36, partly overlapping, sub series of 512 points in which each subseries starts half way along the previous subseries. The Nyquist frequency is 2 Hz and the degree of freedom is about 95.

#### *low-frequency waves*

Recent observations in the nearshore zone have shown that infragravity waves often dominate the spectrum. These infragravity motions can be correlated to suspension events (e.g. Shi and Larson, 1984; Hanes, 1991) and thus have an important impact on sediment transport. To evaluate the differences between the gravity and infragravity part of the spectrum, the time series were high-pass (HP) and low-pass (LP) filtered. The cut-off frequency used was 0.05 Hz because the spectral density is often low around this frequency (see Agaard, 1990; Kroon, 1994).

#### *hydrodynamic zones and parameterisation*

Research on wave hydrodynamics in the nearshore has identified regions of different hydrodynamic properties associated with shoaling and wave breaking (e.g. Miller, 1976; Basco, 1985; Larson and Kraus, 1989). These regions are distributed around a breakpoint and are often defined as a non-breaking zone (seaward of the breakpoint), a breaking zone and a swash/bore zone (landward of the breakpoint (Fig. 4.2). Kroon (1994) found that these zones can be determined using the relative wave height ( $H_s/h$ ) as a steering parameter. A low relative wave height was found in the non-breaking zone while in the swash/bore zone higher values were observed. The observations made in this study lead to the determination of five hydrodynamic zones:

1. a non-breaking wave zone: waves do not break but may be subject to shoaling processes;
2. a (non) breaking wave zone: waves may either break or may pass unbroken;
3. a breaking zone: waves may either break or may pass unbroken and the plunge point of the breaking waves passes the instrument location during the session;
4. a breaking/swash zone: waves may either break or pass as swash, i.e. a uprush of water on the beach;
5. a swash zone: all waves are broken and pass this zone as swash.

Breaking waves are defined here as waves showing foam at the crest of the wave. The plunge point is the location where either the amount of foam reaches its highest volume (spilling breaker) or the wave curls over (plunging breaker). Note that after a wave has broken, it is here denoted as 'swash'. Where the water depth is several decimetres, the broken wave may be better compared with a bore, i.e. a broken wave with an abrupt front and almost no curvature of the water surface after the wave crest. To study if each of these hydrodynamic zones shows specific hydrodynamic features, the results of all analyses are related to the relative wave height.

#### 4.4.2 Results and discussion

##### *overview of wave conditions*

The series averaged values of the general hydrodynamic conditions present during the validated measurements are summarised in Table 4.3. The general hydrodynamic conditions during the measurements can be described as follows:

- $H_s$  = 0.29 - 0.98 m
- $T_s$  = 4.8 - 8.3 s
- $h$  = 0.65 - 1.95 m
- $H_s/h$  = 0.16 - 0.72
- $H_s/L_s$  = 0.040 - 0.087
- breaker type = spilling and plunging
- percentage of breaking waves = 5 - 93 %

Several trends between these parameters and variables can be observed. Steeper waves occur as the depth increases (Fig. 4.4) although there is no clear correlation between wave steepness and the hydrodynamic zones. Nevertheless, the expected trend, i.e. that wave steepness is reduced during the breaking processes, is visible: the highest wave steepness is found in the (non) breaking and breaking zone, the lowest in the breaking/swash and swash zone.

Another trend is visible in the correlation between the relative wave height and the hydrodynamic zones (Fig. 4.5). Low relative wave heights occur during non-breaking conditions. However, if the relative wave height increases then the wave conditions gradually change from non-breaking to (non) breaking to breaking and finally to swash.

The results depicted in Figure 4.5 indicate that all waves are broken when  $H_s/h \sim 0.72$ . The mean value of  $H_s/h$ , using the breaking and (non) breaking wave data, is about 0.55. The scatter is large, suggesting that there are other factors besides water depth that control wave breaking. The mean value is about 25 per cent lower than the most commonly used value of individual waves  $H_b/h_b = \gamma_b = 0.78$ , where  $H_b$  and  $h_b$  represent breaker height and breaker depth respectively (McCowan, 1894). Other studies have also shown that the relative breaker heights for irregular waves (field conditions) are lower than those for regular waves (Guza and Thornton, 1981; Mizuguchi, 1992).

Two different breaker types were observed, namely plunging breakers and spilling breakers. During most of the measuring sessions, however, both breaker types were simultaneously present and they were observed more than once to be present along one wave crest at the same time. It was not surprising, therefore, that the breaker type was found to be unrelated to the relative wave height. The Iribarren parameter (Battjes, 1975), commonly used to determine the breaker type, was tested against the observations. However, no clear correlation between this parameter and the observed breaker type was found. The lack of criteria to distinguish spilling breakers from plunging breakers may influence the analysis of sediment transport (Chapter 5) as the breaker type largely affects the amount of sand brought into suspension (e.g. Nielsen, 1982). In addition, other criteria are either unable to distinguish plunging from spilling breakers under field conditions (Weishar and Byrne, 1976, in Carter, 1988), or they classify the breaker type subjectively (Cowell, 1982; Horikawa, 1988).



**Table 4.3** Hydrodynamic conditions from inner nearshore measurements

Series	h	H <sub>s</sub>	T	H <sub>s,o</sub>	tidal phase	wave conditions	breaker type	breaking waves	H <sub>s</sub> /L <sub>s</sub>
	[m]	[m]	[s]	[m]	[-]	[-]	[-]	[%]	[-]
2310-1	0.65	0.43	6.91	1.21	rising	swash	-	-	0.055
2310-2	1.33	0.87	6.37	1.65	rising	breaking	plunging	61.2	0.072
2310-3	1.34	0.90	6.72	1.66	HW/falling	breaking	plunging	70.1	0.071
2310-4	1.23	0.81	6.90	1.74	falling	breaking	plunging	82.6	0.065
2310-5	1.03	0.73	7.36	1.73	falling	breaking	plunging	74.6	0.057
2510-2	1.95	0.32	5.78	0.57	rising/HW	non breaking	-	0.0	0.056
2510-3	1.85	0.29	5.15	0.45	HW/falling	non breaking	-	0.0	0.056
2610-1	0.77	0.53	7.08	0.74	rising	swash	-	-	0.058
2610-2	1.57	0.66	6.11	0.76	rising	(non) breaking	plung/spill	3.4	0.069
2610-3	1.31	0.73	6.06	0.81	HW/falling	(non) breaking	plung/spill	32.8	0.071
0411-1	0.87	0.49	8.04	1.73	rising	swash	-	-	0.043
0411-2	1.21	0.66	7.72	1.87	rising	breaking	plung/spill	84.9	0.051
0411-3	1.40	0.72	7.73	1.90	rising/HW	breaking	plunging	82.6	0.053
0411-4	1.37	0.70	7.71	1.64	HW/falling	breaking	plung/spill	84.6	0.052
0411-5	1.24	0.60	8.19	1.55	falling	breaking	plung/spill	x	0.046
0411-6	1.05	0.47	8.28	1.61	falling	breaking	spilling	93.1	0.040
0511-1	1.00	0.64	7.04	1.13	rising	swash	-	-	0.060
0511-2	1.20	0.74	6.52	1.25	rising	breaking	plung/spill	84.9	0.065
0511-3	1.20	0.72	6.51	1.10	falling	breaking	plunging	82.6	0.065
0511-4	1.08	0.67	6.73	x	falling	breaking/swash	plunging	84.6	0.061
0511-5	0.89	0.58	6.77	x	falling	breaking/swash	spilling	85.7	0.056
0611-1	0.97	0.57	6.98	1.13	rising	breaking	spilling	91.8	0.056
0611-2	1.50	0.81	5.81	1.18	rising	breaking	plung/spill	71.2	0.079
0611-3	1.58	0.81	5.90	1.22	HW/falling	(non) breaking	plung/spill	64.1	0.078
0611-4	1.42	0.72	5.68	1.06	falling	(non) breaking	plung/spill	69.1	0.075
0611-5	1.25	0.63	5.68	1.08	falling	breaking	spilling	85.7	0.069
0711-1	1.06	0.68	6.64	1.52	rising	swash	-	-	0.064
0711-2	1.61	0.88	6.26	1.60	rising/HW	breaking	plunging	35.5	0.075
0711-3	1.57	0.84	6.24	1.52	falling	breaking	plunging	50.8	0.073
0711-4	1.29	0.68	6.31	1.41	falling	breaking	plunging	x	0.065
0811-1	1.25	0.76	8.23	0.80	rising	breaking	plung/spill	53.3	0.055
0811-2	1.62	0.80	8.20	0.93	HW/falling	(non) breaking	plunging	62.7	0.056
0811-3	1.43	0.79	8.06	0.87	falling	breaking	plung/spill	78.0	0.056
0911-1	1.54	0.56	4.77	0.72	rising	(non) breaking	plung/spill	36.0	0.084
0911-2	1.58	0.74	5.12	0.96	rising/HW	(non) breaking	plung/spill	10.4	0.087
0911-3	1.47	0.74	5.70	1.13	falling	(non) breaking	plung/spill	23.1	0.077
1011-1	1.36	0.98	7.36	1.63	rising	swash	-	-	0.065
1011-2	1.69	0.97	7.22	1.58	HW/falling	breaking	plung/spill	19.4	0.069

= not applicable

h=depth

H<sub>s,o</sub>=significant offshore wave height

x = not measured

H<sub>s</sub>=local significant wave height

L<sub>s</sub>=local significant wave length

T = wave period



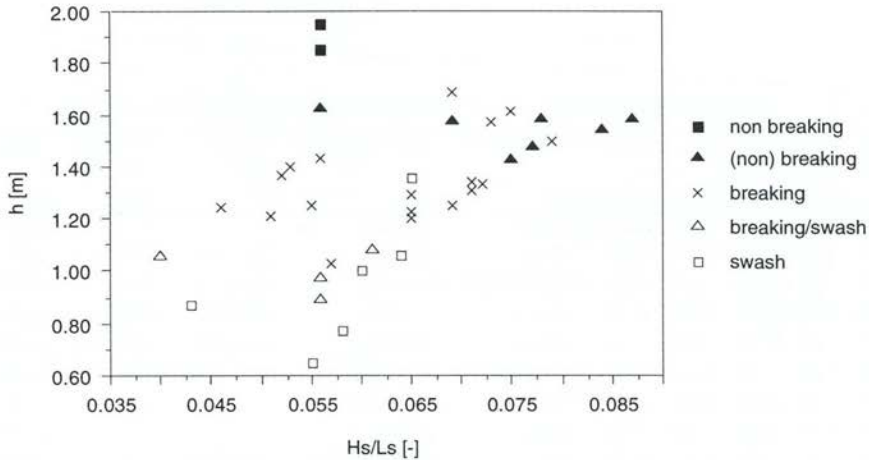


Figure 4.4 Relation between wave steepness ( $H_s/L_s$ ), water depth ( $h$ ) and hydrodynamic conditions.

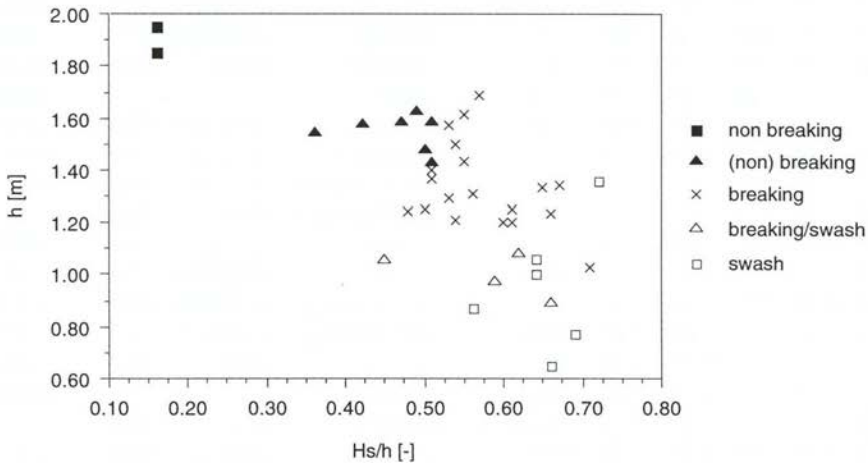


Figure 4.5 Relation between relative wave height ( $H_s/h$ ), water depth ( $h$ ) and hydrodynamic conditions.

#### wave asymmetry

The observed amplitude-asymmetries range from 0.56 to 0.66 and the duration-asymmetries vary from 0.41 to 0.51 (Table 4.4).

There is a weak correlation between amplitude- and duration asymmetry (Fig. 4.6) in that the amplitude asymmetry reduces from more asymmetric to less asymmetric when the duration asymmetry decreases. Note that an asymmetry of 0.5 means a perfect symmetry. Thus a decrease in an asymmetry value does not automatically imply that there is also a reduction in the asymmetry. For instance, a wave with an asymmetry value of 0.4 is more asymmetric than one with a value of 0.45 while a wave with a asymmetry value of 0.60 is less asymmetric than one with a value of 0.65. The waves during (non) breaking conditions have the lowest duration

Table 4.4 Wave asymmetry

Series	Amplitude asymmetry	Duration asymmetry
2310-1	0.60	0.47
2310-2	0.60	0.41
2310-3	0.60	0.44
2310-4	0.61	0.46
2310-5	0.61	0.46
2510-2	0.60	0.48
2510-3	0.61	0.49
2610-1	0.62	0.45
2610-2	0.62	0.42
2610-3	0.62	0.42
0411-1	0.60	0.50
0411-2	0.62	0.49
0411-3	0.63	0.47
0411-4	0.64	0.47
0411-5	0.63	0.47
0411-6	0.61	0.48
0511-1	0.62	0.49
0511-2	0.63	0.45
0511-3	0.63	0.47
0511-4	0.62	0.47
0511-5	0.64	0.49
0611-1	0.66	0.51
0611-2	0.65	0.44
0611-3	0.61	0.43
0611-4	0.63	0.44
0611-5	0.62	0.45
0711-1	0.62	0.45
0711-2	0.57	0.44
0711-3	0.60	0.42
0711-4	0.63	0.45
0811-1	0.61	0.43
0811-2	0.61	0.42
0811-3	0.60	0.43
0911-1	0.56	0.44
0911-2	0.57	0.41
0911-3	0.65	0.43
1011-1	0.64	0.45
1011-2	0.63	0.46

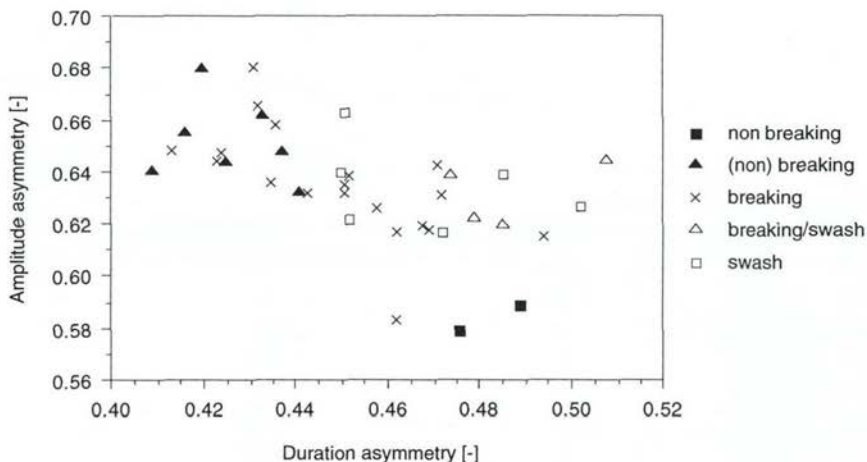


Figure 4.6 Relation between duration asymmetry and amplitude asymmetry.

asymmetric values i.e. are the most duration asymmetric and have the highest amplitude asymmetric values. Hence, the most asymmetric waves are found under (non) breaking-wave conditions which means that the wave profile is strongly peaked as the waves begin to break. The lowest amplitude asymmetric values i.e. the most amplitude symmetric waves are present during non-breaking conditions. Swash and breaking conditions show a large range of asymmetries. Hotta and Mizuguchi (1980, in: Van Rijn, 1990) also observed that the amplitude asymmetry and irregularity of waves are the largest just outside the breaker line. The amplitude asymmetry remains significant (0.60-0.68) after the waves break, but the duration asymmetry decreases (0.46-0.40). The wave profile of the broken waves, therefore, resembles more that of a bore which has a shape with an abrupt front and almost no curvature of the water surface after the wave crest.

The present results show no correlation with the relative wave height ( $H_s/h$ ). This outcome is in contrast to the study of Kroon (1994), who found that the amplitude asymmetry increased with increasing relative wave height. Within a particular hydrodynamic zone, however, some distinct trends are visible. For the swash conditions, for instance, the duration asymmetry of the waves increases when either the wave steepness or the relative wave height increases (not shown).

#### *wave surface profile*

Duration- and amplitude asymmetry are two of the main characteristics of wave shape. In this section further characteristics of wave shape are studied and then compared to various wave theories.

All time series show the trough of the observed waves to be more de-formed than the wave crest (see Fig. 4.7, for example). The first part of the trough (between 0 and 150 degrees) is especially skewed. The part of the wave shape between 200 and 270 degrees runs approximately parallel to a linear wave, although it is displaced in the direction of the crest. The final part of the wave (between 270 and 360 degrees), is reasonably described by the linear wave theory. Identical profiles were also observed by Kroon (1994).



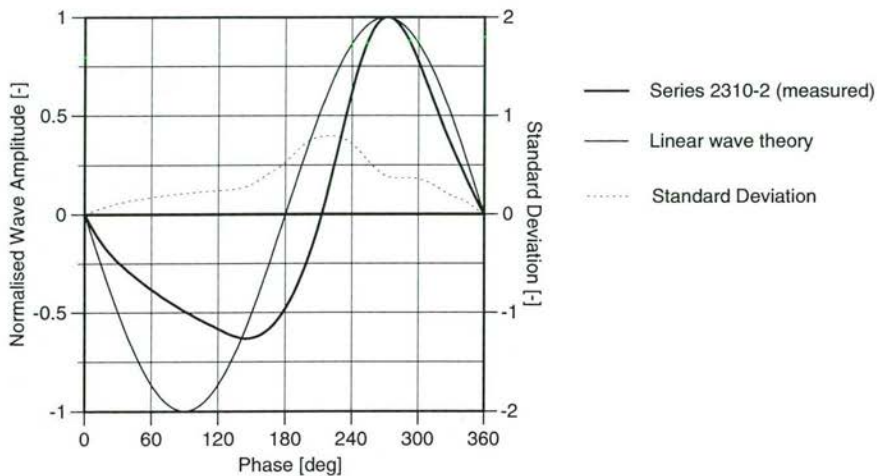


Figure 4.7 Example of wave profile shape.

Nine series were selected to see to what extent the observed surface-wave profile can be described by existing wave theories. Note that these theories were originally not designed for use in breaking waves. The series were selected using two parameters that determine the application domain of the various wave theories (Fig. 4.8). The selected series, assumed to represent all series and designated 1-9 in Figure 4.8, were evaluated and compared to the following theories and methods:

- Linear wave theory ;
- Stokes second order (only series 1-2; e.g. Stokes, 1847);
- Second order Cnoidal theory (e.g. Korteweg and de Vries, 1895);
- Covocoidal theory (e.g. Swart and Crowley, 1991; Fornerino et al., 1992);
- Fourier Approximation Method (e.g. Dean, 1965; Rienecker and Fenton, 1981).

These theories were chosen because they represent different approaches and incorporate different assumptions about wave form. The linear theory was chosen because of its simplicity, despite giving unsatisfactory results for steeper waves. To compensate for this deficiency, theories were developed which approximate non-linear terms but which can also be applied to steeper waves. Here, four higher-order theories are used. The higher order terms of the Stokes theory enhance the amplitude of the crest. Stokes' waves, therefore, have longer and wider troughs and sharper crests than those in the linear wave theory, as is often the case in shallow water. The Cnoidal theory is a second non-linear theory applied when the wave length is much longer than the water depth, i.e. when swell is present. The Stokes theory gives unrealistic results in those cases. The application of the Cnoidal wave theory is limited to shallower water depths (Fig. 4.8).

The empirical Covocoidal theory is the only theory that does not assume a symmetry around the crest and also incorporates the bottom slope.

The Fourier Approximation Method (FAM) is a non-analytical theory, the main advantage of which is that it can be used over a wide range of hydrodynamic

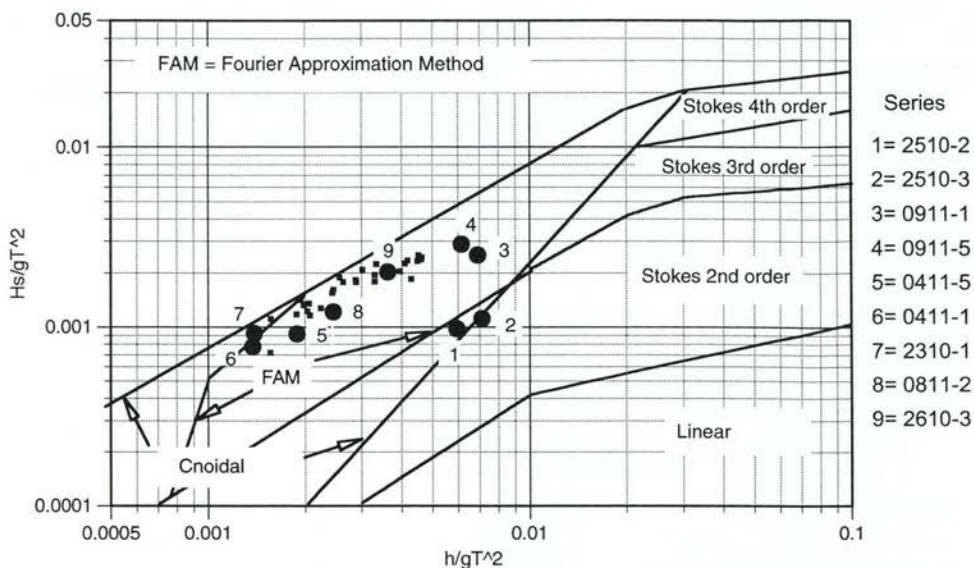


Figure 4.8 Application domain of various wave theories (after Le Mehaute, 1969, in *Shore protection manual*, 1984) and position of measurements; big dots are series further analysed, small squares are the other measurements.

conditions. The method uses a Fourier series capable of accurately approximating any periodic quality. The coefficients of the series are solved numerically rather than analytically (Fenton, 1990).

Some results are depicted in Figure 4.9. As expected, the series 2510-2 (1) and 2510-3 (2) (Fig. 4.9a) are best described by the second order Stokes theory which, although it overestimates the amplitude asymmetry, adequately describes the duration asymmetry. The FAM and the Linear wave theory do not compare with the observed amplitude and duration asymmetry.

None of the theories is able to describe the wave shape of the series 0911-1 (3) and 0911-2 (4) despite the fact that these series are in the application domain of the Cnoidal theory and FAM (Fig. 4.9b). Apart from the linear wave theory, all theories overestimate the amplitude asymmetry and the duration asymmetry. The linear wave theory gives the best prediction of series 0411-5 (5), 0411-1 (6) and 2310-1 (7) (Fig. 4.9c). The results for all other theories are even worse than for series 0911-1 (3) and 0911-2 (4). The surface-wave profile shape of series 0811-2 (8) is approximately the same as the series 5-7 so that the conclusions for the one are therefore also valid for the other series. The amplitude and duration asymmetry of series 2610-3 (9) is correctly described by the FAM (Fig. 4.9d) and all other theories fail in this case.

In conclusion, the observed waves cannot accurately be described by the wave theories mainly because in almost all the series, breaking waves are present and these theories were not designed for use with breaking waves. In addition, in almost all cases, the observed waves are, re-formed waves that broke earlier on the outer nearshore bar, the inner nearshore bar or even just in front of the BERT. In particular,



all theories fail with respect to one particular feature of the wave form - the trough. Apart from the *Covocoidal* theory, those theories applied assume that a wave is symmetrical between  $0-\frac{1}{2}T$  and between  $\frac{1}{2}T-T$ , where  $T$  is the wave period. This is indeed the case in most of the observed waves as far as the crest is concerned i.e. that part of the wave above SWL, but the theories mainly fail to describe the trough, as this feature is not symmetrical.

One important assumption of the Linear wave theory is that the wave amplitude is small compared to the wave length. Hence, the less steep the wave, the better the linear wave theory predicts the measured wave form, as can be derived from Figure 4.9 and Table 4.3. Assumptions regarding the Stokes and Cnoidal theory lead to the conclusion that Stokes' theory is valid for 'deeper' water and the Cnoidal theory for 'shallow' water (e.g. Horikawa 1988). This study confirms the first conclusion, but rejects the second one. The failure of the Cnoidal theory may be due to the fact that the waves were very steep. Waves which are less steep propagate into smaller depths before breaking, and the major part of their shoaling process may be described by the Cnoidal theory.

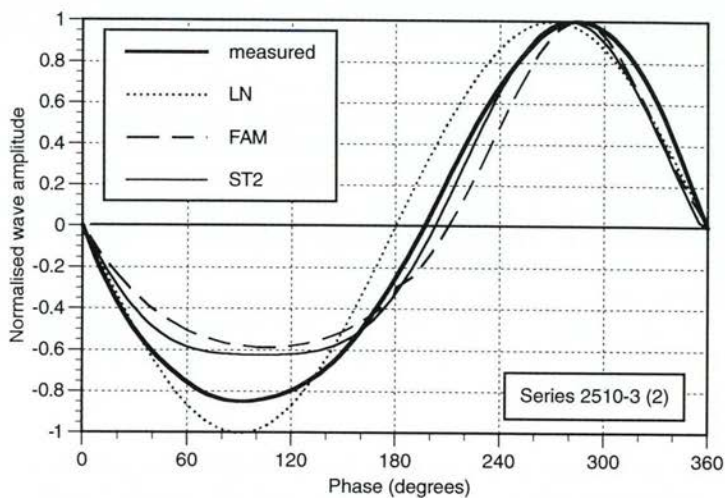
#### *wave spectra*

The spectra for water surface elevations show that most of the energy is concentrated in a relatively narrow peak with a rapid decay to the lower and higher frequencies, and a second peak is sometimes visible in the lower frequencies. There is a large temporal variation in the shape of the spectra. Within one day's measurements, however, a correlation can be seen between the wave and water level conditions. As an example, the spectra of series 0411-1 to 0411-6 are depicted in Figure 4.10. These spectra cover the tidal phases and wave-related conditions present during one day's measurements. While measuring in the swash zone, during the rising tide, the spectra show a peak between the 0.1 and 0.2 Hz (5-10 s). These peaks resemble gravity (wind) waves. Neither the frequency of the peaks nor the energy involved varies much during the rising tide, although the peaks become more pronounced. A second peak, with a much lower spectral density, is often present between 0.06 and 0.1 Hz (10-17 s) but this disappears as the water level rises and reaches its highest level. During a rising tide, the energy ratio between infragravity ( $T > 20$  s) and gravity ( $T \leq 20$  s) waves decreases. The spectrum reaches its maximum density around high tide, decreasing again as the tide falls, although the peakedness of the spectrum remains the same and the frequency of the peaks only changes a little ( $< 0.05$  Hz) and in no particular direction.

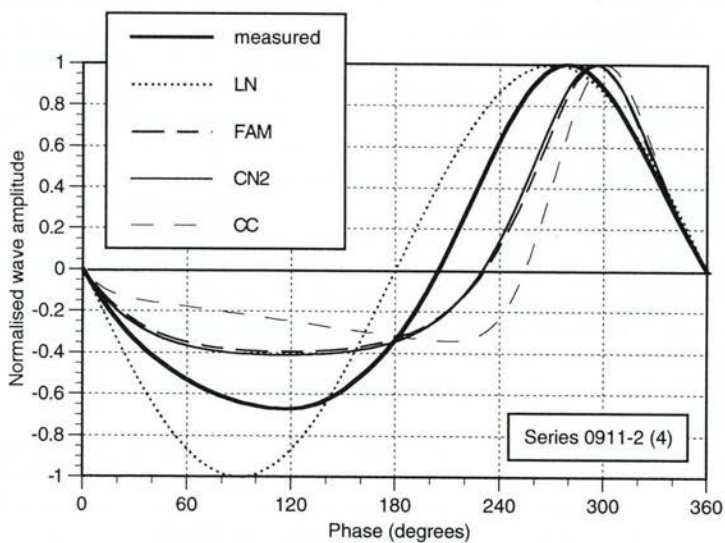
The wave spectra show that the incident wave frequency remains more or less the same, despite the occurrence of breaking waves and a rising tide. Apparently, breaking waves often produce a bore of the same wave period as (unbroken) incident waves. Hence, an incident wave is never completely destroyed. This hypothesis is supported by the analysis of asymmetry and surface-wave profiles.

The spectral density at the incident wave frequency changes when different wave conditions are present. There was approximately the same percentage of breaking waves in all cases registered on 4 November (Fig. 4.10). Thus, this percentage does not influence the spectral density during incident wave conditions. Consequently, a decrease in the spectral density of incident waves can only be determined by registering their position relative to the break point.





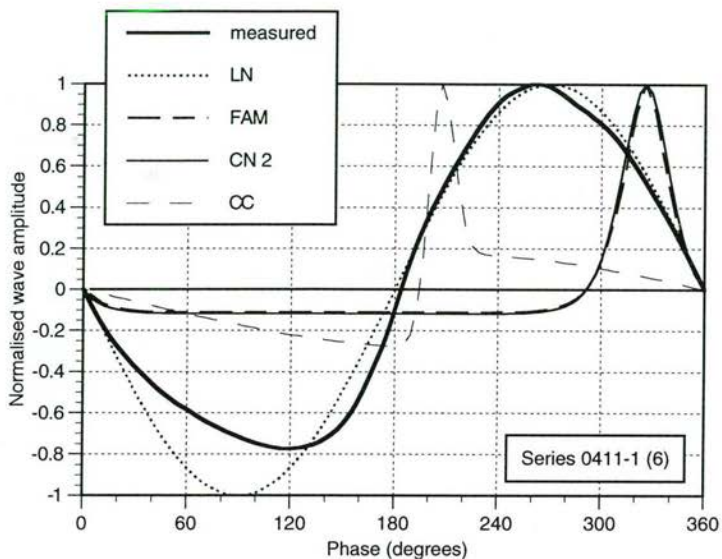
**A**



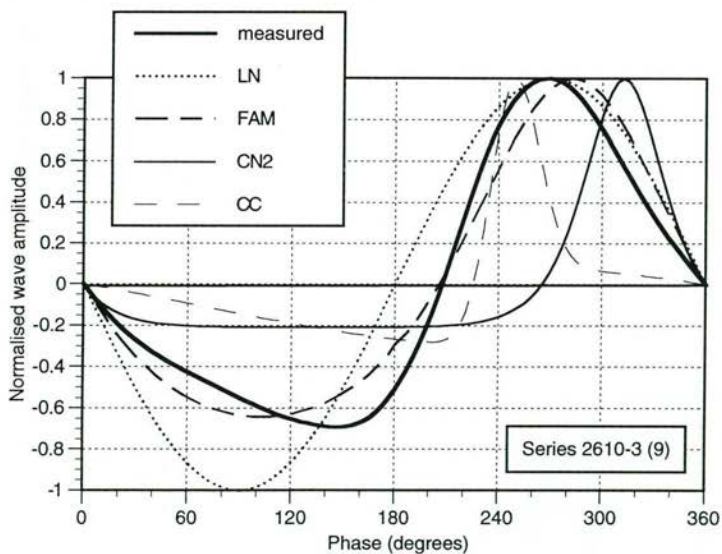
**B**

Figure 4.9

Shape of wave profile, measured and theoretical (LN = linear theory, FAM = Fourier Approximation Method, ST2 = Stokes second order, CN2 = cnoidal second order, CC = covocoidal). Numbers between brackets refer to Fig. 4.8.



**C**



**D**

Figure 4.9  
(continued)

Shape of wave profile, measured and theoretical (LN = linear theory, FAM = Fourier Approximation Method, ST2 = Stokes second order, CN2 = cnoidal second order, CC = covocoidal). Numbers between brackets refer to Fig. 4.8.

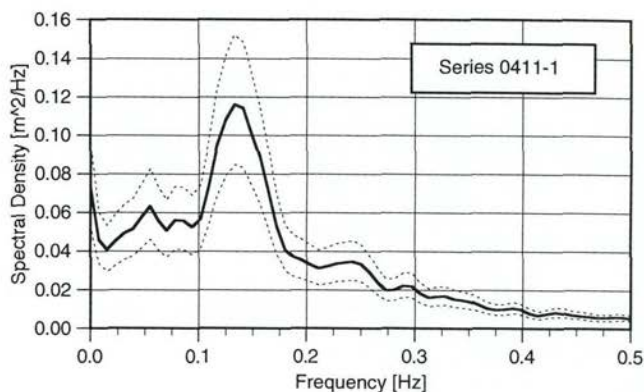
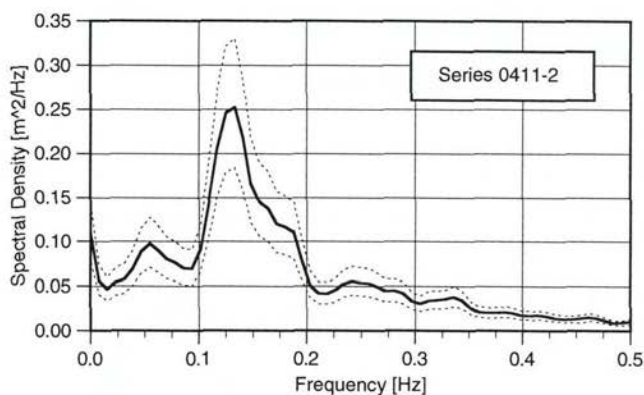
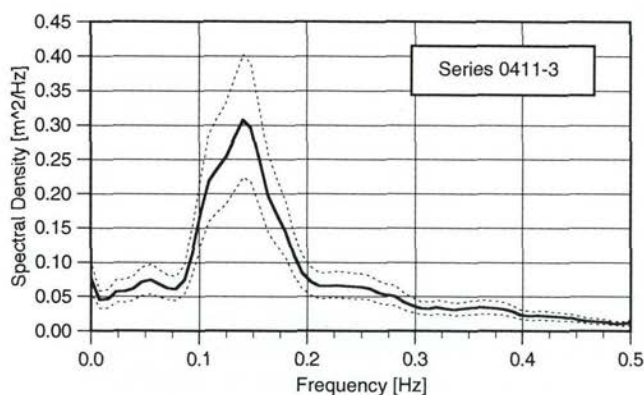
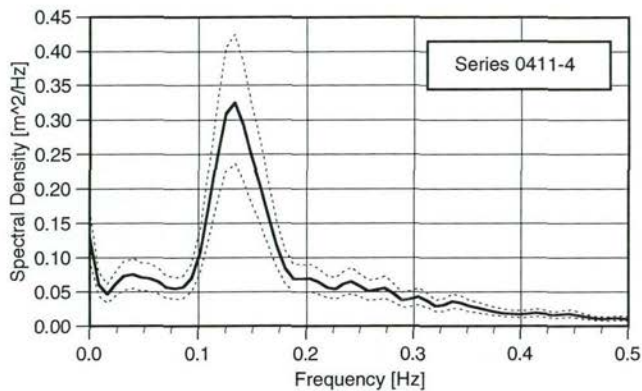
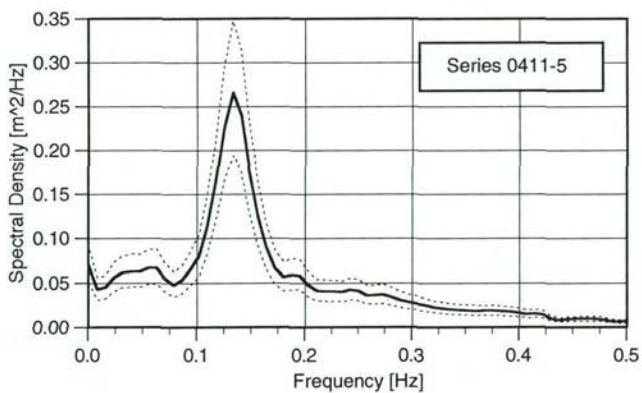
**A****B****C**

Figure 4.10 Wave frequency spectra (with 95% conf. interval) of surface wave recordings (Df = 93.6) (different vertical scale).

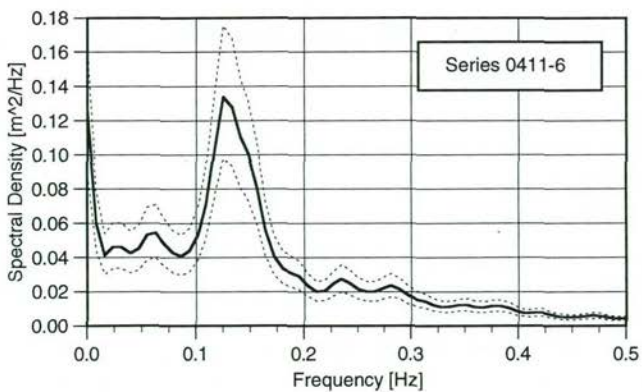


**D**

% br : 84.6  
 tide : high tide/falling  
 h : 1.37 m  
 zone : breaking

**E**

% br : (not measured)  
 tide : falling  
 h : 1.24 m  
 zone : breaking

**F**

% br : 93.1  
 tide : falling  
 h : 1.05 m  
 zone : breaking

Figure 4.10 Wave frequency spectra (with 95% conf. Interval) of surface wave recordings (continued) (Df = 93.6) (different vertical scale).

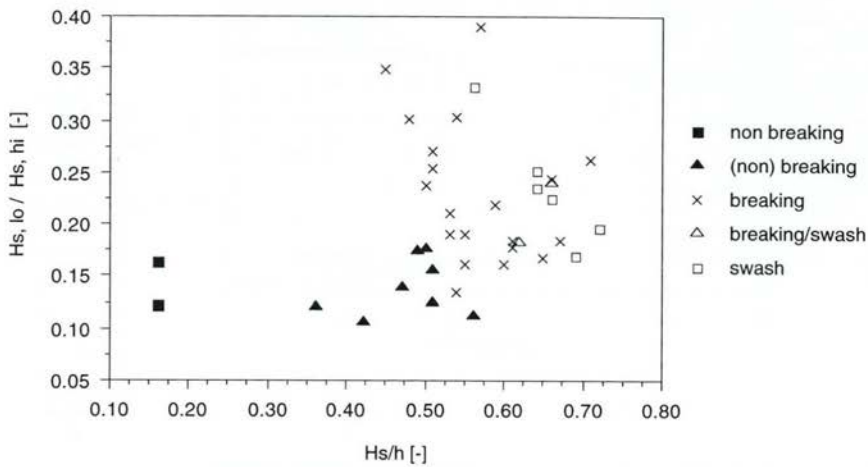


Figure 4.11 Relation between relative wave height and the low-frequency, high-frequency ratio of the surface wave height.

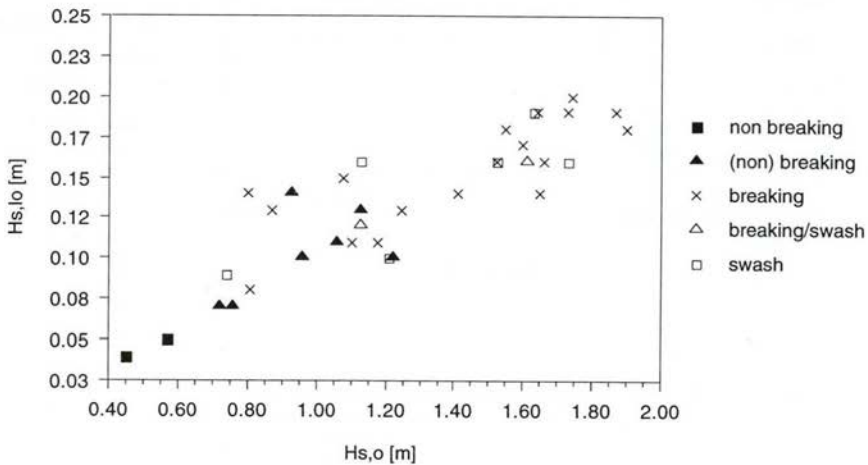


Figure 4.12 Relation between offshore wave height ( $H_{s,o}$ ) and low-frequency wave height ( $H_{s,lo}$ ).

#### low-frequency waves

The spatial variability of the gravity and infragravity bands is further studied by examining filtered time-series. The significant wave height of the filtered series of high-frequency waves ( $H_{s,hi}$ ) is nearly the same as the wave height for the unfiltered series (Table 4.5), with differences smaller than 3 percent. The significant wave heights of low-frequency waves ( $H_{s,lo}$ ) are always smaller than high-frequency waves. The highest values of the  $H_{s,lo}$  are registered during high energy conditions (Table 4.5). A clear relation between the relative wave height and  $H_{s,lo}$  was, however, not present. The significant wave periods of  $H_{s,lo}$  vary from 40 to 86 s, but are mostly

**Table 4.5** Wave height and period in different frequency domains

Series	All waves		High-frequency waves		Low-frequency waves	
	$T_s$	$H_s$	$H_{s,hi}$	$T_{s,hi}$	$H_{s,lo}$	$T_{s,lo}$
2310-1	6.91	0.43	0.43	6.86	0.10	52.13
2310-2	6.37	0.87	0.86	6.31	0.14	43.77
2310-3	6.72	0.90	0.89	6.65	0.16	41.61
2310-4	6.90	0.81	0.81	6.87	0.20	47.05
2310-5	7.36	0.73	0.71	7.12	0.19	48.81
2510-2	5.78	0.32	0.32	5.53	0.05	46.91
2510-3	5.15	0.29	0.29	5.09	0.04	51.08
2610-1	7.08	0.53	0.52	6.80	0.09	65.18
2610-2	6.11	0.66	0.67	6.15	0.07	54.61
2610-3	6.06	0.73	0.73	6.05	0.08	48.79
0411-1	8.04	0.49	0.48	7.74	0.16	48.33
0411-2	7.72	0.66	0.64	7.49	0.19	47.27
0411-3	7.73	0.72	0.72	7.62	0.18	45.16
0411-4	7.71	0.70	0.69	7.64	0.19	46.84
0411-5	8.19	0.60	0.59	7.94	0.18	46.92
0411-6	8.28	0.47	0.46	8.15	0.16	54.05
0511-1	7.04	0.64	0.63	6.85	0.16	56.18
0511-2	6.52	0.74	0.73	6.51	0.13	46.00
0511-3	6.51	0.72	0.71	6.46	0.11	51.52
0511-4	6.73	0.67	0.67	6.64	0.12	59.15
0511-5	6.77	0.58	0.57	6.56	0.14	45.25
0611-1	6.98	0.57	0.56	6.63	0.12	57.59
0611-2	5.81	0.81	0.80	5.81	0.11	60.99
0611-3	5.90	0.81	0.81	5.85	0.10	54.66
0611-4	5.68	0.72	0.72	5.65	0.11	55.12
0611-5	5.68	0.63	0.62	5.55	0.15	56.03
0711-1	6.64	0.68	0.67	6.50	0.16	52.53
0711-2	6.26	0.88	0.88	6.17	0.17	43.80
0711-3	6.24	0.84	0.83	6.17	0.16	43.53
0711-4	6.31	0.68	0.67	6.25	0.14	46.74
0811-1	8.23	0.76	0.74	8.09	0.14	50.12
0811-2	8.20	0.80	0.79	8.05	0.14	51.21
0811-3	8.06	0.79	0.78	7.91	0.13	51.38
0911-1	4.77	0.56	0.56	4.70	0.07	85.53
0911-2	5.12	0.74	0.74	5.00	0.10	58.50
0911-3	5.70	0.74	0.74	5.63	0.13	42.62
1011-1	7.36	0.98	0.97	7.28	0.19	51.82
1011-2	7.22	0.97	0.97	6.97	0.19	54.88

$T_s$  = significant wave period  
 $H_s$  = significant wave height  
 hi = high frequency waves  
 lo = low frequency waves



about 40-60 s. The ratio between the low-frequency waves ( $H_{s, lo}$ ) and high-frequency waves ( $H_{s, hi}$ ) varies between 0.1 and 0.2 during non-breaking conditions, increases up to 0.4 during breaking conditions and decreases to 0.15 - 0.25 in swash (Fig. 4.11). Hence, low-frequency waves never become dominant in the inner nearshore zone and there is no correlation between relative wave height and the ratio  $H_{s, lo} / H_{s, hi}$  (Fig. 4.11). The heights of the low-frequency waves show less correlation with the local wave heights (not shown) than with the offshore wave height (Fig. 4.12), which confirms the findings of a number of other studies (e.g. Holman, 1981; Guza and Thornton, 1982, 1985; Kroon, 1994).

#### 4.4.3 Conclusions

The hydrodynamics of the surface waves in the inner nearshore zone were studied. The measurements were performed under conditions with a relative wave height varying from 0.16 - 0.72. The analysis leads to the following conclusions:

##### *general wave conditions*

- The relative wave height increases towards the shore, i.e. with the hydrodynamic conditions varying from non-breaking, breaking, to swash.
- The breaker type shows no relation to hydrodynamic condition; spilling and plunging breakers, though dominate.

##### *asymmetry of the waves*

- Almost all waves in the inner nearshore show an asymmetry around the vertical axis (duration asymmetry) and an asymmetry around the horizontal axis (amplitude asymmetry).
- The breaking of waves leads to more sinusoidal waves, although large duration and amplitude asymmetries remain.

##### *wave theories and wave profile shape*

- None of the applied wave theories is able to describe the surface-wave shape correctly, mainly because of the asymmetry of the wave trough.

##### *wave spectra*

- Most of the spectral energy is confined to incident (wind) wave frequencies.
- The shape of the wave spectra remains fairly constant during the different wave conditions.

##### *low frequency waves*

- Low-frequency energy is insignificant in the inner nearshore wave field.

#### 4.5 Analysis of the velocity field

##### 4.5.1 Introduction

In the previous section, a division into five hydrodynamic zones was made on the basis of the characteristics, e.g. breaking, non-breaking, of surface (wind-) waves. The surface-wave hydrodynamics of each of these zones was described and related

to the relative wave height and to wave steepness. The next section concludes the analysis of the surface and sub-surface hydrodynamics of these zones. The velocity field under the surface-waves is investigated and related to the surface-wave hydrodynamics.

Forty-minute recordings of the velocity data were made using electromagnetic flow meters (EMFs) 0.1, 0.3 and 0.7 m above the bed (Section 3.6). Some of the routines used for the analyses of the EMF data are largely similar to those used to analyse the capacitance wire (CW) data already explained in Section 4.4.1. These routines will be treated briefly in the following sections.

The following aspects of near-bed velocities, i.e. the velocities measured at 0.1 m above the bed, are analysed:

- significant peak velocities;
- mean cross-shore and longshore velocities and undertow;
- asymmetry of the velocity;
- velocity spectra;
- low frequency velocities;
- relation with surface-wave hydrodynamics;
- application of wave theories.

Finally, the vertical structure of the velocity field is studied by comparing the mean, the significant velocities, the duration asymmetry and the amplitude asymmetry at the three heights above the bed.

#### 4.5.2 Analysis and interpretation methods

##### *significant peak velocities*

Significant peak velocities are important for sediment transport because they determine the pick-up of sediment. Significant peak velocity is the mean value of the highest one-third of measured peak velocities. The characteristics of the individual velocity cycles were determined between two upward zero crossings and the trend in the time series was determined using a second order polynomial.

##### *mean velocities and undertow*

A net movement of sediment can be determined by superimposing a mean cross-shore current on the oscillatory wave motions. The mean velocity may, therefore, be responsible for the movement of inter-tidal and nearshore bars (e.g. Osborne and Greenwood, 1992). To avoid confusion between the term 'mean cross-shore current' and 'undertow', these terms are here defined. Undertow is the result of breaking waves which produce a radiation stress that is not uniform over depth whereas the opposing pressure gradient is, the result being a wave set-up. This always results in a seaward directed current. A net seaward directed current could also be the result of a weak or non-stationary rip-current. This is, however, less likely because at the start of each measuring day, the location of possible rip-currents was visually determined and the BERT was placed at the largest possible distance from them. The mean cross-shore current is the result of *all* wind and wave induced currents e.g. undertow, Stokes' drift, streaming and wind set-up. The mean cross-shore current may also be onshore directed.

One of the main difficulties in modelling cross-shore sediment transport is how to model the undertow (Nielsen, 1992). Therefore existing formulations are, tested against the measured time-averaged (40 minute) velocities to investigate the applicability of these formulations.

The next three formulations are investigated:

Svendsen (1984):

$$U_{mean,off} = c \cdot \left( \frac{H_s}{h} \right) \cdot \left( B_o \frac{A}{H_s^2} \cdot \frac{h}{L} \right) \quad (4.3)$$

- $U_{mean,off}$  = mean offshore directed return flow velocity [ $ms^{-1}$ ]
- $c$  = propagation velocity of waves [ $ms^{-2}$ ]
- $H_s$  = significant wave height [m]
- $h$  = water depth [m]
- $B_o$  = non-dimensional energy flux factor [-] ( $\approx 0.07$ )
- $A$  = surface roller parameter [-]
- $A \approx 0.9 H$  (Duncan, 1981 in Svendsen, 1984),  $B_o$  and  $A$  are factors which describe the wave profile, which, in turn, determines the distribution of the mean currents.
- $L$  = wave length [m].

Stive and Wind (1986):

$$U_{mean,off} = 0.1 \cdot \left( \frac{g}{h} \right)^{0.5} \cdot H_s \quad (4.4)$$

- $g$  = acceleration of gravity [ $ms^{-2}$ ]

and van Rijn (1990):

$$U_{mean,off} = 0.125 \cdot \left( \frac{g}{h} \right)^{0.5} \cdot \left( \frac{H_s^2}{h_t} \right) \quad (4.5)$$

- $h_t$  = water depth under the wave trough [m]

The authors of these formulae are not clear about the representative wave height that should be used. The authors only mention 'wave height' without explaining whether this is the significant wave height ( $H_s$ ) the root-mean-square wave height ( $H_{rms}$ ) or the mean wave height ( $H_m$ ). The undertow is generated to compensate for the onshore directed flow caused by the wave drift and the surface rollers carrying water shoreward. Surface rollers are only present when a wave breaks, usually a large wave while the lower ones may still propagate without breaking. In order to include the effect of breaking waves on the undertow, therefore, the significant wave height has been chosen as representing the wave height in the three formulas describing the undertow.



The water depth and significant wave height used in the three formulas are determined using the CW series of the BERT. Velocity, depth and significant wave height are thus based on 40 minute averaged values.

An important assumption of this study is that the morphology is determined by the cross-shore hydrodynamics (Chapter 1). If longshore velocities are very large compared to cross-shore velocities than small gradients in the former may have a large impact on cross-shore morphological developments. The mean longshore velocities have, therefore, also been calculated to determine the ratio between the mean longshore and cross-shore velocities, i.e. to verify the earlier assumption.

#### *asymmetry of the velocity*

Both the amplitude- and duration asymmetry are calculated. The amplitude asymmetry of the velocity is defined as:

$$A_{a,u} = \frac{u_{s,on}}{u_{s,on} + u_{s,off}} \quad (4.6)$$

$A_{a,u}$  = amplitude asymmetry ratio of the velocity [-]  
 $u_{s,on}$  = significant onshore peak velocity [m/s]  
 $u_{s,off}$  = significant offshore peak velocity [m/s]

The duration asymmetry is defined as:

$$A_{d,u} = \frac{T_{onshore}}{T_{onshore} + T_{offshore}} \quad (4.7)$$

$A_{d,u}$  = duration asymmetry ratio of the velocity [-]  
 $T_{onshore}$  = significant time-interval between a zero up (onshore) crossing and the next zero down (offshore) crossing [s]  
 $T_{offshore}$  = significant time-interval between a zero down (offshore) crossing and the next zero up (onshore) crossing [s]

Significant peak velocities, i.e. the mean of the highest one-third onshore and offshore peak velocities are used to calculate the asymmetries, which are thus significant. The de-meaning procedures and the calculation of the time-averaged onshore and offshore velocities were similar to the procedures described for the calculation of surface-wave asymmetries (see Section 4.4.1).

#### *velocity spectra and low-frequency velocity*

The calculations of velocity spectra and low-frequency velocities are identical to the method used to calculate wave spectra and low-frequency waves (see Section 4.4.1).

#### *relation of surface hydrodynamics to the velocity field*

The relation between surface-wave characteristics and near-bed velocities is studied. The following characteristics of the surface-wave and near-bed velocity are compared, pairwise: period, amplitude, amplitude and duration asymmetries and spectra.

#### *application of wave theories*

The shape of the orbital velocity profile, whereby orbital velocity is represented as a function of time from  $t = 0$  to  $t = T$ , is calculated to facilitate an evaluation of the applicability of different wave theories for the different hydrodynamic zones.

The shape of the orbital velocity profile was computed for all series using Houwman and Hoekstra's (1994) method (see Section 4.4.1). Nine measured velocity time series were selected to compare the orbital velocity shape with several wave theories. The outcome of earlier analysis showed that no single theory could predict the surface-wave profile correctly under all wave conditions. Therefore, all theories used in surface-wave analysis are again used to calculate the near-bed hydrodynamics: linear wave theory, Stokes' second order theory, the second order Cnoidal theory, the Covocoidal theory and the Fourier Approximation Method (FAM).

All measured series were further examined with respect to two aspects of the orbital velocity profile viz. significant peak velocities in the on- and offshore direction and the resulting amplitude asymmetry. The data from the field measurements were compared with the values predicted by the above mentioned theories to test the applicability of the various wave theories used in sediment transport models. The data set for the theories was derived from the capacitance wire and comprises the significant wave height ( $H_s$ ), the wave period ( $T$ ) and the water depth ( $h$ ). In addition, the slope of the bed ( $\alpha$ ) was determined.

#### *vertical variability of the velocity field*

This analysis investigates the vertical structure of the velocity field under waves. All measured series were examined for mean velocity, significant onshore peak velocity, significant offshore peak velocity, amplitude asymmetry and duration asymmetry at three heights, 0.1, 0.3 and 0.7 m above the bed, because these parameters have a dominant influence on sediment transport (e.g. Soulsby et al., 1993). The analysis should determine the elevation above the bed at which peak velocities, mean velocities and velocity asymmetries may be regarded as being uniform. This is important for the sediment transport analysis because the sediment dynamics was intended to be related to the velocities measured at 0.1 m (Chapter 5), if appropriate.

### **4.5.3 Results and discussion**

#### *general characteristics of the velocity field*

The wave conditions are characterised by a significant wave height varying between 0.29 and 0.98 m while the relative wave height varied between 0.16 and 0.72. Under these hydrodynamic conditions, the following characteristics of the near-bed (0.1 m above the bed) velocity field were observed (see also Table 4.6):

- onshore significant peak velocity = 0.38 - 1.63 ms<sup>-1</sup>
- offshore significant peak velocity = 0.34 - 1.22 ms<sup>-1</sup>
- mean velocity = 0.03 - 0.37 ms<sup>-1</sup> (always offshore directed)
- amplitude asymmetry = 0.52 - 0.63
- duration asymmetry = 0.41 - 0.53

#### *significant peak velocities*

The highest onshore peak velocities were measured during swash and breaking wave conditions; the lowest during non-breaking wave conditions. No relation was found

Table 4.6 Mean velocities, significant, orbital peak velocities and velocity asymmetries in the cross-shore direction at 0.1 m above the bed.

Series	$H_b/L_s$	$H_b/h$	hydrodynamic zone	Cross-shore						Longshore					
				$u_{mean}$ [m/s]	$u_s$ [m/s]	$T_s$ [s]	$u_{s,on}$ [m/s]	$u_{s,off}$ [m/s]	$A_{s,u}$ [-]	$A_{d,u}$ [-]	$u_{mean}$ [m/s]	$u_s$ [m/s]	$T_s$ [s]	$u_{s,north}$ [m/s]	$u_{s,south}$ [m/s]
2310-1	0.055	0.66	swash	-0.28	2.18	7.35	1.47	-1.06	0.580	0.498	0.06	1.14	6.62	0.72	-0.64
2310-2	0.072	0.65	breaking	-0.08	2.27	6.41	1.57	-1.00	0.609	0.425	-0.04	0.89	5.25	0.54	-0.49
2310-3	0.071	0.67	breaking	-0.11	2.28	7.02	1.60	-1.07	0.599	0.458	-0.24	1.15	7.02	0.65	-0.68
2310-4	0.065	0.66	breaking	-0.14	2.17	6.99	1.56	-0.98	0.614	0.449	-0.19	1.01	7.25	0.57	-0.59
2310-5	0.057	0.71	breaking	-0.21	2.23	7.33	1.53	-1.01	0.602	0.465	-0.20	1.05	7.05	0.64	-0.63
2510-2	0.056	0.16	non breaking	-0.03	0.69	5.78	0.40	-0.37	0.521	0.500	0.12	0.31	4.69	0.18	-0.17
2510-3	0.056	0.16	non breaking	-0.03	0.67	5.22	0.39	-0.35	0.526	0.494	0.06	0.28	4.12	0.15	-0.16
2610-1	0.058	0.69	swash	-0.17	2.03	6.71	1.37	-0.96	0.586	0.458	-0.07	0.85	6.28	0.53	-0.46
2610-2	0.069	0.42	(non) breaking	-0.07	1.76	6.22	1.20	-0.75	0.615	0.413	0.01	0.49	6.22	0.30	-0.27
2610-3	0.071	0.56	(non) breaking	-0.13	1.95	6.13	1.33	-0.87	0.603	0.420	-0.09	0.68	5.04	0.41	-0.37
0411-1	0.043	0.56	swash	-0.17	1.40	7.32	1.00	-0.68	0.596	0.486	-0.25	0.85	7.49	0.47	-0.55
0411-2	0.051	0.54	breaking	-0.35	1.47	6.70	1.03	-0.76	0.575	0.479	-0.33	0.88	7.15	0.49	-0.56
0411-3	0.053	0.51	breaking	-0.34	1.51	7.33	1.04	-0.76	0.577	0.475	-0.33	0.86	6.30	0.46	-0.54
0411-4	0.052	0.51	breaking	-0.37	1.54	7.25	1.05	-0.79	0.570	0.489	-0.36	0.83	6.62	0.45	-0.53
0411-5	0.046	0.48	breaking	-0.35	1.37	5.79	0.95	-0.75	0.559	0.499	-0.36	0.77	6.13	0.41	-0.48
0411-6	0.040	0.45	breaking	-0.28	1.22	5.22	0.85	-0.71	0.547	0.503	-0.19	0.67	5.55	0.39	-0.42
0511-1	0.060	0.64	swash	-0.21	1.69	5.54	1.16	-0.89	0.565	0.479	0.08	0.92	5.67	0.54	-0.54
0511-2	0.065	0.61	breaking	-0.11	2.04	6.74	1.39	-1.00	0.582	0.459	0.04	0.94	6.10	0.53	-0.57
0511-3	0.065	0.6	breaking	-0.07	2.10	6.41	1.44	-1.05	0.579	0.467	0.04	0.89	6.27	0.49	-0.54
0511-4	0.061	0.62	breaking/swash	-0.12	1.99	4.73	1.31	-1.12	0.538	0.486	0.02	0.86	5.06	0.51	-0.49
0511-5	0.056	0.66	breaking/swash	-0.20	2.09	4.58	1.34	-1.25	0.518	0.489	-0.04	0.90	4.57	0.53	-0.55
0611-1	0.056	0.59	breaking	-0.27	1.69	6.40	1.16	-0.84	0.581	0.524	0.58	0.89	5.33	0.58	-0.48
0611-2	0.079	0.54	breaking	-0.09	1.89	5.91	1.25	-0.93	0.572	0.458	0.25	0.79	4.70	0.47	-0.42
0611-3	0.078	0.51	(non) breaking	-0.09	1.98	6.21	1.34	-0.92	0.591	0.442	0.20	0.70	5.01	0.43	-0.37
0611-4	0.075	0.51	(non) breaking	-0.07	1.38	5.44	0.93	-0.64	0.593	0.444	0.08	0.54	4.31	0.32	-0.29
0611-5	0.069	0.5	breaking	-0.13	1.35	5.40	0.88	-0.73	0.547	0.465	0.15	0.70	4.34	0.44	-0.35
0711-1	0.064	0.64	swash	-0.18	1.99	6.36	1.38	-0.97	0.586	0.460	0.47	0.94	5.38	0.60	-0.50
0711-2	0.075	0.55	breaking	-0.33	1.99	6.77	1.38	-0.99	0.584	0.456	0.52	0.97	5.81	0.64	-0.50
0711-3	0.073	0.53	breaking	-0.30	1.88	6.79	1.27	-0.93	0.577	0.469	0.37	0.95	6.33	0.63	-0.49
0711-4	0.065	0.53	breaking	-0.31	1.63	6.74	1.13	-0.82	0.578	0.474	0.25	0.91	6.38	0.59	-0.46
0811-1	0.055	0.61	breaking	-0.08	1.85	7.14	1.31	-0.88	0.599	0.434	-0.04	0.59	6.29	0.31	-0.36
0811-2	0.056	0.49	(non) breaking	-0.12	1.25	7.50	0.85	-0.58	0.594	0.459	-0.15	0.50	8.41	0.25	-0.33
0811-3	0.056	0.55	breaking	-0.17	1.80	8.36	1.22	-0.80	0.605	0.445	-0.30	0.64	7.94	0.34	-0.40
0911-1	0.084	0.36	(non) breaking	-0.11	1.25	4.96	0.79	-0.61	0.564	0.448	0.37	0.65	4.14	0.39	-0.35
0911-2	0.087	0.47	(non) breaking	-0.07	1.54	5.21	1.01	-0.71	0.587	0.418	0.22	0.68	4.60	0.40	-0.34
0911-3	0.077	0.5	(non) breaking	-0.19	1.65	5.75	1.12	-0.76	0.595	0.438	0.35	0.70	4.87	0.43	-0.36
1011-1	0.065	0.72	swash	-0.09	2.46	7.39	1.68	-1.13	0.598	0.451	0.14	0.92	6.61	0.54	-0.52
1011-2	0.069	0.57	breaking	-0.14	2.43	7.61	1.66	-1.10	0.602	0.441	0.09	0.96	6.82	0.57	-0.56

$u_{mean}$  = mean cross-shore velocity

- = offshore/south

+ = onshore/north

$T_s$  = significant period

$u_s$  = significant cross-shore peak velocity

$u_{s,on}$  = onshore significant cross-shore peak velocity

$u_{s,off}$  = offshore significant cross-shore peak velocity

$u_{s,south}$  = south directed significant longshore peak velocity

$u_{s,north}$  = north directed significant longshore peak velocity

$A_{s,u}$  = amplitude-asymmetry of the cross-shore peak velocity

$A_{d,u}$  = Duration-asymmetry of the cross-shore peak velocity



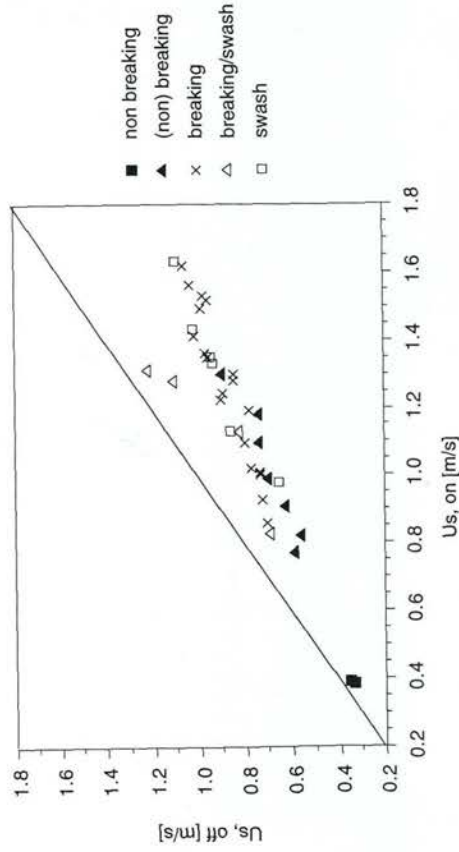


Figure 4.13 Relation between onshore- ( $U_{s,on}$ ) and offshore ( $U_{s,off}$ ), significant, orbital peak velocities at 0.1 m above the bed.

between the strength of the offshore velocity and either the hydrodynamic zones (Fig. 4.13) or the type of breaker (not shown). Also, the significant offshore peak velocities were found to be smaller than the onshore peak velocities in all hydrodynamic zones. The significant onshore peak velocity is related to the relative wave height (Fig. 4.14) and because the relation between the onshore and offshore significant peak velocities (Fig. 4.13), a higher relative wave height will lead to both higher onshore and offshore velocities near the bed.

#### *mean velocities and undertow*

The mean velocity varied between  $-0.37$  and  $-0.03 \text{ ms}^{-1}$ . Hence, there was always an offshore directed mean current near the bed, even with non-breaking waves.

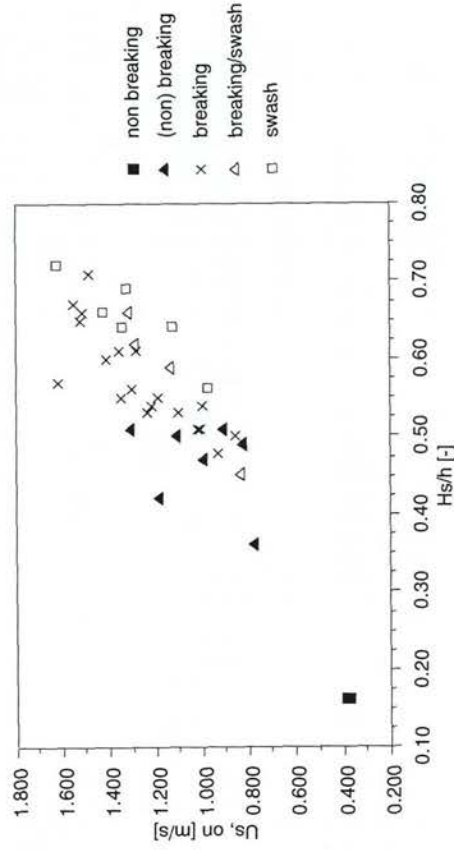


Figure 4.14 Relation between relative wave height ( $H_s/h$ ) and onshore, significant, peak velocity ( $U_{s,on}$ ) at 0.1 m above the bed.

The highest offshore-directed mean currents were measured during conditions with breaking waves (Fig. 4.15). The strength of the mean flow was not related to the breaker type (not shown) although such a relation could be expected according to previous research (see Section 2.2; Fig. 2.1). It is concluded from Table 4.6 that there is no relation between the strength of the mean cross-shore current and the hydrodynamic zones. This is somewhat peculiar because, for instance, in the breaking wave zone the occurrence and magnitude of surface rollers is larger than in the non-breaking zone. These surface rollers induce an onshore flow which in theory is compensated by the undertow. Thus, one would expect either a relation between the hydrodynamic zone or between the relative wave height and the undertow, but these relations were, not found.

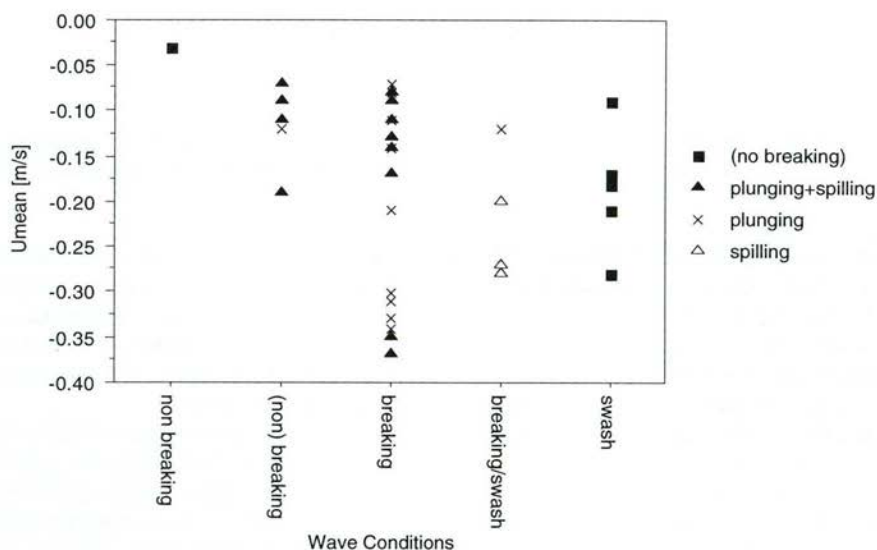


Figure 4.15 Relation between mean velocity ( $U_{\text{mean}}$ ) at 0.1 m above the bed and breaker type for the different hydrodynamic zones (negative flow = offshore direct flow).

The mean cross-shore currents are in the same order as the mean longshore currents (Table 4.6). After examination of the sediment transport (next chapter) it may be clear to what extent these results reject the assumption that the sediment transport in the nearshore zone is dominated by cross-shore sediment transport. It appears from Table 4.6 that the longshore significant peak velocities are about a factor 0.5 smaller than the significant peak velocity in the cross-shore direction. Thus, the cross-shore velocities are the main stirring agent for the sediment, although the longshore velocities cannot be ignored.

The measured mean cross-shore velocities are compared with predictions based on formulas 4.3-4.5. Note that these formulas only predict the undertow and not the mean cross-shore current which was measured. The results, presented in Figure 4.16, show that there is no relation between the predicted and measured values, which is no real surprise. All formulas assume that there is a relation between undertow and wave height, relative wave height or wave steepness. None of these relations was found, however, in the previous analysis. Apparently other factors, not included in the formulas, e.g. non-local processes such as wind set-up, are important under

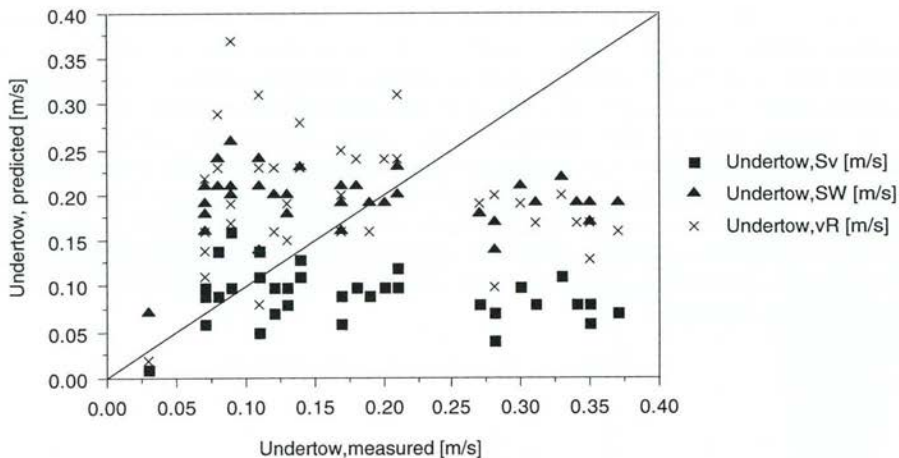


Figure 4.16 Relation between measured undertow and predicted undertow according to Svendsen (1984) (Sv), Stive and Wind (1986) (SW) and Van Rijn (1990) (vR).

measured conditions. Kuriyama (1991) in Kroon (1994) mentions that the surface roller parameter is not constant but may vary by a factor of 10. This may also explain the differences between measured undertow and undertow according to the Svendsen formula (4.3). Finally, a three-dimensional current pattern may have been present which means that the shoreward mass transport by breakers did not have to be (fully) compensated in the vertical plane, i.e. by undertow alone.

Van Rijn's (1990) formula uses the depth below the trough ( $h_t$ ) as input variable. Van Rijn (1990) suggests that this value can be approximated by  $0.8 \cdot h$  and this was the value used in the above comparison. Because there are considerable differences between the undertow as predicted by the Van Rijn (1990) formula and measured values, an improvement on the Van Rijn (1990) formula was attempted.

Kroon (1994), suggested that the value of  $h_t$  can be found using  $h_t = h - 0.36 \cdot H_s$ . The relation between formula 4.5, and the measured undertow was, therefore, investigated, using  $h_t = h - 0.36 H_s$ . However, this did not lead to an improved relationship between the predicted and measured values. Therefore, it is concluded that none of the formulas (4.3-4.5) is able to predict accurately the strength of the mean cross-shore current because the assumed relation between the surface wave parameters and the undertow was not present. Besides, other factors than the undertow (e.g. wind set-up) are important in determining the local measured mean cross-shore current.

#### *asymmetry of the velocity*

The differences between on- and offshore velocities result in the amplitude asymmetry of the near-bed velocities, varying from 0.52 to 0.62 (Table 4.6). Low amplitude-asymmetries were measured during non-breaking wave conditions. The highest amplitude asymmetries were not restricted to a particular wave condition but occurred during swash, breaking and (non) breaking conditions (Fig. 4.17). Note that the asymmetries in the swash zone are always measured on the seaward side of this zone and not in the run-up zone. These asymmetries are thus the asymmetries of bores. Thus the highest amplitude-asymmetries are not necessarily found near the



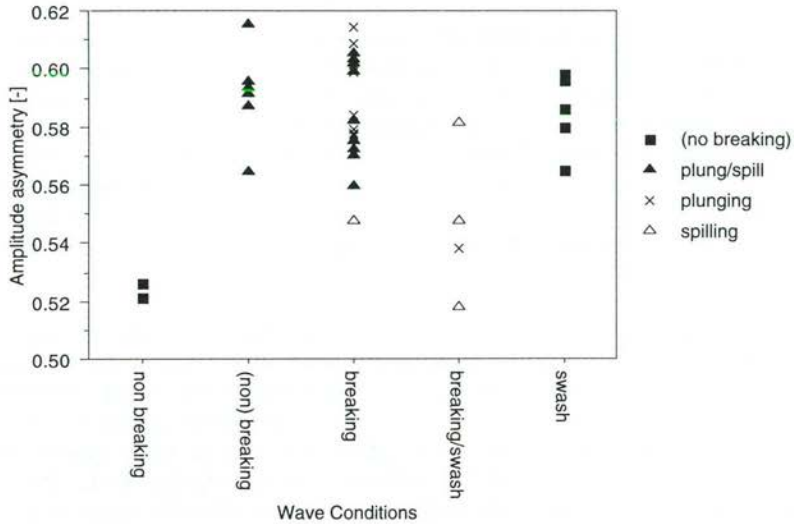


Figure 4.17 Relation between amplitude asymmetry of the velocity at 0.1 m above the bed and breaker type.

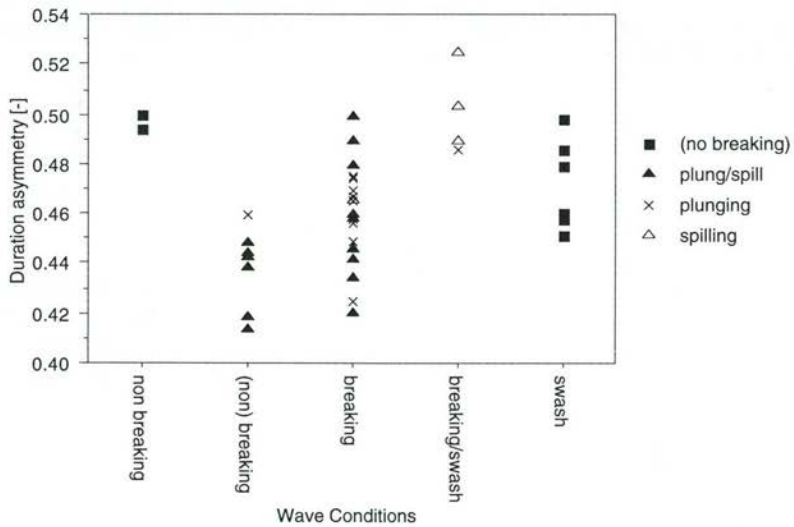


Figure 4.18 Relation between duration asymmetry of the velocity at 0.1 m above the bed and breaker type.

break point as was suggested by Nadaoka and Kondoh (1982, in Soulsby et al., 1993). The magnitude of the amplitude asymmetries is in the same range as that observed by Kroon (1994).

The duration asymmetry varies from 0.41 to 0.53 (Fig. 4.18). However, all but five series show duration asymmetries of between 0.41 and 0.50, which means shorter onshore duration and longer offshore duration of the orbital cycle. Waves with a duration asymmetry of 0.5, i.e. waves symmetric around a horizontal axis, are found during all conditions. The lowest duration asymmetry values, i.e. the most duration asymmetric waves are found during breaking and non-breaking waves with plunging or a combination of plunging and spilling breakers. Spilling breakers alone were related to more duration symmetric waves (Fig. 4.18). A lower duration asymmetry value is found in waves with a higher amplitude asymmetry (Fig. 4.17-4.18). Hence, orbital excursions characterised by a highly asymmetric velocity signal are often asymmetric along both the vertical and horizontal axis.

The extent to which the observed tendencies in amplitude and duration asymmetry are related to the relative wave height were examined. Kroon (1994) found that amplitude asymmetry increases with relative wave height, but these findings were largely influenced by high values of amplitude asymmetries (0.6-0.63) measured under swash, with a large relative wave height of 0.8-1.15. As lower values - relative wave heights between 0.16 and 0.72 - were recorded during this study, the relation between amplitude asymmetry and relative wave height was not found. It is only in breaking waves, that higher relative wave heights produce more amplitude-asymmetric waves (see Fig. 4.19). For all other hydrodynamic conditions, no relation was found between relative wave height and amplitude asymmetry (Fig. 4.19). Especially during breaking/swash conditions, relative wave height was found to show a decrease in amplitude asymmetry. This may be explained by the percentage of breaking waves. High percentages (> 80 %) measured during breaking/swash conditions result in a rapid decrease in amplitude asymmetries (Fig. 4.20).

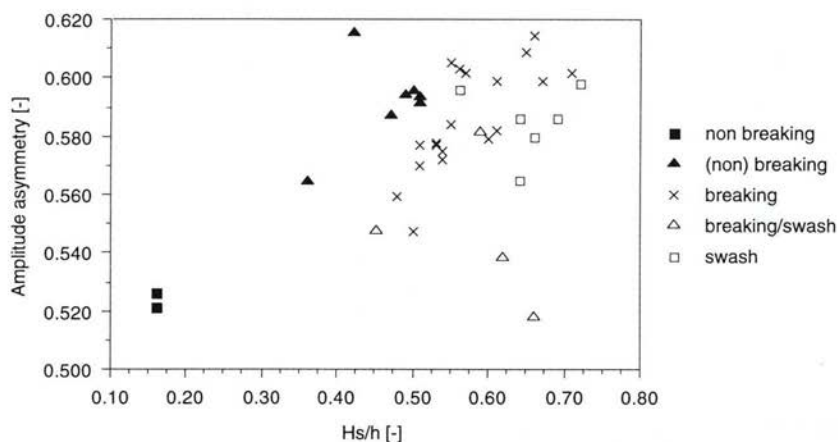


Figure 4.19 Relation between relative wave height ( $H_s/h$ ) and amplitude asymmetry of the velocity at 0.1 m above the bed

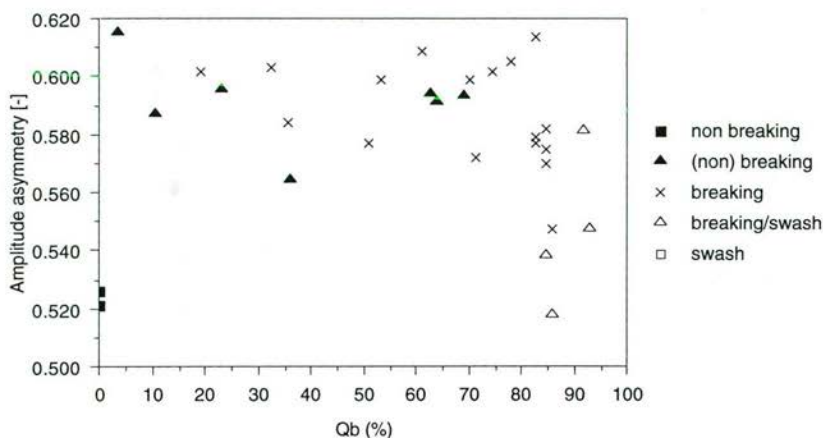


Figure 4.20 Relation between percentage of breaking waves ( $Q_b$ ) and amplitude asymmetry of the velocity at 0.1 m above the bed

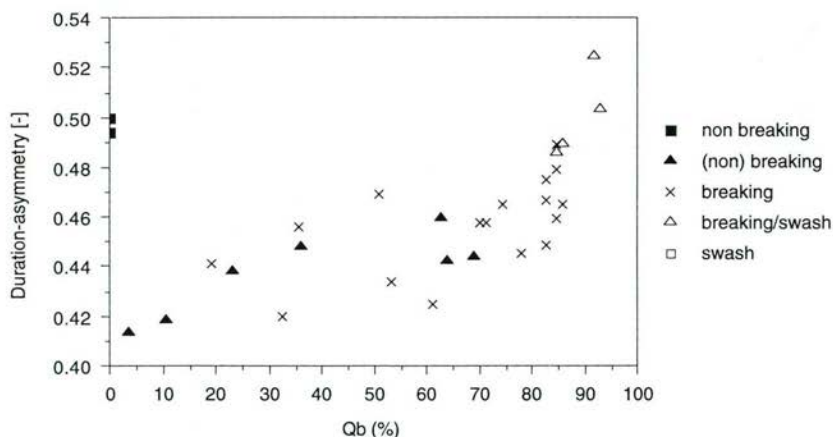
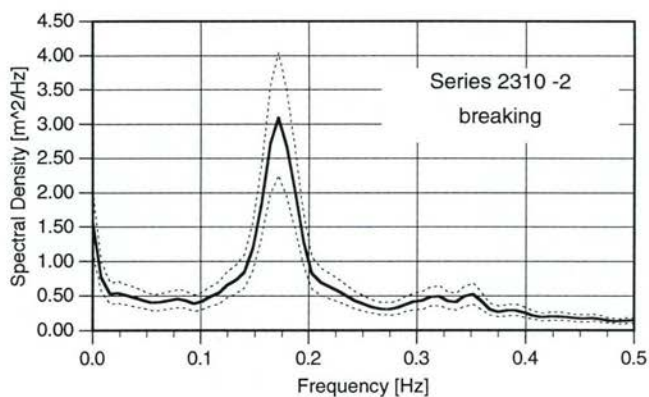


Figure 4.21 Relation between percentage of breaking waves ( $Q_b$ ) and duration asymmetry of the velocity at 0.1 m above the bed.

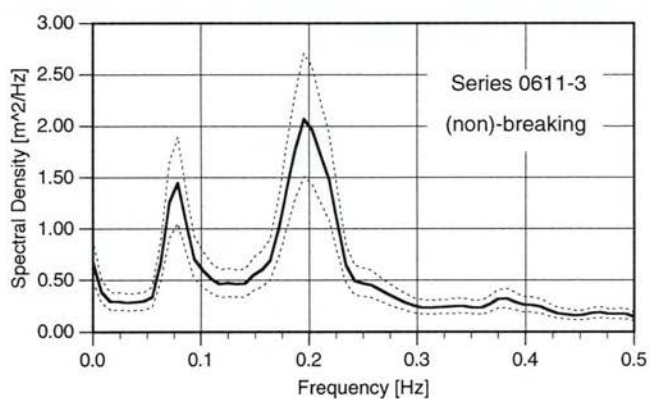
A relation between relative wave height and duration asymmetry was not found. As with the outcome of the amplitude asymmetry analysis, this is in contrast to Kroon's (1994) study, but can be explained by the lack of observations with a relative wave height of 0.8-1.15.

A final observation is the percentage of breaking waves which, as with amplitude asymmetry, is not correlated to the duration asymmetry for lower ( $< 80\%$ ) percentages of breaking waves. Higher percentages of breaking waves ( $> 80\%$ ), however, strongly reduce duration asymmetry (Fig. 4.21).

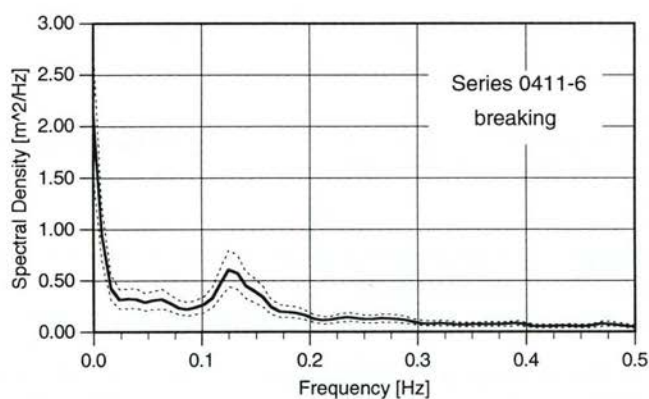




**A**



**B**



**C**

Figure 4.22 Examples of frequency spectra (with 95% conf. int.) of near bed velocities ( $D_f = 93.6$ )

Table 4.7 Cross-shore peak velocities (high/low-frequency) at 0.1 m above the bed

File	High-Frequency				Low-Frequency			
	$u_s$ [m/s]	$u_{s,on}$ [m/s]	$u_{s,off}$ [m/s]	$u_s$ [m/s]	$T_s$ [s]	$T_s$ [s]	$u_{s,on}$ [m/s]	$u_{s,off}$ [m/s]
2310be-1	2.11	1.32	0.97	0.85	6.91	52.86	0.48	0.49
2310be-2	2.20	1.51	0.90	0.57	6.08	49.82	0.34	0.31
2310be-3	2.21	1.45	0.93	0.84	6.48	58.29	0.50	0.45
2310be-4	2.12	1.43	0.88	0.73	6.54	56.60	0.45	0.43
2310be-5	2.15	1.42	0.93	0.72	6.87	56.38	0.45	0.40
2510be-2	0.69	0.39	0.35	0.08	5.68	48.86	0.04	0.05
2510be-3	0.67	0.38	0.34	0.08	5.15	50.09	0.04	0.05
2610be-1	1.98	1.29	0.89	0.57	6.35	45.32	0.31	0.32
2610be-2	1.77	1.19	0.70	0.27	6.17	75.73	0.14	0.17
2610be-3	1.95	1.31	0.81	0.34	6.01	71.93	0.19	0.20
0411be-1	1.33	0.90	0.62	0.64	6.58	64.00	0.42	0.36
0411be-2	1.43	0.96	0.69	0.61	6.20	74.49	0.40	0.32
0411be-3	1.46	0.96	0.68	0.58	6.75	57.57	0.37	0.29
0411be-4	1.48	0.97	0.72	0.54	6.81	61.47	0.36	0.28
0411be-5	1.31	0.88	0.68	0.60	5.19	73.37	0.35	0.31
0411be-6	1.18	0.79	0.64	0.49	4.74	67.73	0.29	0.28
0511be-1	1.63	1.08	0.81	0.64	5.06	65.40	0.37	0.36
0511be-2	1.98	1.29	0.91	0.68	6.09	72.37	0.42	0.41
0511be-3	2.08	1.37	0.98	0.57	6.04	71.96	0.35	0.34
0511be-4	1.98	1.25	1.06	0.61	4.54	65.32	0.34	0.37
0511be-5	2.00	1.26	1.15	0.63	4.12	56.30	0.42	0.38
0611be-1	1.64	1.07	0.77	0.72	5.88	54.68	0.43	0.38
0611be-2	1.86	1.21	0.87	0.44	5.73	60.70	0.22	0.27
0611be-3	1.97	1.29	0.88	0.39	5.99	48.19	0.23	0.22
0611be-4	1.37	0.91	0.60	0.32	5.31	58.00	0.19	0.17
0611be-5	1.33	0.84	0.67	0.36	5.20	59.92	0.20	0.22
0711be-1	1.95	1.27	0.90	0.76	5.91	65.42	0.44	0.44
0711be-2	1.96	1.27	0.85	0.69	6.25	77.43	0.42	0.46
0711be-3	1.78	1.15	0.79	0.73	5.99	62.25	0.44	0.43
0711be-4	1.53	0.98	0.70	0.72	5.81	76.54	0.46	0.41
0811be-1	1.79	1.26	0.81	0.48	6.67	48.60	0.27	0.28
0811be-2	1.20	0.82	0.51	0.33	7.08	90.55	0.16	0.20
0811be-3	1.74	1.18	0.71	0.43	7.93	66.94	0.22	0.24
0911be-1	1.24	0.78	0.58	0.19	4.90	54.83	0.11	0.10
0911be-2	1.55	1.01	0.67	0.25	5.15	49.88	0.13	0.14
0911be-3	1.65	1.10	0.71	0.34	5.63	55.72	0.18	0.21
1011be-1	2.44	1.61	1.02	0.65	7.12	61.47	0.38	0.37
1011be-2	2.34	1.54	0.97	0.76	7.09	60.31	0.45	0.45

$u_s$ = significant cross-shore peak velocity

$T_s$ = significant period

$u_{s,on}$ = onshore significant cross-shore peak velocity

$u_{s,off}$ = offshore significant cross-shore peak velocity

### velocity spectra

The spectra of the near-bed velocity have no uniform shape although those near the BERT show one to three peaks, the first peak, located around 0.125-0.25 Hz (4-8s) (Fig. 4.22a), is associated with the incident wave frequency.

In 8 cases, there is a second peak near 0.05-0.075 Hz (13-20s), and for 7 of the 8 cases, this peak is lower than the first peak (Fig. 4.22b). The frequency and spectral density of the second peak remain largely unchanged during the shift from one hydrodynamic zone to another. This second peak may be due to a swell component of the nearshore wave field or may be induced by gravity edge waves. In 26 of the 38 cases, a third peak is visible on the left side of the spectra at frequencies lower than 0.02 Hz (50s) (Fig. 4.22c). This peak is visible despite the removal, using a second-order polynomial, of the trend in the time-series for the detection of individual waves.

Although the frequency of the spectral peak of the incident wave frequency differs from day to day, it shows only minor changes during any one day, i.e. during the shift from one hydrodynamic zone to another. The frequency of the incident waves (first peak) is thus unrelated to the relative wave height or wave steepness.

### low frequency orbital velocities

The cross-shore and longshore velocity time series were high-pass ( $T < 20$  s) and low-pass ( $T > 20$  s) filtered to examine the contribution of the high frequency and low frequency velocities to the velocity series (Table 4.7). Cross-shore, high-frequency orbital velocities dominate the cross-shore velocity field. For the significant velocities, the average difference between the unfiltered series and the high-pass filtered series is less than  $0.05 \text{ ms}^{-1}$  (3%), while the significant low-frequency orbital velocities vary between  $0.08$  and  $0.85 \text{ ms}^{-1}$ , and increase with relative wave height (Fig. 4.23). Thus, wave-breaking leads to an increase in the low-frequency energy. The ratio between the low- and high frequency velocities varies between 0.11 and 0.48, which is in the same range as reported by Kroon (1994). However, this ratio shows no relation with the relative wave height but shows the same tendency as the ratio between the low- and high-frequency surface waves (Fig. 4.11), i.e. the highest ratios were found in the breaking zone.

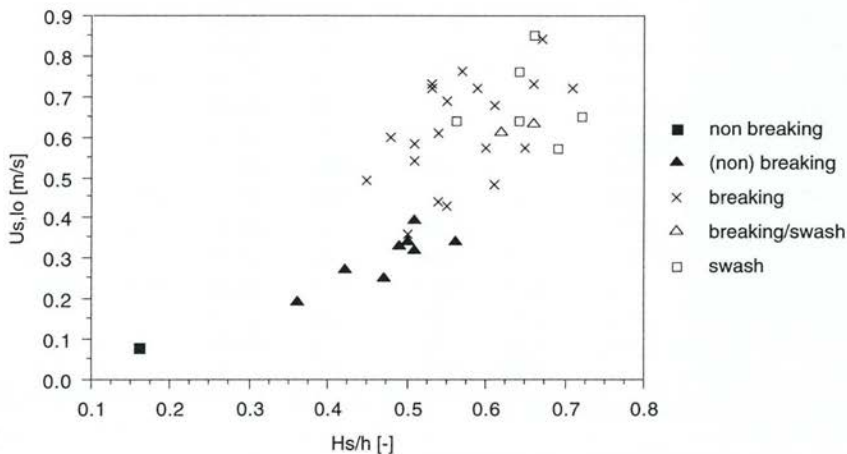


Figure 4.23 Relation between relative wave height and significant, low-frequency, orbital peak velocity at 0.1 m above the bed.



*relation between surface-wave characteristics and near-bed velocities*

The period and amplitude of surface-waves were first compared with those of the near-bed velocities (at 0.1 m). It was found that the significant wave period of surface waves is only weakly correlated with the period of velocity signals, the best resemblance ( $r^2 \sim 0.75$ ) being found during (non)-breaking wave conditions; a large scatter is observed for all other conditions ( $r^2 < 0.3$ ). The same outcome is found when, instead of the significant period, the mean period of the surface-waves and the near-bed velocities is compared. The amplitude related variables, i.e. the significant and mean amplitude of the waves and velocity, result in a reasonable correlation for certain hydrodynamic zones but no linear relations were found to be valid for all zones. The above results show that the surface-wave period and amplitude cannot be related with the period and amplitude of the near-bed velocity.

That surface-wave statistics and velocity statistics do not easily compare may be partially explained by the method used to distinguish the individual waves i.e. a second-order polynomial. The coefficients for the polynomial were found using a least-squares solution, but were, separately determined for the surface-wave series and the near-bed velocity series. As a result, the number of waves, for instance, differ in the wave and velocity series recorded or analysed during the same time-span, thereby leading to differences in other wave related variables. In addition, certain hydrodynamic processes, e.g. turbulence, and -conditions, e.g. air entrapment by breaking waves may also have disturbed the relation between surface-wave characteristics and near-bed velocities

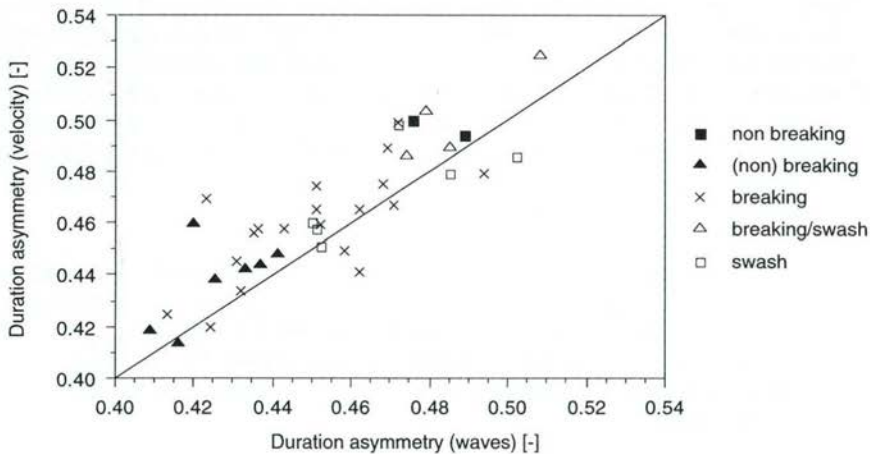


Figure 4.24 Relation between duration asymmetry of the waves and duration asymmetry of the velocity at 0.1 m above the bed.

Secondly, the amplitude- and duration asymmetries of the surface-wave and near-bed velocity series were compared, and it was found that the amplitude asymmetry of the surface-waves does not correspond with that of the velocity near the bed ( $r^2 = 0.28$ ). In contrast, the duration asymmetry of both series shows a reasonable linear correlation (Fig. 4.24).

The overall shape of the spectra shows a good resemblance. The incident wave peak of the surface-wave spectra is always visible in the spectra of the near-bed velocity. Secondary peaks with a frequency lower than that of the incident wave are also nearly always visible in both spectra. The largest differences between surface-wave spectra and velocity spectra are found in the lower frequencies ( $< 0.1$  Hz,  $> 10$  s). In particular, the peak to the left end of the spectra (Fig. 4.22c) can be found in either spectrum, but not in both simultaneously.

In conclusion, it is difficult to obtain a simple statistical-empirical correlation between surface-wave and near-bed velocity characteristics. The period, amplitude and duration asymmetries of surface-waves and velocity show no linear relation although much more similarity is shown between the spectra and duration asymmetry of surface-waves and velocity. An empirical approach seems to be less successful and, potentially, the theoretical relation between surface-wave and near-bed velocity may be better described by the wave theories investigated next.

#### *application of wave theories*

Before the wave theories can be tested, the shape of the orbital profile of the near-bed velocity has to be calculated. The results of the asymmetry analysis indicate that the shape of the orbital velocity profile is asymmetric along both the amplitude and time (phase) axes. The result of the orbital shape calculations confirms this double asymmetry as, together with the linear wave theory, is illustrated in Figure 4.25: Fig. 4.25a for non-breaking, Fig. 4.25b for breaking and Fig. 4.25c for swash conditions. The figures resemble the general tendency present in the orbital velocity profile, viz. the trough that is more de-formed and of longer duration than the crest. Only the non-breaking waves have a nearly symmetrical profile. The standard deviation of the orbital velocity profile is high in some cases, with, in one case, values up to 60. For a high standard deviation, the mean shape of the orbital velocity profile is the result of very irregular waves and does not resemble the measured orbital velocity of the entire time series. This means that, in those cases, the application of wave theories is not very fruitful. However, the larger part of all series (33 of the 38 series) has an orbital wave shape with a standard deviation of less than 5.

As a next step, the surface-wave shape is compared with that of the orbital velocity profile near the bed. The largest deviation between the surface elevation and velocity curves is in the first and last quarter of the wave. Between the wave trough and the wave crest, the curves often show an almost identical shape (Fig. 4.26a-c). As this part determines the duration asymmetry of the waves, it confirms the outcome of the asymmetry comparison.

The shape of the orbital velocity profile was compared with some wave theories. Nine series were further examined (see Fig. 4.8), distributed over the various application domains of the investigated wave theories. It was found that none of the wave theories accurately describes both the amplitude and the duration asymmetry of the series with non-breaking waves, 2510-2 and 2510-3 (Table 4.6; Fig. 4.27). In some cases, though, a particular theory may predict the observed amplitude asymmetry as with the linear theory and series 0411-1 (Fig. 4.27c). The second-order Stokes theory also gives a reasonable assessment of the amplitude asymmetry of series 2510-3 (Fig. 4.27a). However, in none of the nine cases examined is duration asymmetry properly predicted by any of the theories.

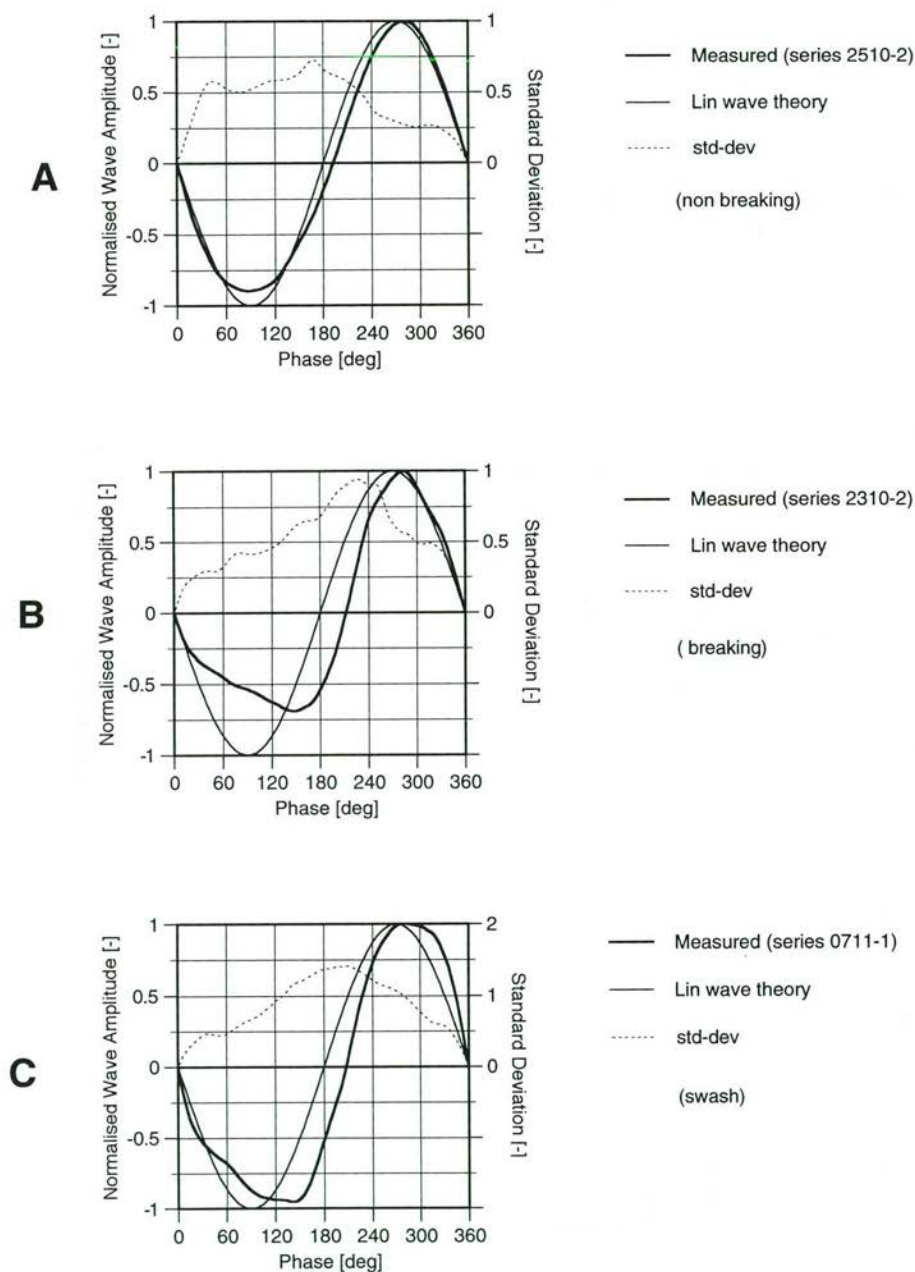


Figure 4.25 Examples of orbital velocity profile of the velocity at 0.1 m above the bed.



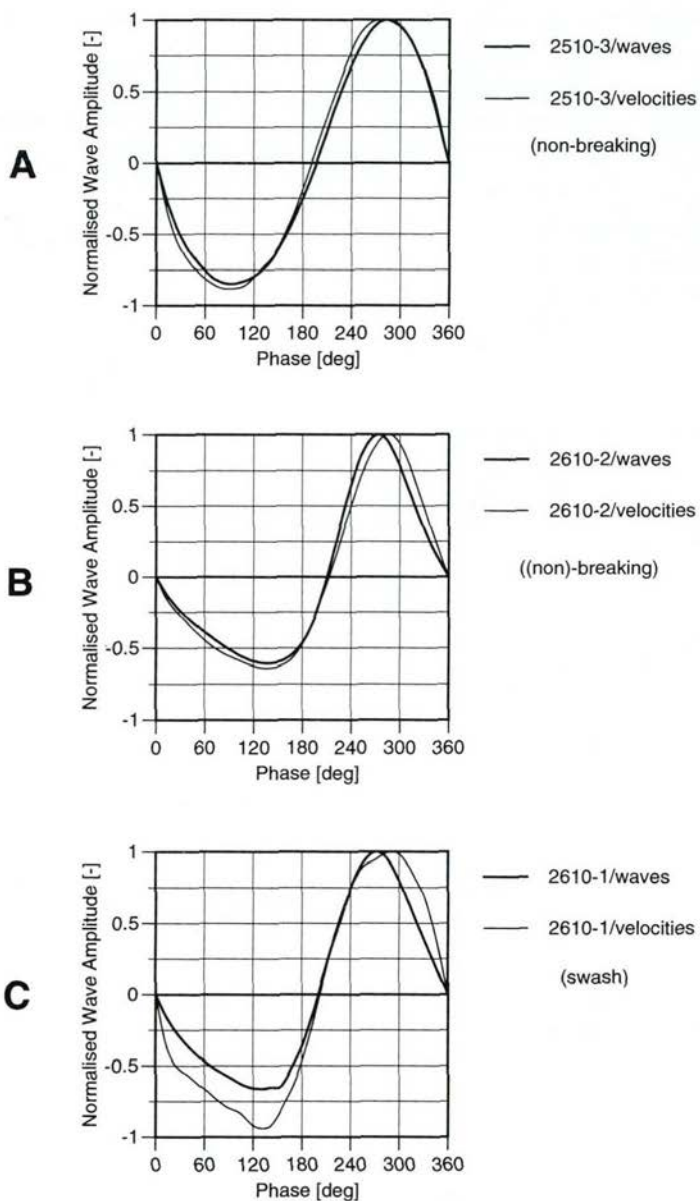


Figure 4.26 Wave profile and orbital velocity profile of near-bed velocity.

The standard deviation of the minimum and maximum value of the orbital profile, used for calculating amplitude asymmetry (Fig. 4.25), is nearly always smaller than that at the point where the orbital profile crosses the phase axis. The latter determines the duration asymmetry. Thus the variation of the standard deviation over the profile may be the reason why the theoretical and measured amplitude asymmetries match better than those of the duration-asymmetries.

Many sediment transport models use wave theories relating the surface-wave height and wave period to near-bed velocities. The above analysis, however, has shown that no theory accurately describes the entire orbital-velocity-profile shape or even the amplitude- or duration asymmetry. The applicability of the theories were further examined by studying to what extent three particular features of the near-bed hydrodynamics - the significant onshore peak velocity, the significant offshore peak velocity and the amplitude asymmetry of the significant velocity - can be calculated using the different theories. Significant velocities are used because the significant wave height is used in the various theories. In this comparison, all measured series are used. The significant velocities are important because they are strongly related to the pick-up of sediment. The amplitude asymmetry largely determines the direction and magnitude of sediment transport (e.g. Soulsby et al., 1993).

The Stokes second order theory could only be applied in the two cases of non-breaking waves. As all other cases gave numerical difficulties, this theory was not considered in this extended analysis. All theories underestimate the onshore peak velocities and in particular, the highest measured onshore velocities are much higher than predicted values (Fig. 4.28). Nevertheless, the onshore peak velocities predicted by the linear, Cnoidal and Fourier Approximation methods show a high correlation ( $r^2 > 0.7$ ) with the measured values, in contrast to the Cnoidal theory where no correlation was shown: while the measured velocities vary between 0.39 and 1.68  $\text{ms}^{-1}$ , the Cnoidal theory predicts significant onshore velocities of between 0.75 and 0.98  $\text{ms}^{-1}$ . The ratio between the predicted significant onshore velocities and the measured velocities increases with the relative wave height, but in all cases is less than two (Fig. 4.29). The relative wave height is related to the hydrodynamic zones (Fig. 4.5). Thus, the applicability of the examined wave theories in predicting the onshore velocity decreases when going from the non-breaking zone (low relative wave height) to the swash zone (high relative wave height). It is noted that the results of this study are more in line with the expectations. Because all these theories were originally designed for use with non-breaking waves, the ratio between measured and theoretical values should increasingly deviate from unity when going from the non-breaking wave (lower  $H_s/h$ ) to the breaking wave zone (higher  $H_s/h$ ).

The result of the analysis of the onshore velocities is in contrast to the findings of Kroon (1994), although the measured velocities are in the same range. He found that the predicted velocities by the Cnoidal theory agreed well with the observed values. He also found that the ratio between the theoretical and the observed onshore velocities decreased with an increasing relative wave height. However, Kroon (1994) observed relative wave heights larger than 1, while in this study the maximum relative wave height is 0.72. These large relative wave heights heavily influence the correlation between relative wave heights and the ratio of theoretical to observed velocities and contribute to the lack of agreement on this point between this study and that of Kroon (1994).

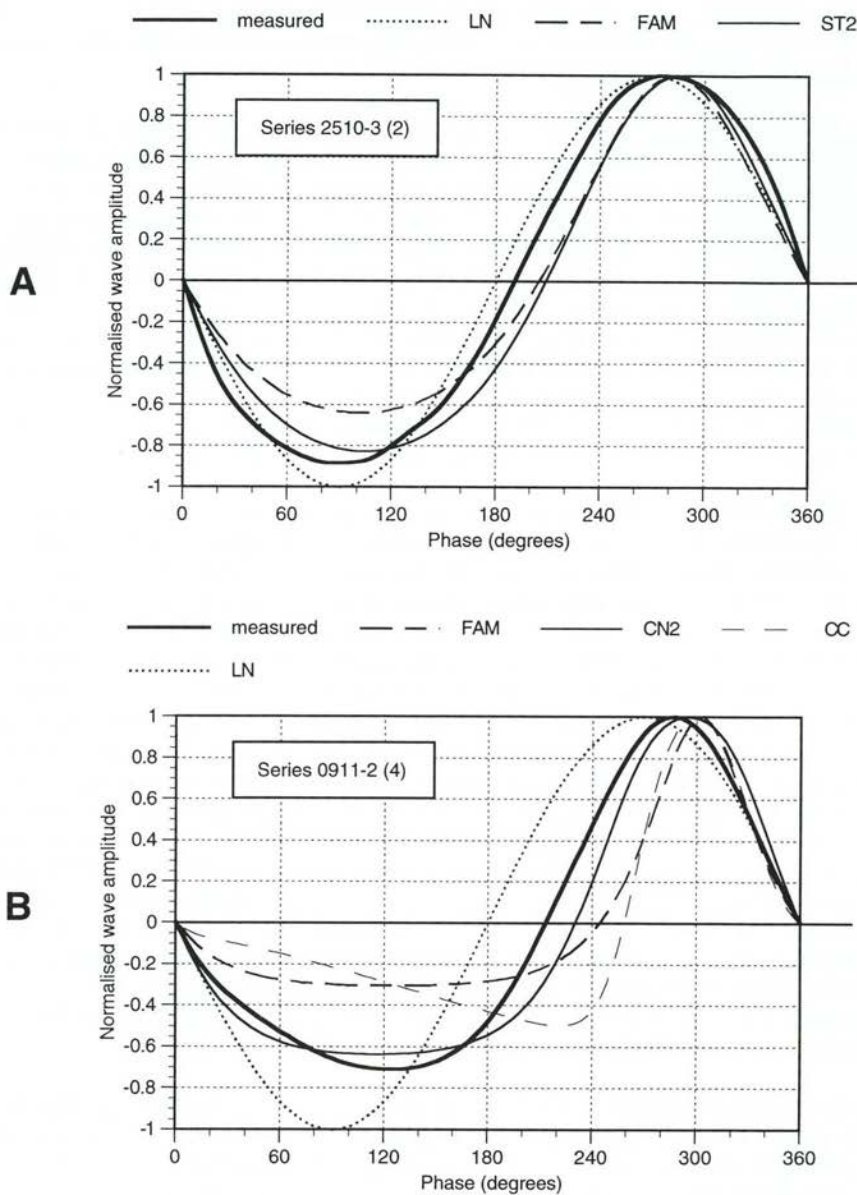
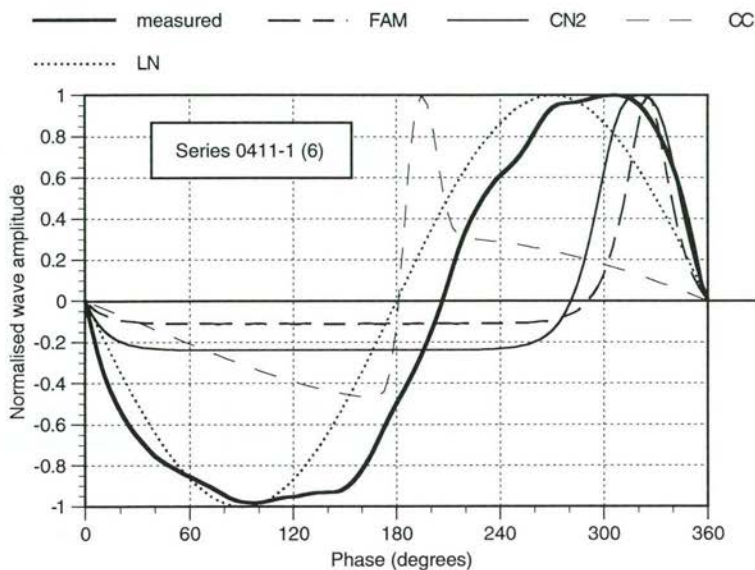


Figure 4.27 Shape of orbital velocity profile, measured and theoretical (LN = linear theory, FAM = Fourier Approximation Method, ST2 = Stokes second order, CN2 = cnoidal second order, CC = covocoidal). Numbers between brackets refer to Fig. 4.8.



C



D

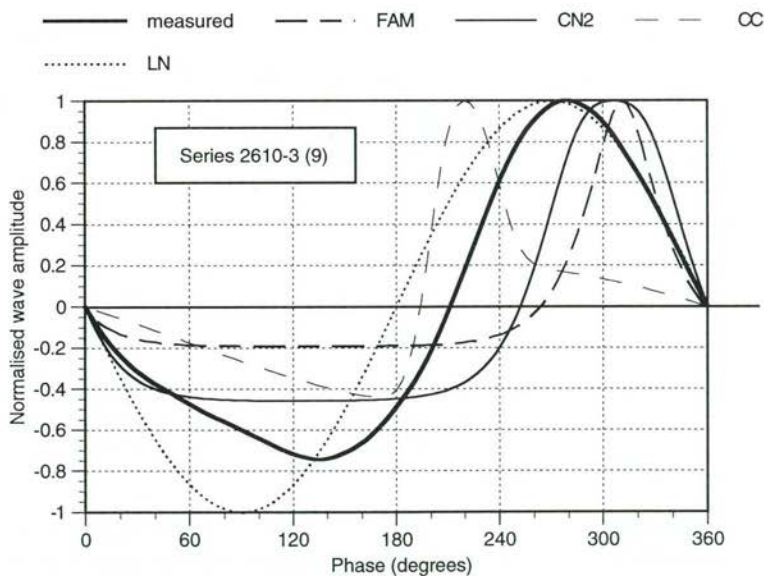


Figure 4.27  
(continued)

Shape of orbital velocity profile, measured and theoretical (LN = linear theory, FAM = Fourier Approximation Method, ST2 = Stokes second order, CN2 = cnoidal second order, CC = covocoidal). Numbers between brackets refer to Fig. 4.8.

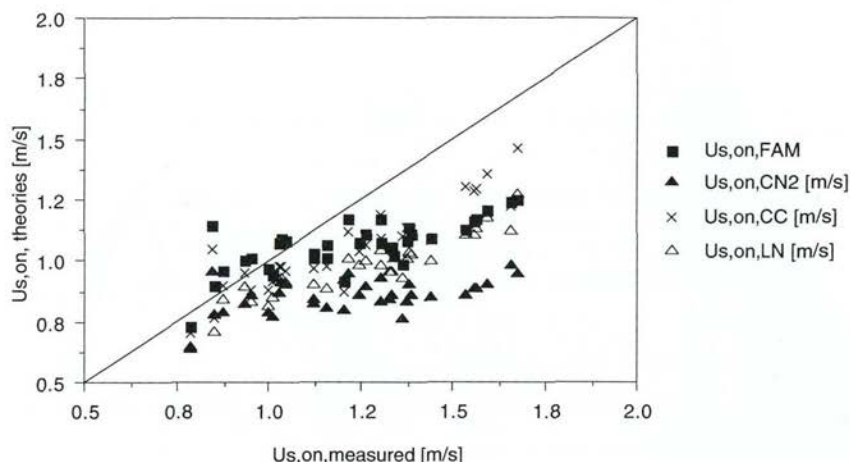


Figure 4.28 Relation between measured and theoretical significant, onshore, orbital peak velocity at 0.1 m above the bed (FAM = Fourier Approximation Method, CN2 = cnoidal second order, CC = covocoidal, LN = linear theory).

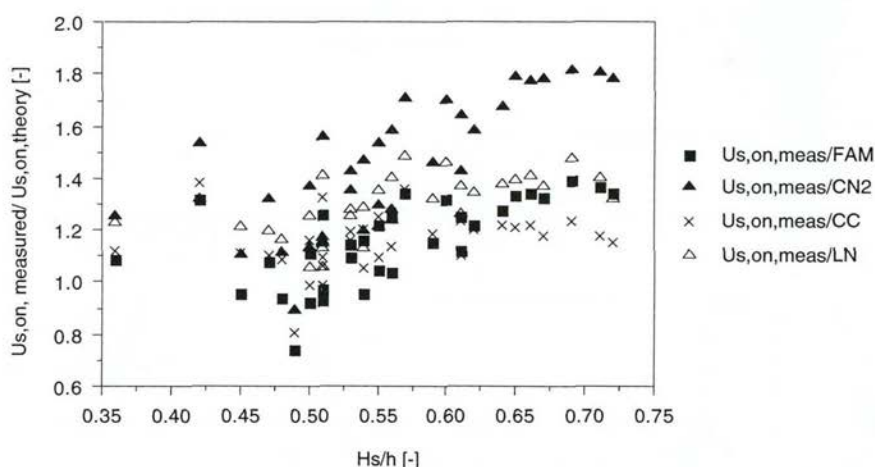


Figure 4.29 Relation between the ratio measured to theoretical, significant, onshore peak velocity at 0.1 m above the bed and the relative wave height ( $H_s/h$ ) (FAM = Fourier Approximation Method, CN2 = cnoidal second order, CC = covocoidal, LN = linear theory).

swash zone (high relative wave height). It is noted that the results of this study are more in line with the expectations. Because all these theories were originally designed for use with non-breaking waves, the ratio between measured and theoretical values should increasingly deviate from unity when going from the non-breaking wave (lower  $H_s/h$ ) to the breaking wave zone (higher  $H_s/h$ ).

The result of the analysis of the onshore velocities is in contrast to the findings of Kroon (1994), although the measured velocities are in the same range. He found that the predicted velocities by the Cnoidal theory agreed well with the observed values.

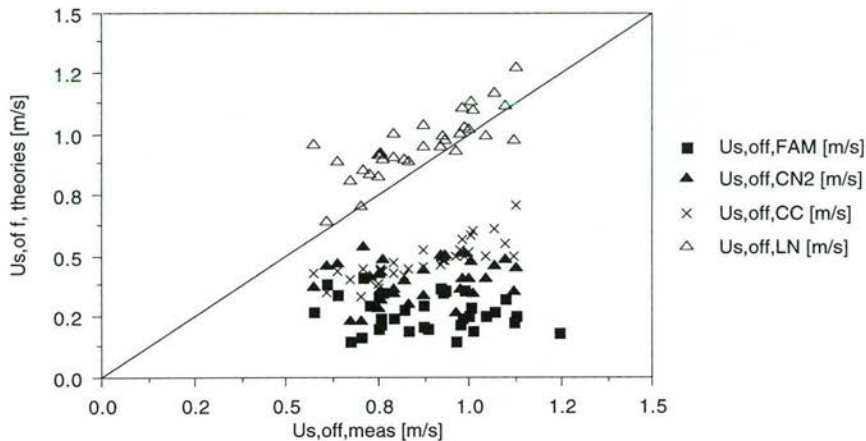


Figure 4.30 Relation between measured and theoretical, significant, offshore, orbital peak velocity at 0.1 m above the bed (FAM = Fourier Approximation Method, CN2 = cnoidal second order, CC = covocoidal, LN = linear theory).

He also found that the ratio between the theoretical and the observed onshore velocities decreased with an increasing relative wave height. However, Kroon (1994) observed relative wave heights larger than 1, while in this study the maximum relative wave height is 0.72. These large relative wave heights heavily influence the correlation between relative wave heights and the ratio of theoretical to observed velocities and contribute to the lack of agreement on this point between this study and that of Kroon (1994).

The measured significant offshore peak velocities show a good agreement with the outcome derived from the linear wave theory (Fig. 4.30). The other theories produce lower values than those measured, with the exception of the offshore peak velocities predicted by the linear and the Covocoidal theories where some correlation with the measured values is shown with the ratios between the measured and predicted values varying from 1 to 6. For the Fourier Approximation Method the ratio rapidly increases with the relative wave height and the outcome of the offshore velocity analysis fully agrees with Kroon's (1994) study.

The Fourier Approximation Method (FAM), the Cnoidal theory and the Covocoidal theory underestimate the onshore and the offshore velocity. These theories, however, overestimate the amplitude asymmetry (Fig. 4.31). The FAM and the Cnoidal theory show a large scatter and no relation with the measured asymmetries. The amplitude-asymmetries predicted by the Covocoidal theory are less scattered, but also have no relation with the measured asymmetries and the prediction accuracy of the amplitude asymmetry of all theories shows no relation with the relative wave height.

It is difficult to give directions on how to improve the predictions made by the various theories. Kroon (1994) multiplied the theoretical predictions of the linear wave theory with a factor which was related to the relative wave height, and in this way improved



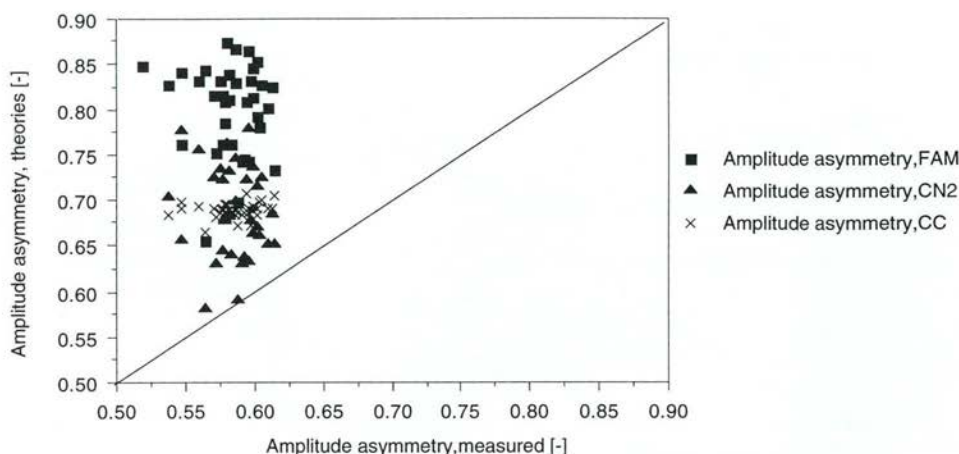


Figure 4.31 Relation between measured and theoretical amplitude asymmetry of the velocity at 0.1 m above the bed (FAM = Fourier Approximation Method, CN2 = cnoidal second order, CC = covocoidal).

the predictive capacity of the theory. For this study, however, the application of this factor does not lead to an improvement of the prediction capability of the linear wave theory. The correlation coefficient between the measured and theoretical values improves slightly for the onshore peak velocities from  $r^2 = 0,79$  to  $r^2 = 0,81$ , but decreases for the offshore peak velocities from  $r^2 = 0,63$  to  $r^2 = 0,54$ . The lack of improvement is because the assumed relation between relative wave height and the prediction accuracy was not found by this study. Hence Kroon's (1994) approach is here less useful.

Surprisingly enough, the above analysis makes clear that for the determination of on- and offshore velocity in breaking waves, the linear theory generally gives the best results. Unfortunately, none of the theories give reasonable results for the calculation of the amplitude asymmetry of the velocity in all the hydrodynamic zones.

#### *vertical variability of the velocity field*

Some of the series started when the upper EMF (0.7 m above the bed) was near to SWL, or even sometimes above water level. To exclude errors due to exposure to air, 7 series were excluded from this analysis.

First, the vertical variability of the cross-shore mean current and the on- and offshore significant velocities were considered. The mean currents of the lowest EMF (0.1 m above the bed) and the middle EMF (0.3 m above the bed), were found to show a high correlation ( $r^2 \sim 0.9$ , Fig. 4.32, Table 4.8). The mean currents of both EMFs were found to be always offshore directed and the average difference between the mean current of both sensors is less than  $0.01 \text{ ms}^{-1}$ . There is almost no correlation between the middle EMF and the highest EMF (0.7 m above the bed) and while the lowest two EMFs only show a mean offshore velocity, the highest one shows mean currents that are either onshore or offshore directed. The differences in mean currents between the middle and upper EMF vary up to  $0.9 \text{ ms}^{-1}$  within anyone series.

Table 4.8 Mean velocities, significant peak velocities and velocity asymmetries at three heights (0.1, 0.3 and 0.7 m above the bed) in cross-shore direction.

Series	at 0.1 m					at 0.3 m					at 0.7 m				
	$u_{mean}$	$u_{s,on}$	$u_{s,off}$	$A_{a,u}$	$A_{d,u}$	$u_{mean}$	$u_{s,on}$	$u_{s,off}$	$A_{a,u}$	$A_{d,u}$	$u_{mean}$	$u_{s,on}$	$u_{s,off}$	$A_{a,u}$	$A_{d,u}$
	[m/s]	[m/s]	[m/s]	[-]	[-]	[m/s]	[-]	[-]	[m/s]	[m/s]	[m/s]	[m/s]	[m/s]	[-]	[-]
2310be-2	-0.08	1.53	0.98	0.61	0.43	-0.12	1.65	1.11	0.60	0.43	-0.12	1.81	1.11	0.62	0.43
2310be-3	-0.11	1.56	1.04	0.60	0.46	-0.07	1.56	1.00	0.61	0.46	-0.04	1.89	1.14	0.63	0.43
2310be-4	-0.14	1.52	0.96	0.61	0.45	-0.13	1.48	0.94	0.61	0.45	-0.04	1.83	1.08	0.63	0.42
2510be-2	-0.03	0.39	0.36	0.52	0.50	-0.06	0.41	0.39	0.52	0.49	-	-	-	-	-
2510be-3	-0.03	0.38	0.34	0.53	0.49	-0.06	0.37	0.33	0.53	0.48	-	-	-	-	-
2610be-2	-0.07	1.18	0.74	0.62	0.41	-0.12	1.14	0.74	0.61	0.43	-0.16	1.28	0.81	0.61	0.41
2610be-3	-0.13	1.30	0.85	0.60	0.42	-0.20	1.25	0.82	0.60	0.42	-	-	-	-	-
0411be-2	-0.35	1.00	0.74	0.58	0.48	-0.31	1.08	0.83	0.57	0.48	-0.57	0.64	0.67	0.49	0.50
0411be-3	-0.34	1.01	0.74	0.58	0.48	-0.33	1.02	0.72	0.59	0.47	-0.57	0.57	0.66	0.47	0.51
0411be-4	-0.37	1.02	0.77	0.57	0.49	-0.34	1.01	0.76	0.57	0.47	-0.69	0.54	0.64	0.46	0.50
0411be-5	-0.35	0.93	0.73	0.56	0.50	-0.31	0.96	0.89	0.52	0.50	-	-	-	-	-
0411be-6	-0.28	0.83	0.69	0.55	0.50	-0.22	0.95	0.86	0.52	0.48	-0.69	0.54	0.64	0.46	0.49
0511be-2	-0.11	1.36	0.97	0.58	0.46	-0.13	1.39	1.02	0.58	0.46	-0.13	0.70	0.76	0.48	0.51
0511be-3	-0.07	1.41	1.02	0.58	0.47	-0.09	1.33	1.05	0.56	0.49	-0.14	0.64	0.69	0.48	0.50
0511be-4	-0.12	1.28	1.10	0.54	0.49	-0.12	1.30	1.15	0.53	0.49	-0.19	0.73	0.74	0.50	0.50
0611be-2	-0.09	1.22	0.91	0.57	0.46	-0.14	1.22	0.96	0.56	0.47	0.30	0.59	0.53	0.53	0.50
0611be-3	-0.09	1.30	0.90	0.59	0.44	-0.12	1.24	0.90	0.58	0.45	0.20	0.55	0.47	0.54	0.48
0611be-4	-0.07	0.91	0.62	0.59	0.44	-0.14	1.16	0.83	0.58	0.46	0.16	0.56	0.50	0.53	0.49
0611be-5	-0.13	0.86	0.71	0.55	0.47	-0.21	1.16	0.82	0.58	0.46	0.33	0.66	0.58	0.53	0.50
0711be-1	-0.18	1.35	0.95	0.59	0.46	-0.15	1.36	0.96	0.59	0.47	0.37	1.51	1.22	0.55	0.44
0711be-2	-0.33	1.35	0.96	0.58	0.46	-0.32	1.34	0.99	0.58	0.45	0.57	0.75	0.63	0.54	0.49
0711be-3	-0.30	1.24	0.90	0.58	0.47	-0.29	1.28	0.93	0.58	0.44	0.44	0.72	0.61	0.54	0.50
0711be-4	-0.31	1.10	0.80	0.58	0.47	-0.28	1.16	0.84	0.58	0.49	0.33	0.78	0.64	0.55	0.51
0811be-1	-0.08	1.28	0.85	0.60	0.43	-0.09	1.32	0.90	0.59	0.44	-0.12	0.45	0.55	0.45	0.53
0811be-2	-0.12	0.82	0.56	0.59	0.46	-0.17	1.08	0.69	0.61	0.43	-	-	-	-	-
0811be-3	-0.17	1.19	0.78	0.61	0.45	-0.23	1.22	0.78	0.61	0.44	-0.47	0.38	0.43	0.47	0.51
0911be-1	-0.11	0.77	0.59	0.56	0.45	-0.13	0.80	0.61	0.57	0.45	-	-	-	-	-
0911be-2	-0.07	0.99	0.70	0.59	0.42	-0.12	0.99	0.74	0.57	0.41	-	-	-	-	-
0911be-3	-0.19	1.10	0.74	0.60	0.44	-0.24	1.11	0.84	0.57	0.45	0.47	0.58	0.49	0.54	0.47
1011be-1	-0.09	1.63	1.10	0.60	0.45	-0.06	1.66	1.12	0.60	0.46	0.09	0.79	0.76	0.51	0.48
1011be-2	-0.14	1.62	1.07	0.60	0.44	-0.08	1.56	1.05	0.60	0.44	0.09	0.67	0.65	0.51	0.50

$u_{mean}$ = mean cross-shore velocity

- = offshore/south

+ = onshore/north

"-"= excluded from analysis because EMF at 0.7 m was temporarily above water level

$u_{s,on}$ = onshore significant cross-shore peak velocity

$u_{s,off}$ = offshore significant cross-shore peak velocity

$A_{a,u}$ =amplitude-asymmetry of the cross-shore peak velocity

$A_{d,u}$ =duration-asymmetry of the cross-shore peak velocity

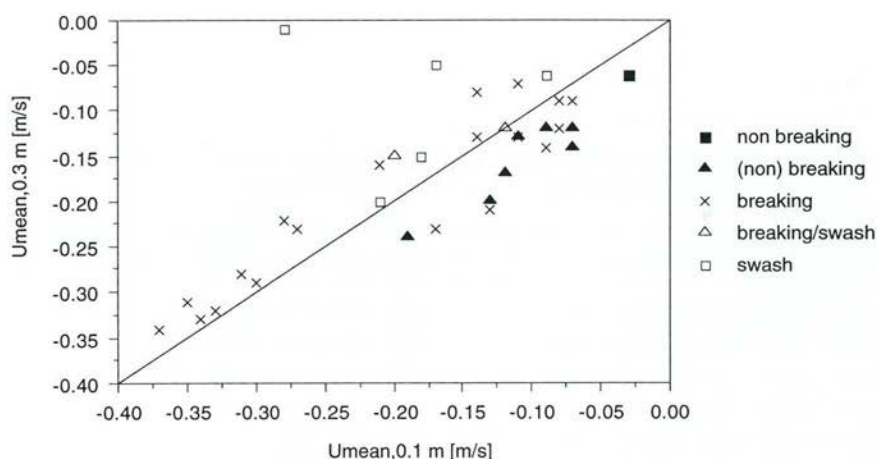


Figure 4.32 Relation between mean, cross-shore velocity at 0.1 m and at 0.3 m above the bed.

An identical conclusion is reached regarding the comparison between the offshore and onshore significant peak velocities. A high correlation between the significant peak velocities is present for the lowest and the middle EMF whereas the middle and the highest EMF show no correlation.

Besides the vertical variability of the significant- and mean current, the vertical variability of the velocity asymmetry was also investigated. Both the amplitude- and the duration asymmetry of the lowest two EMFs show a very high degree of correlation (Table 4.8) and the mean values averaged over all series, are the same. There was no correlation between the amplitude- and duration-asymmetries of the two highest EMFs. The amplitude-asymmetries of the middle EMF shows higher values than the upper EMF. Moreover, the series averaged amplitude asymmetries at the middle EMF are larger than 0.5 while the amplitude asymmetries of the upper EMF indicate amplitude symmetry with a ratio of about 0.5. The middle EMF shows lower values for the duration asymmetry than the upper EMF. As in the case of the amplitude asymmetries, the values of the duration asymmetries for the upper EMF are closer to 0.5 than those of the middle EMF. Thus, the shape of the orbital velocity profile is more symmetrical in the upper part of the profile than in the lower part. This is somewhat unexpected as most wave theories and also measurements (e.g. Greenwood and Osborne, 1990) show that the velocity asymmetry (slightly) decreases or remains unchanged towards the bed. The tendency observed here may be due to the fact that the water level varied during the 40-minutes recordings. As a result, the time-averaged velocity at the upper EMF may have been varying from onshore to offshore, i.e. undertow was only temporarily present. This leads to a more symmetrical orbital velocity profile.

The above analysis shows that the significant peak velocities, the mean velocities and the asymmetry of the velocity vary with the elevation above the bed. The relative depth of the EMFs varies with the tide. However, no tidal dependency of the vertical structure of one of the variables could be found. In conclusion, whereas the near-bed velocities are highly correlated between 0.1 m and 0.3 m above the bed, the cross-shore velocities between 0.3 m and 0.7 m above the bed show no correlation.



#### 4.5.4 Conclusions

The near-bed velocities in the inner nearshore zone were studied and measurements were performed under conditions with a relative wave height varying from 0.16 - 0.72. The analysis leads to the following conclusions:

##### *significant and mean velocities*

- The near-bed significant peak velocities of the inner near shore zone show a dominance of the cross-shore velocities over the longshore velocities in all hydrodynamic zones.
- A higher relative wave height results in a higher significant onshore- and offshore velocity near the bed.
- The strength of the cross-shore, near-bed mean current is not related to either the relative wave height or to the wave steepness.
- Existing formulas for undertow do not accurately estimate the measured strength of the mean cross-shore current.

##### *asymmetry of the velocities*

- Non-symmetric orbital velocities show both an amplitude asymmetry and a duration asymmetry.
- Higher relative wave heights only result in higher near-bed velocity asymmetries in breaking waves.
- A high (>80%) percentage of breaking waves leads to more symmetrical orbital velocities near the bed.

##### *velocity spectra*

- Most of the spectral energy is confined to incident (wind) wave frequencies.
- The shape of the velocity spectra remains fairly constant during the different wave conditions.

##### *wave theories and orbital profile shape*

- The shape of the orbital velocity profile near the bed demonstrates a trough that is more de-formed, and of longer duration, than the crest.
- None of the applied wave theories are able to describe the orbital shape correctly, mainly due to the asymmetry of the wave trough.
- All investigated theories underestimate the significant onshore velocities near the bed. The ratio between the measured and estimated near-bed velocities is, in all cases, less than two.
- Apart from the linear wave theory, all other investigated theories underestimate the significant offshore velocities near the bed.
- All theories overestimate the amplitude-asymmetries of the near-bed velocities. No linear correlation is present between the theoretical values and the measured values.

##### *low frequency velocities*

- High-frequency energy dominates the inner nearshore velocities.
- The relative contribution of low frequency velocities increases towards the breaker zone but decreases thereafter.

of high-frequency suspended sediment transport. It also suggests that the mean sediment transport will be directed to the sea because undertow is always offshore directed. However, the relative contributions of these sediment transport components, their spatial distribution and the influence of the wave asymmetry on the total (net) sediment transport cannot be determined from hydrodynamic data alone, as it depends as well on the phase relationship between the instantaneous velocity and concentration and on the magnitude of the bedload transport. Hence, it is necessary to determine the modes, magnitudes and directions of the nearshore sediment transport and to relate these to the observed hydrodynamics. Only then, a complete picture of the sediment dynamics, responsible for inner nearshore bar developments, can be established. This sediment transport analysis is performed in the next chapter.